TRITA-MMK 2002:10
ISSN 1400-1179
ISRN KTH/MMK--02/10--SE

# Stability analysis and synthesis of statically balanced walking for quadruped robots

**Freyr Hardarson**

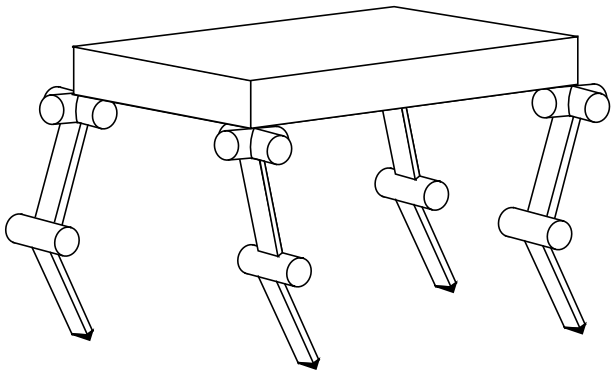

DAMEK

Stockholm
2002

Doctoral Thesis
Mechatronics Lab
Department of Machine Design
Royal Institute of Technology, KTH
S-100 44 Stockholm, Sweden

Akademisk avhandling som med tillstånd från Kungliga Tekniska Högskolan i Stockholm, framläggs till offentlig granskning för avläggande av teknologie doktorsexamen, torsdagen den 13 juni 2002, kl. 13.00 i sal M3, på Institutionen för Maskinkonstruktion, Kungliga Tekniska Högskolan, Stockholm.



Stockholm 2002, Universitetsservice US AB

**Mechatronics Lab**
**Department of Machine Design**
**Royal Institute of Technology**
**S-100 44 Stockholm, Sweden**

TRITA-MMK 2002:10
ISSN 1400-1179
ISRN KTH/MMK/R--02/10--SE

*Document type*
Doctoral Thesis

*Date*
020613

*Author(s)*
Freyr Hardarson

*Supervisor(s)*
Jan Wikander

*Title*
Stability analysis and synthesis of statically balanced walking for quadruped robots

*Sponsor(s)*
The Foundation for Strategic Research through its Centre for Autonomous Systems, Royal Institute of Technology

*Abstract*

Walking robots have a potential to traverse certain types of terrain in a more efficient and stable manner than more conventional robots, using wheels or tracks. The property of walking robots that the contact with the ground is discontinuous gives them the ability to select footholds such that obstacles or holes are avoided. Other advantageous properties of walking robots are that they cause less damage to the terrain, active suspension is an intrinsic part of their structure, and they are omnidirectional, which gives them an advantage in maneuvering through cluttered and tight environments.

The control of walking robots requires that the issue of stability against tipping over is treated in a more specific fashion than for wheeled robots, as there are discrete changes in the support of the robot when the legs are lifted or placed. The stability of the robot is dependent on how the legs are positioned relative to the body and on the sequence and timing in which the legs are lifted and placed. In order to reduce the risk of the robot losing stability while walking, a measure for the stability of the robot is typically used in the gait and motion planning, in order to avoid, or detect, that the robot could become unstable.

The main contribution of the thesis is in the analysis of the stability of statically balanced quadrupedal gaits and how statically balanced walking can be achieved. The center of pressure, i.e. the point where the resultant of the ground reaction forces at the feet acts, is used to develop a stability measure, which is then used in the planning of the body motion. The stability measure is used to set appropriate bounds on the motion of the robot, to account for potentially destabilizing forces or moments. The motion of the robot is planned by determining the supporting force for each leg, which in turn will determine how the robot should shift its weight in order to remain statically balanced. The approach proposed in this thesis, therefore, solves simultaneously the problem of determining a statically balanced motion trajectory for the body, as well as, the distribution of forces to the feet, to compensate for the weight of the robot. A description of the implementation and experimental results are provided, using the quadruped robot WARP1. The experimental results demonstrate the walking capability of the robot, and its ability to handle inclined surfaces.

*Keywords*
legged locomotion, walking robots, mobile robots, stability measures, center of pressure, force distribution, kinematics, dynamics, gaits

*Language*
English

## ACKNOWLEDGMENT

First of all, my sincere thanks to Professor Jan Wikander for the guidance, encouragement and support he has given me during the years. I also appreciate the careful reading and editing of this thesis, and for providing valuable comments.

I would also like to thank my colleagues at Damek for creating the stimulating and enjoyable atmosphere to work in. Especially, I would like to thank my colleagues in the WARP group, both past and present, for the collaboration. The great work of Christian Ridderström and Johan Ingvast in providing the development and experimental setup, that has been vital for the success of this project, is most gratefully acknowledged. Also, the work of Dr. Henrik Rehbinder has provided an important component to the work presented here.

Special thanks go to my old comrades in arms throughout all these years, Henrik Flemmer and Ola Redell, for being great friends. Special thanks go also to all the people who have helped me with setting up the equipment and assisted with the experiments. Further I would like to thank Professor Henrik Christensen for providing a very stimulating research environment through the Centre for Autonomous Systems.

This work was supported by the Swedish Foundation for Strategic Research through its Centre for Autonomous Systems at the Royal Institute of Technology, Stockholm.

Stockholm, May 2002

Freyr Hardarson

## NOTATION

*Abbreviations*

| | |
|---|---|
| CoG | Center of Gravity |
| CoP | Center of Pressure |
| $\mathrm{CoP_d}$ | Desired center of Pressure |
| DSM | Dynamic Stability Margin |
| ESM | Energy Stability Margin |
| FRI | Foot Rotation Indicator |
| PCoG | vertical Projection of the Center of Gravity onto a plane |
| SSI | Support Stability Indicator |
| SSM | Support Stability Margin |
| ZMP | Zero Moment Point |

*Index points*

| | |
|---|---|
| $B$ | index point for the robot body |
| $\overline{B}$ | vertical projection of the index point $B$ onto a plane |
| $C$ | the center of pressure |
| $D$ | index point for the virtual vehicle |
| $E$ | point where an external force acts |
| $G$ | center of gravity of the robot |
| $\overline{G}$ | vertical projection of the center of gravity onto a plane |
| $H_i$ | position of hip of leg $i$ |
| $L_{i,j}$ | index point of link $j$ of leg $i$ |
| $N$ | world origin |
| $O$ | general point in the ground plane |
| $P_i$ | index point of foot $i$ |
| $Q$ | point on an edge of the support surface |

*Frames*

| | |
|---|---|
| $fA$ | the attitude frame of the body |
| $fB$ | the frame fixed to the robot body |
| $fC$ | the ground frame with third axis normal to the ground plane |
| $fD$ | frame fixed to the virtual vehicle |
| $fL_{i,j}$ | frame fixed to link $j$ of leg $i$ |
| $fN$ | the world frame or inertial frame |
| $fR_{i,j}$ | frame fixed to the rotor at joint $j$ of leg $i$ |

*Variables and constants*

| | |
|---|---|
| $a_i$ | shortest distance between the CoP and an edge of the support surface |
| $a_G$ | acceleration of gravity, $a_G \approx 9.8 m/s^2$ |
| $\underline{a}^{NB}$ | acceleration of point $B$ |
| $\underline{a}^{NL}_{i,\,j}$ | acceleration of point $L_{i,j}$ |
| $\boldsymbol{B}_i$ | velocity feedback gain matrix of leg $i$ |
| $\boldsymbol{B}_B$ | velocity feedback gain matrix for body controller |
| $\underline{b}_i$ | vector representing axis $i$ of frame $fB$, for $i$ = 1...3 |
| $\boldsymbol{C}$ | matrix of centrifugal and coriolis force |
| $\underline{c}$ | vector of centrifugal and coriolis forces |
| $\underline{c}_i$ | vector representing axis $i$ of frame $fC$, for $i$ = 1...3 |
| $\boldsymbol{D}$ | the inertia matrix |
| $d_i$ | shortest distance of foot $i$ from an |

opposite edge of a triangle

$\underline{e}$ unit vector pointing along an edge of the support surface

$\underline{e}^{P_iP_j}$ unit vector of a vector from point $P_i$ to $P_j$

$\underline{F}_G$ the resultant of the inertial and external forces acting at point $G$

$\underline{F}_E$ external force acting at point $E$

$|\underline{F}_{G,n}|_{max}$ maximum of $\underline{F}_G$ normal to the ground plane

$|\underline{F}_{G,t}|_{max}$ maximum of $\underline{F}_G$ tangential to the ground plane

$\underline{f}$ vector of generalized forces

$\underline{f}_{i,r}^{P}$ force reference for foot $i$

$\underline{g}$ vector of gravitational forces

$\underline{H}$ vector of support ratio parameters

$\underline{H}_G$ the angular momentum of the robot around the CoG

$h$ the vertical height of point $G$ above the ground plane

$h_n$ the height of point $G$ above the ground plane along the normal

$\boldsymbol{I}_B$ the inertia matrix of robot body

$\boldsymbol{I}_{ij}$ the inertia matrix of link $j$ of leg $i$

$\boldsymbol{I}_R$ the inertia matrix of the rotor

$\underline{I}_i$ the vector of currents of leg $i$.

$J$ the inertia of a rotor around its axis of rotation

$\boldsymbol{J}_i$ diagonal matrix of the reflected inertias of the rotors of leg $i$

${}^{B}\boldsymbol{J}_i^{P}$ jacobian matrix of the kinematic relationship of point $B$ and $P_i$

$\boldsymbol{K}_i$ diagonal matrix of the stiffness coefficients of leg $i$

$\boldsymbol{K}_{t,i}$ diagonal matrix of the gear ratio and torque constants of leg $i$

$k_{i,j}$ stiffness coefficient for joint $j$ of leg $i$

$k_{emf,i,j}$ back electro-motive constant of the motor in joint $j$ of leg $i$

$k_{t,i,j}$ the torque constant of the motor in joint $j$ of leg $i$

$L$ the Lagrangian, $L = T - P$

$l_{i,j}$ inductance of the motor in joint $j$ of leg $i$.

$l_{i\text{-}j}$ line parallel with the edge formed by feet $i$ and $j$

$\underline{M}_G$ the resultant moment of the inertial and external forces acting around point $G$

$\underline{M}_E$ external moment acting on robot

$M_i$ moment acting around edge $i$

$|\underline{M}_G|_{max}$ maximum of $\underline{M}_G$ acting around an edge of the support surface

$m$ the total mass of the robot

$m_B$ the mass of robot body

$m_{ij}$ the mass of link $j$ of leg $i$.

$n$ gear ratio

$n_{i,j}$ gear ratio of joint $j$ of leg $i$

$\underline{n}_i$ vector representing axis $i$ of frame $fN$, for $i = 1...3$

$P$ the total potential energy of the robot

$P_G$ the gravitational potential energy of the robot

$P_K$ the elastic potential energy of the robot

$\boldsymbol{P}_i$ position feedback gain matrix of leg $i$

$\boldsymbol{P}_B$ position feedback gain matrix of the body controller

$\underline{q}$ vector of generalized coordinates

$\underline{q}_B$ vector of generalized coordinates, associated with the body

$\underline{R}_i$ vector of ground reaction forces acting at foot $i$

${}^N\boldsymbol{R}^B$ rotation matrix from $fB$ to $fN$.

${}^B\boldsymbol{R}^L_{i,j}$ rotation matrix from $fL_{i,j}$ to $fB$

${}^L_{i,j-1}\boldsymbol{R}^L_{i,j}$ rotation matrix from $fL_{i,j}$ to $fL_{i,j-1}$

${}^A\underline{r}^{BC}$ position vector from point $B$ to point $C$, expressed in frame $fA$

${}^A r^{BC(j)}$ element $j$ of a vector ${}^A\underline{r}^{BC}$

$\underline{r}^{NP}_i$ position of point $P_i$

$\underline{r}^{BP}_{i,r}$ position reference trajectory of point $P_i$

$\underline{r}^{BL}_{i,j}$ position of point $L_{i,j}$, relative to $B$

$\underline{r}_B = \underline{r}^{NB}$

$\underline{r}_{ij} = \underline{r}^{NL}_{ij}$

$\underline{r} = {}^D\underline{r}^{DP}_i$

$\underline{r}_{i,c}$ boundary condition

$r_{i,j}$ resistance of the motor in joint $j$ of leg $i$

$\tilde{\underline{r}}_i$ defined by equation (6.34)

$T$ the cycle time

$T_a$ duration of transfer phase

$T_s$ duration of support phase

$T$ the total kinetic energy of robot

$T_B$ kinetic energy of the body

$T_R$ kinetic energy of rotor

$T_i$ the kinetic energy of leg $i$

$t$ time

$t_j$ time elapsed from beginning of stride to event $j$

$\Delta t_j$ time difference between event $j$+1 and $j$, i.e. $\Delta t_j = t_{j+1} - t_j$

$\underline{t}$ unit vector in the ground plane, pointing into the support surface, orthogonal to an edge

$\underline{t}_{i-j}$ unit vector $\underline{t}$ orthogonal to the edge formed by the feet $i$ and $j$

$u_{i,j}$ input voltage to the motor in joint $j$ of leg $i$

$\underline{u}$ vector of input voltage to motors

${}^A\underline{v}^{BC}$ velocity of point $C$ relative to point $B$, expressed in frame $fA$

$\underline{v}^{NP}_i$ velocity of point $P_i$ relative to point $N$

$\underline{v}^{BP}_{i,r}$ reference velocity of point $P_i$ relative to point $B$

$\underline{v}^{NB}_r$ reference velocity of point $B$

$\underline{v}^{BL}_{i,j}$ the velocity of index point $L_{i,j}$ relative to index point $B$

$\underline{v}_B = \underline{v}^{NB}$

$\underline{v}_{ij} = \underline{v}^{NL}_{ij}$

$\underline{v}^{ND}_d$ desired velocity of point $D$ relative to point $N$

$\underline{v}_d = \underline{v}^{ND}_d$

$\tilde{\underline{v}}_j$ defined by equation (6.35)

$W$ total weight of robot

$\underline{x}_B$ vector of generalized coordinates associated with the translation of the body

$\beta$ the duty factor

${}^N\boldsymbol{\Phi}^B$ matrix relating ${}^N\underline{\omega}^B$ with $\dot{\underline{q}}$

$\underline{\phi}_B$ vector of generalized coordinates associated with the rotation of the body

$\underline{\phi}_c$ vector of rotations defining $fC$ relative to $fN$

$\underline{\phi}_{bc}$ vector of rotation defining $fC$ relative to $fB$

$\underline{\gamma}$ the gravity vector

$\eta_i$ the support ratio of leg *i*

$\bar{\eta}_{i,k}$ support ratio parameter for leg *i*, where $k = \{d, sd, l, sl\}$

$\varphi_i$ the relative phase of leg *i*

$\Lambda$ the distance of point $\overline{G}$ to an edge of the support surface, also the support stability indicator

$\Lambda_m$ support stability margin

$\Lambda_{m(i\text{-}j)}$ support stability margin for the edge, formed by the feet *i* and *j*

$\Lambda_{m,i}$ support stability margin for edge *i*

$\lambda_i$ the stroke of leg *i*

$\underline{\theta}_i$ vector of generalized coordinates associated with the joints of leg *i*

$\underline{\theta}_i^{(1 \to j)}$ the first to the j:th element of vector $\underline{\theta}_i$

$\underline{\theta}_{R,i}$ vector of generalized coordinates associated with the rotors of the joints of leg *i*

$\underline{\theta}_{M,i}$ vector of generalized coordinates associated with the output of the transmission of leg *i*

$\bar{\theta}_i^{(j)} = \theta_{Mi}^{(j)} - \theta_i^{(j)}$

$\tau_i$ the time phase difference of the foot trajectory of leg *i* relative to leg 1

$\underline{\tau}_{a,i}$ the vector of applied torques at the joints of leg *i*

$\underline{\tau}_{f,i}$ the vector of dissipative or frictional torques at the joints of leg *i*

$\underline{\tau}_{e,i}$ the vector of external torques acting at the joints of leg *i*

$\underline{\tau}_{k,i}$ the vector of spring torques at the joints of leg *i*

${}^N\Omega^B$ dual matrix of the angular velocity vector ${}^N\underline{\omega}^B$

${}^N\Omega_{i,j}^L$ dual matrix of the angular velocity vector ${}^N\underline{\omega}_{i,j}^L$

${}^N\underline{\omega}^B$ vector of angular velocity between frames *fN* and *fB*

${}^N\underline{\omega}_{i,j}^L$ vector of angular velocity between frames *fN* and $fL_{i,j}$

${}_{i,j-1}^L\underline{\omega}_{i,j}^L$ vector of angular velocity between frames $fL_{i,j-1}$ and $fL_{i,j}$

$\omega_B = {}^N\underline{\omega}^B$

$\omega_{ij} = {}^N\underline{\omega}_{ij}^L$

$\underline{\omega}_M = \frac{1}{n}\underline{\omega}_R$

$\underline{\omega}_R$ the angular velocity of *fR* relative to $fL_{i,j-1}$

$\omega_d$ desired turning rate of the robot

$\psi_i$ the relative phase of the event when leg *i* is lifted

## PUBLICATIONS


F. Hardarson (1998), *Locomotion for difficult terrain*, Technical report, Dept. of Machine Design, Royal Institute of Technology, Stockholm, TRITA-MMK 1998:3

T. Wadden, K. Benjelloun, F. Hardarson, J. Wikander, Ö. Ekeberg (1998), Biologically inspired design of a leg for dynamic walking, *Proc. of Euromech 375*, p. 228-235

F. Hardarson, K. Benjelloun, T. Wadden, and J. Wikander (1998), Biologically inspired design and construction of a compliant robot leg for dynamic walking, *Proc. of the 6th UK Mechatronics Forum International Conference*, p. 367-72

F. Hardarson, B. Eriksson, C. Ridderström, T. Wadden, and J. Wikander (1999), Experiments with impedance control of a single compliant leg, *Int. Conf. on Climbing and Walking Robots (CLAWAR'99)*, p. 319-32

F. Hardarson (1999), *On the design of legs for walking robots*, Technical report, Dept. of Machine Design, Royal Institute of Technology, Stockholm, TRITA-MMK 1999:8

F. Hardarson (1999), *Principles of legged robots: Design and control of a single leg prototype*, Licentiate Thesis, Dept. of Machine Design, Royal Institute of Technology, Stockholm, TRITA-MMK 1999:10, ISSN1400-1179,ISRN KTH/MMK--99/10--SE

F. Hardarson, and J. Wikander (2000), Robust torque control of a flexible, geared, DC-motor driven robot joint, *Proc. 1st IFAC Conf. on Mechatronic Systems*, **2**: 659-64

C. Ridderström, J. Ingvast, F. Hardarson, M. Gudmundsson, M. Hellgren, J. Wikander, T. Wadden, and H. Rehbinder (2000), The basic design of the quadruped robot WARP1, *Int. Conf. on Climbing and Walking Robots (CLAWAR)*, p. 87-94

F. Hardarson, and J. Wikander (2002), Statically balanced walking of a quadruped robot based on the center of pressure of the ground reaction forces, *to be submitted for journal publication*

## TABLE OF CONTENTS

# 1. INTRODUCTION

Autonomous mobile robots are finding applications in areas, such as cleaning, running errands, and assisting handicapped or elderly. Mobile robots are also being developed to be used in areas that are inaccessible and/or dangerous for humans, for instance in demining, maintenance in hazardous environments, military, and exploration of volcanoes and space (Wettergreen, et al. 1993; Shirley, and Matijevic 1995). For such robots to function autonomously, advanced sensing and algorithms are needed, for instance, to do localization, path planning, and decision making. Still, one important aspect of the development of autonomous mobile robots is the design and construction of the platform that provides the robot with the mobility necessary to fulfill its purpose. The subject of this thesis will be in this area, where walking robots are being developed to provide autonomous mobile robots the ability to traverse certain types of terrain in a more efficient and stable manner than more conventional robots, using wheels or tracks. The types of terrain that walking robots may potentially have an advantage in, are those that can be classified as uneven or extreme terrain, that would for instance comprise obstacles, holes, steps or ditches. Examples of such terrain would be found, for instance, in forests, mountains, or other rocky terrain, but also in indoor environments, where steps, stairways or high thresholds can cause conventional robots some difficulty.

One advantage with walking robots is that their contact with the ground is not a rolling contact. Instead, the contact with the ground is discontinuous and footholds can be selected such that obstacles or holes are avoided, whereas a wheel would have to follow the contour of the ground. In soft terrain, wheels may have to plow

their way through the terrain, causing a large resistance in the direction of motion, as well as damage to the terrain. Walking robots, on the other hand, leave only isolated foot marks on the ground, and as their locomotion does not rely on slipping, for instance when turning, they cause less damage to the terrain. Walking robots are, therefore, more suitable to perform tasks in environments that are sensitive to intrusion. A walking robot can also benefit from that active suspension is an intrinsic part of its structure and allows the robot to adapt to uneven terrain. This would allow for smoother ride for any passengers or cargo, and furthermore, if the robot were, for instance, equipped with a manipulator, the legs could provide an active but stable base while tasks are being performed. Furthermore, a walking robot is an omnidirectional robot, as it can walk forward, sideways, or turn on the spot, and additionally has the ability to raise or lower its body or tilt it, by varying the length of its legs, i.e. by bending its knees. This ability gives walking robots an advantage in maneuvering through cluttered and tight environments.

All the above mentioned advantages of walking robots are dependent on the design of their mechanical structure and the control system. There are many challenges with designing and building legged robots. The large number of actuated degrees of freedom makes them heavier, more complex and expensive than wheeled systems. Most walking robots of today are quite slow and have bad payload-weight-to-own-weight ratio compared to more conventional wheeled or tracked robots. The control of a walking robot has to cope with a highly nonlinear system with many degrees of freedom, changes in the system dynamics as the legs are being lifted and placed, and unknown dynamics such as the interaction of the foot with the ground. The control of walking robots also requires that the issue of stability against tipping over be treated in a more specific fashion than for wheeled robots, as there are discrete changes in the support of the robot when legs are lifted or placed.

One approach to designing legged robots is to study the solutions that nature has provided to the locomotion of animals through millions of years of evolution. The argument is that the way animals are built or move may in some sense represent an optimum, which may be beneficial in the design and control of legged robots. For instance the study of gaits has led to mathematical models that can explain why some gaits are preferred by animals (Hildebrand, 1965; McGhee, and Frank, 1968;

Alexander, 1989). The structure of different animals has also inspired the design of robots (Arikawa, and Hirose, 1996; Cordes, et al., 1997; Nelson, et al., 1997; Pratt, et al., 1997), and study of the mechanics has shown energy conserving methods (McGeer 1990; Pratt, and Pratt, 1999). The role of compliance in animal locomotion, in conserving energy and absorbing shocks (Alexander, 1988, 1990; McMahon, 1985), has inspired robot mechanical and control design (Hogan, 1984; Yamaguchi, and Takanishi, 1995; Yamaguchi, and Takanishi 1997; Pratt, et al., 1997; Ahmadi, and Buehler, 1997). Studies of the muscle-neural system has led to the development of controllers for walking robots (Beer, et al., 1990; Quinn, and Espenscheid, 1993; Pfeiffer, et al., 1995; Espenschied, et al., 1996; Wadden, 1998). Todays technology is however far from being able to replicate complexity of the muscle-skeleton system and the neural system controlling it. On the other hand, machines can be built in ways that animals can not replicate, for instance, rotating actuators are not found in animals. Various innovative designs of legged robots have been tried (Raibert, 1986; Song, and Waldron 1989; Hirose, et al., 1991; Bares, and Whittaker, 1993; Halme, et al., 2001). Furthermore, the development of very simplified mechanisms, in terms of number of degrees of freedom and actuators, has also proven that legged locomotion can be accomplished without trying to mimic the complexity of animals (Buehler, et al., 1998; Moore, and Buehler, 2001).

## 1.1. The walking robot project

The work, presented in this thesis, has been carried out within the Walking Robot Project (WARP) at the Centre for Autonomous Systems (CAS), Royal Institute of Technology. The aim has been to do research on concepts and methods that would enable the design of an autonomous mobile robots for difficult terrain, where the main direction, that has been taken, is to build a self-contained four-legged walking robot, capable of dynamic walking. WARP1 is a four legged robot, with a cursorial mammalian configuration (figure 1.1). It weighs approximately 60 kg, which is distributed such that the body weighs approximately 20 kg, and the legs weigh 10 kg each. The length and width of the body are 80 cm and 50 cm, respectively. The height of the robot, when standing with straight legs, is approximately 80 cm. The legs have club feet made of a rubber half sphere of diameter 5 cm. Each leg is composed of three links and has three degrees of freedom, with respect to the body. The first link is, however, designed such that it does not contribute to the length of

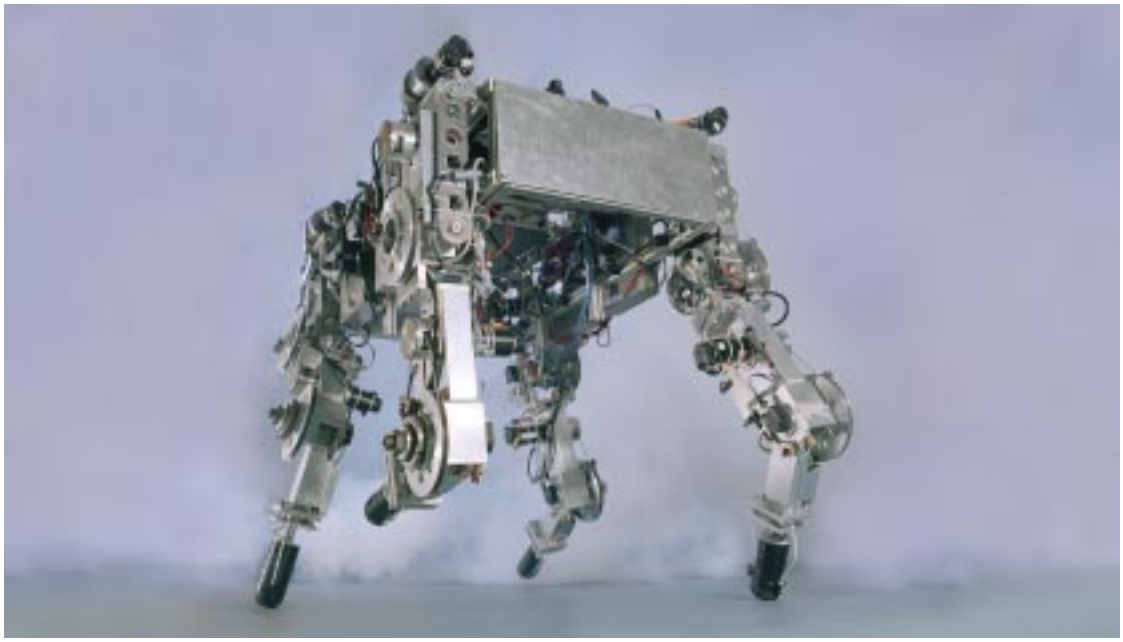

*Figure 1.1. The quadruped robot WARP1.*

the leg. The length of the thigh and the shank (i.e. the second and third link) is 30 cm, respectively. The first joint of each leg is an abduction/adduction in the hip, i.e. a rotation around the longitudinal axis of the robot. The second joint is a flexion/extension joint also in the hip, i.e. a rotation around the lateral axis of the body. The axes of rotation for the first two joints in the hip are set such that the axes of rotation intersect orthogonally. Finally, the third joint is a flexion/extension joint in the knee. The total number of degrees of freedom is therefore eighteen, where there are three actuated degrees of freedom for each of the four legs and six for the motion of the body. The leg joints are actuated by Maxon DC-motors, where a 150 W motor is used for the flexion/extension joints and a 90 W motor for the abduction/adduction joint. The transmission consists of a harmonic drive, with gear ratio 100:1, and a wire-pulley system, giving a total gear ratio of 285:1 for the flexion/extension joints and 250:1 for the abduction/adduction joints. Each motor is equipped with an incremental encoder to measure the joint angle, and three hall effect switches to calibrate the encoder. The robot is equipped with a sensor package, consisting of three rate gyros, two inclinometers and one three axes accelerometer, which allows estimation of the robots attitude (Rehbinder, 2001). For a more thorough description of WARP1, see Ridderström, et al. (2000).

The project has resulted in general studies of control architectures (Petterson, 1999), control methods (Eriksson, 1998; Ridderström, 1999), and the mechanical design (Hardarson, 1999) for walking robots. A computer tool-chain has been developed that allows for fast generation of models and controllers for simulation and implementation purposes (Ridderström, and Ingvast, 2001a). A method for the generation of stepping for a single leg, based on a state machine, has been studied (Hardarson, et al., 1999), as well as the development of a torque controlled elastic joint (Hardarson, and Wikander, 2000). A method for controlling the attitude and the height of the robot body has been proposed (Ridderström, and Ingvast, 2000b), as well as a method to increase the performance of a trot gait (Ingvast, et al., 2001). Rehbinder (2001), has developed methods to estimate the attitude of the robot, by fusing signals from inclinometers, gyros and accelerometers.

## 1.2. Problem formulation

The first task oriented goal with the walking robot project is to accomplish blind walking, i.e. that the robot can traverse a terrain without the use of any range finding sensors. The robot will have to feel its way forward, by lifting one foot and search for the next foothold, while remaining stable and avoid tipping over. For that, the use of statically stable gaits are suitable, as they can be executed arbitrarily slow, while allowing the robot to be balanced at all times.

McGhee, and Frank (1968) define *static stability* as “An ideal legged locomotion machine is statically stable at time *t* if all the legs in contact with the support plane at the given time remain in contact with that plane when all the legs of the machine are fixed at their location at time *t* and the translational and rotational velocities of the resulting rigid body are simultaneously reduced to zero”. An ideal legged locomotion machine they defined as a rigid body with mass less legs which are able to supply an unlimited force into the contact surface. Given these assumptions they show that the machine is statically stable if the vertical projection of the center of mass of the body onto a horizontal plane is within the support area.

The above definition of static stability by McGhee, and Frank (1968), is highly idealized as it assumes that the feet can provide unlimited forces, and does not treat external forces. The use of the term static stability in this thesis will be limited to setting a necessary condition for the state of the robot. This condition will be

referred to as necessary condition for static balance, rather than for static stability, although the two will often be used interchangeably throughout the thesis. First the *support surface* will be defined as the convex surface, which boundary is formed by the lines connecting the feet ground contact points, i.e. the surface is formed by the edges around which the robot can tip over. A necessary condition for a walking robot with point feet to be *statically balanced* is that at least three feet have to be in ground contact at all times, placed such that they form a support surface with an area that is not equal to zero, and the vertical projection of the center of gravity has to be within the boundary of the support surface. This is not a sufficient condition for stability, as motion dependent forces can still make the robot tip over, for example if the robot is moving and suddenly stops and tumbles over. Furthermore, an external force can always be found that can tip the robot over. Finally, the terrain, on which the robot is walking, may not be sufficiently rigid to support the robot (Ridderström, 2002). Instead, a measure of the stability of the robot should be found, which can indicate how large the motion dependent and external forces can be, without the robot becoming instable. The problem to be addressed in this thesis is then what is an appropriate measure for the static balance of the robot, and how can statically balanced walking be achieved.

## 1.3. Related work

The synthesis of controllers for a walking robot requires combining several components, ranging from the control of body motion to the control of each individual joint. A motion for the body has to be planned such that the robot is stable and will not tip over. Furthermore, the stability of the robot is dependent on how the legs are positioned relative to the body and on the sequence and timing in which the legs are lifted and placed. As the motion of the robot is determined by the legs in ground contact, the legs have to be coordinated in such manner that they provide propulsion and suspension to the body.

The planning of stable body motion for quadruped robots has been addressed in several papers. Yoneda, and Hirose (1995) included a preplanned sideways sway in their intermittent trot gait, based on the zero moment point, which they define as the point on the ground where the force and the moment, acting on the center of gravity, can be resisted by applying a simple force and no moment. The sideways sway reduced the rate of change in the acceleration of the body, and made the

motion of the robot more smooth and energy efficient. The authors further developed the algorithm in Kurazume, et al. (2001), and included longitudinal and vertical motion to a more general sway trajectory, which they show to be more energy efficient than their original sideways sway trajectory. Kang, et al. (1997) developed a method of adapting a statically stable gait to compensate for the influence of external forces. Force sensors in the feet were used to calculate the *effective mass center*, which they define and which is similar to the calculation of the center of pressure, i.e. the point where the resultant of the ground reaction forces acts. The deviation between the effective mass center and the real mass center is used for two compensation strategies. One is to vary the height above ground of the robot's center of gravity, to affect the moment arm for the external forces, and the second is to change the direction of the motion of the body. Hugel, and Blazevich (1999) included sway in a static crawl gait with duty factor 0.75 by letting the center of gravity follow a sinusoidal sideway motion. By this they were able to reduce the risk of the robot tipping over.

Given the desired motion of the body, the feet have to be coordinated to provide the motion. One approach is to specify a force and a moment acting on the body to provide the motion, and then distribute this force and moment to the feet in ground contact. However, if there are more than three feet in ground contact, the force distribution problem is indeterminate as each foot has three unknown force components, and there are only six force and moment balance equations. In order to determine the forces that each foot should provide, pseudo-inverse solutions have been used (Klein, et al., 1983; Lehtinen, 1996). Waldron (1986), and Kumar, and Waldron (1988), decomposed the foot force field into an interaction force field and an equilibrating force field, and obtained foot forces based on the zero interaction force constraint, which states that foot forces should not work against each other. They show, however, in Kumar, and Waldron (1988), that this method is equivalent to the pseudo-inverse solution. Several optimization methods have been tried to solve the indeterminate problem, which can be formulated as a linear or quadratic programming problem, using the six force and moment equilibrium equations as constraints, along with other inequality constraints, for example, non negative normal force and limit on tangential forces based on the coefficient of friction (Cheng, and Orin, 1990; Gorinevsky, and Schneider, 1990; Gardner, 1991; Klein, and Kittivatcharapong, 1990; Liu, and Wen, 1997; Marhefka, and Orin, 1998;

Chen, et al., 1998; Zhou, and Low, 1999). Gao and Song (1992) proposed the stiffness matrix method, where the compliance of the legs, the actuating system and the supporting terrain, are included to get a determinate solution.

The purpose of the leg controller is to provide the body with suspension and propulsion during the leg support phase. During the swing phase the leg controller has to move the leg forward and position the foot for the next step. The control problem involves, therefore, both dealing with varying dynamics and changes in the control objectives. The control of the legs has many similarities with the control of manipulators performing contact tasks (De Schutter, et al., 1997), and many of the control methods for control of legs have been adopted from there. For instance, compliance control have been used (Klein, et al., 1983; Pratt, et al., 1997; Hardarson, et al., 1999), and impedance control, proposed by Hogan (1985), has been adopted to leg control by Tzafestas, et al., (1997), and Guihard, and Gorce (1996). To make the leg controller better able to compensate for the unknown ground dynamics, methods to estimate some of the ground properties have been proposed (Tzafestas, et al., 1997; Zhou, and Low, 2001).

## 1.4. Contributions of the thesis

The aim of the work, presented in this thesis, is to develop and implement a statically balanced crawl gait on the quadruped robot WARP1. As with all mobile robots, the task is to get from point A to point B following a specific path, either preplanned or planned on-line. It is assumed that an operator, either human or a higher level controller, provides velocity commands to the robot. Ideally the robot should then move with the desired velocity in a smooth manner, similar to a wheeled robot. However, the operator should not necessarily have to take into account the stability of the robot, for instance that the center of gravity should remain within the support surface or that the feet have to be lifted and repositioned. The robot should then itself determine how to shift its body weight such that the center of gravity is always within the support surface, and maintain a certain stability margin. The robot will then deviate from the desired velocity, set by the operator, but on the average, the velocity of the robot should equal the desired velocity.

The main contribution of the thesis is in the analysis of the stability of statically balanced quadrupedal gaits and how statically balanced walking can be achieved.

The center of pressure of the ground reaction forces of the feet is used to develop a stability measure, which is then used in the planning of the body motion. The body motion is determined by planning a motion of the desired center of pressure, under the assumption that only gravitational forces are acting on the robot, in which case the center of pressure equals the vertical projection of the center of gravity. The stability measure is used to set appropriate bounds on the motion of the desired center of pressure, to account for the neglected inertial and external forces. The motion of the desired center of pressure is planned by determining the supporting force for each leg, which in turn will determine how the robot should shift its weight in order to remain statically balanced. The approach proposed here, therefore, solves simultaneously the problem of determining a statically balanced motion trajectory for the body, as well as, the distribution of forces to the feet to compensate for the weight of the robot.

## 1.5. Summary of earlier work

The scope of this thesis has been limited to the stability analysis and the synthesis of a controller for statically balanced walking. Relevant issues, such as the control of the legs and the joints are, however, not discussed in detail or simply omitted, but are based on previous work by the author and the colleagues in the WARP project.

Much of the earlier work of the author is collected in the Licentiate thesis Hardarson (1999). The licentiate thesis consists of two technical reports and two conference papers. The first report is a general review of different locomotion paradigms used for mobile robots in difficult terrain and gives an overview of the different existing systems. It also briefly addresses choice of locomotion system and terrain properties, and concludes by making a comparison of the advantages and disadvantages of each type of locomotion system. The second report is a study of the general principles of legged locomotion, and gives the necessary background. It focuses on the relevant issues for the design of robot legs, including, the energetics of legged locomotion, leg geometry and motion strategies.

The first paper included in the Licentiate thesis, Hardarson, et al. (1998), presents the design of a prototype leg for a four-legged walking robot. The most important design issues were to make the leg as energy efficient as possible and to provide

the power necessary for dynamic walking. The leg has a configuration similar to a mammal leg with three rotational degrees of freedom. To reduce the moment of inertia of the leg, the motors and respective gears for the hip and knee joints are placed close to the body and balanced around the hip joint, aligned with the thigh. Rubber torsion springs are placed in series with the extension/flexion actuators in the hip and the knee joints. The springs add a shock tolerance to the system as they smooth out impact forces and thereby reduce the peak forces that has to be taken by the gearing. The use of springs also has a potential for storing energy during the support phase. An experimental setup was built, where the leg was placed on a non-motorized treadmill with the hip attached to a small wagon that is free to move in the vertical direction. A mechanical stop prevents the leg from falling completely to the ground during the air phase. Experiments included in the paper demonstrate the properties of the springs. The leg was dropped from a height of 60 cm measured from ground to abduction joint. The leg was slightly bent and the foot was approximately 10 cm above the ground. A controller, based on the impedance control paradigm, was used to implement spring-like behavior between body and foot in cartesian coordinates. The result showed a gradual build up of torque in the springs that had none of the characteristics of an impact.

The second paper included in the Licentiate thesis, Hardarson, et al. (1999), describes the control of the leg stepping on a treadmill. The impedance control paradigm was chosen as it has advantages such as providing a generalized approach to force and position control, being continuous in the transition from free to constrained motion. Also, the position of the end-effector can be controlled in cartesian coordinates without inverting the kinematic equations. The impedance controller was combined with a finite state machine for generating the stepping. The step cycle is divided into four different states where for each state, the reference trajectories and the control parameters are changed depending on the control objective. Special focus is given to the selection of the impedance parameters and strategies discussed for the selection. The control problem is divided into three different control objectives which allows for simpler selection of impedance parameters and reference trajectories. The leg was able to step at different velocities on a treadmill and handle various perturbations, such as variations in ground level.

In Hardarson, and Wikander (2000), an effort was made to improve on the control of torque output at the joints by utilizing the rubber springs in the joints as a torque sensors. A robust control technique, quantitative feedback theory (QFT), was used to make the controller robust against parameter uncertainties, such as changes in the load inertia, ranging from a known minimum value (e.g. a link's inertia) and infinity (constrained link), while rejecting external torque disturbances. The resulting controller is tested experimentally on a copy of the hip joint of WARP1.

## 1.6. Structure of the thesis

The structure of the thesis is that chapters 2 to 4 provide the necessary background for the work presented in the subsequent chapters, where chapter 2 gives a general introduction to legged locomotion, chapter 3 describes the kinematic modelling, and chapter 4 describes the dynamic modelling necessary for the analysis and simulation of the robot. The main contribution of the thesis are presented in chapters 5 and 6, where chapter 5 develops a stability measure for statically balanced walking, and chapter 6. develops a statically balanced walk for quadruped robots. Chapter 7 describes the implementation and provides experimental results. Finally, chapter 8 provides a discussion on the results and future expansion, and draws conclusions.

# 2. INTRODUCTION TO LEGGED LOCOMOTION

Research on legged locomotion has a long history. Biologists and other scientists have long studied the structure and motion of animals. In connection to the interest of the engineering community in building walking vehicles, there has been a search for more mathematical models for the study of gaits. Such models could be used in the design and control of walking vehicles. This section discusses some of the gait related issues relevant to the subsequent sections. The focus is mainly on quadrupeds, but much of the terminology is more general and applies to walkers with other number of legs. For further reading see Alexander (1984), Todd (1985), Song, and Waldron (1989), and Wadden (1998).

## 2.1. Terminology

The definitions are in alphabetical order, and based on Alexander (1984), Kumar, and Waldron (1989), Song, and Waldron (1989), and Wadden (1998).

**Duty factor ($\beta$):** The fraction of the duration of the *stride* for which a foot is on the ground (in the *support phase*).

**Cycle time ($T$):** Time duration of one *stride*, i.e. the time to complete one cycle of leg movements.

**Events of the gait:** The placing or lifting of any of the feet during locomotion. For an $n$-legged machine, there are $2n$ events in one stride.

**Relative phase ($\varphi_i$):** The time elapsed from the setting down of a chosen reference foot until the foot of leg $i$ is set down, given as the fraction of the *cycle time*.

**Stability margin:** The shortest distance from the vertical projection of the center

of gravity of the robot onto a horizontal plane, to the boundary of the support area.

**Stride:** The complete cycle of leg movements, for example, from the setting down of a particular foot to the next setting down of the same foot, where all the legs have been lifted and placed exactly once.

**Stride length:** The distance travelled by the center of gravity of the walker in one *stride*.

**Stroke ($\lambda_i$):** The distance that foot *i* translates relative to the hip during the *support phase*.

**Support area/polygon:** The minimum convex polygon in a horizontal plane, with its vertices formed by the vertical projection of the feet being in support.

**Support phase:** The phase when a foot is in contact with the ground and able to support and propel the body. Also called *stance* or *retraction* phase.

**Swing phase:** The phase when a foot is in the air and repositioned for the next *support phase*. Also called *air* or *protraction* phase.

## 2.2. Description and classification of gaits

Fundamental to the locomotion of animals is that they move by lifting their legs and placing them at new positions. While walking, the legs should be coordinated with respect to stability, propulsion and energy efficiency. The coordinated manner of lifting and placing the legs is called a gait. A gait is characterized by the sequence in which the legs are lifted and placed. The lifting or placing of a leg is called an event of the gait, and the sequence in which the legs are lifted and placed is called a gait event sequence. Theoretically the total number of possible gait event sequences for a quadruped is 5040, but only a very small portion of them are suitable as gaits and used by animals (McGhee, and Frank, 1968). Most people are familiar with the names of some of these gaits, for instance, a horse will switch between different gaits when increasing speed, first walk, then trot, then canter, and finally gallop. Animals switch gaits depending on speed in order to be more energy efficient, and the speed at which animals switch gait is dependent on the size of the animal. It has been noted that animals of different species use similar gaits for certain types of motion. A possible conclusion is that under some conditions of motion, a certain gait is optimum, for reasons that are related to stability, speed, energy efficiency, terrain properties, mobility or structure of the animal (Song, and Waldron, 1989).

A gait is usually cyclic in the sense that the same sequence of lifting and placing the legs is repeated. A complete cycle of leg movements, where all the legs have been lifted and placed exactly once, is called a stride, and the time duration of one stride is called the cycle time. A quadruped gait has exactly eight events in one stride, as each of the four legs is lifted and placed once. McGhee, and Frank (1968) proposed a system, which is widely used today, where gaits are described in terms of duty factor and relative phase. The duty factor $\beta_i$ for leg $i$ is the fraction of the cycle time for which the foot is in ground contact, so the duty factor is a number between 0 and 1. The relative phase of leg $i$ is the time elapsed from the setting down of an arbitrarily chosen reference foot until the foot of leg $i$ is set down, given as the fraction of the cycle time. Thus the reference foot will be assigned the number 1, and has the relative phase $\varphi_1 = 0$. The relative phases of the other legs are then $\varphi_i = \Delta t_i / T$, $0 \le \varphi_i < 1$, where $\Delta t_i$ is the time elapsed since the reference foot was set down, and $T$ is the cycle time. The convention used here is that the left front leg is number 1, right front leg is number 2, left hind leg is number 3, and right hind leg is number 4. The gait event sequence can now be specified using the duty factors and the relative phases, where the first event, and the start of the stride, is chosen as the event when the reference leg is set down. The time, at which the following events of the gait will occur, are given as fractions of the cycle time at which the feet are set down or lifted. The timing of the events when the feet are set down are consequently equal to the relative phase $\varphi_i$. The timing of the events when the feet are lifted will be denoted $\psi_i$, and happens a fraction $\beta_i$ of the cycle time after that the foot is set down. Alternatively, a foot has been lifted a fraction $1 - \beta_i$ of the cycle time before it is set down again. However, as the events should be expressed within the duration of the stride, the events should be a number between 0 and 1. The event of lifting the leg $i$ is given by

$$\psi_i = \begin{cases} \varphi_i + \beta_i, & \text{if } \varphi_i + \beta_i < 1 \\ \varphi_i + \beta_i - 1, & \text{else} \end{cases} \tag{2.1}$$

For example, if the relative phase and the duty factor are $\varphi_i = 0.5$ and $\beta_i = 0.8$, respectively, then the event when leg $i$ is lifted is $\psi_i = 0.3$. A gait is called singular if there is a simultaneous lifting or placing of two or more legs during the stride. A singular gait would correspond to that $\varphi_i = \varphi_j$, $\varphi_i = \psi_j$, or $\psi_i = \psi_j$, for any legs $i$ and $j$ where $i \neq j$. Any singular gait can be obtained as a limit of a non singular gait.

Gaits are divided into walking and running, where the main difference between a walking and running gait is seen in the duration of the support phase, i.e. in the size of the duty factor. The distinction, in general, is that running gaits have a duty factor less than 0.5, and walking gaits have duty factor greater than 0.5. Consequently, running gaits have stages when both feet of a front or back leg pair are off the ground, whereas walking gaits have stages where both feet are on the ground simultaneously (Alexander, 1984). McGhee, and Frank (1968) further define creeping gaits for quadrupeds as a subgroup of walking gaits, in which there are always at least three legs in ground contact at all times, requiring a duty factor greater than 0.75. In addition, gaits are classified as alternating and non alternating gaits (or symmetric and asymmetric gaits). In alternating gaits, the left and right feet of a front and back leg pair have equal duty factors and relative phase differing by 0.5, i.e. by half a cycle. In non alternating gaits, the phase difference is 0, i.e. the front and back leg pairs move in unison. For instance, human walking is an alternating gait while a kangaroo jumping is a non alternating gait. Generally, quadrupeds use alternating gaits for walking and slower running, and non alternating gaits for faster running. Furthermore, a gait is called regular if all the legs have the same duty factor.

## 2.3. Gaits and stability

While walking or running, a legged locomotor has to remain balanced in order to avoid unwanted body motion or falling. Gaits are classified, depending on the strategy used in order to maintain balance, into statically and dynamically stable gaits. The strategy chosen is related to speed, as slower walking gaits, i.e. creeping gaits, are generally statically stable whereas faster gaits are dynamically stable. The main difference is that dynamically stable gaits remain balanced by moving whereas statically stable gaits remain balanced by relying on the support area formed by the legs in ground contact. An analogy is found with the difference of riding a tricycle and a bicycle. When riding a tricycle it can be driven arbitrarily slowly without falling while a bicycle can be hard to balance at low speeds whereas it is easier at higher speeds.

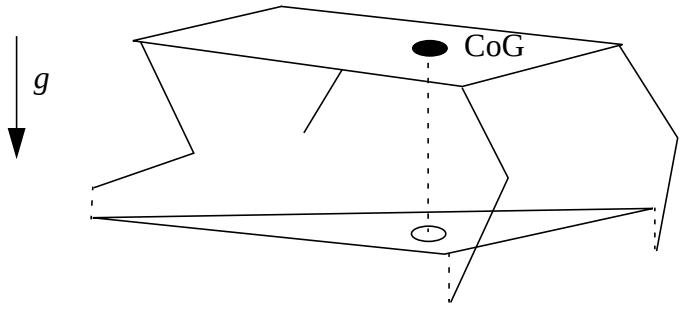


*Figure 2.1. Vertical projections of feet contact points and center of gravity (CoG) on a horizontal plane.*

In a statically stable gait, the vertical projection of the center of gravity (CoG) onto a horizontal plane, is kept within the support area at all times, as shown in figure 2.1 (McGhee, and Frank, 1968; Song, and Waldron, 1989). In the absence of any inertial or external forces and if the ground is sufficiently rigid, the robot can remain stable as long as the CoG is within the support area. For robots with point feet, a necessary condition for static stability is that the robot has at least three legs on the ground at all times. This is necessary in order to form an area of support that can contain the projection of CoG within its borders. In figure 2.2. an example is given for a four-legged robot. In the left part of the figure, three legs provide support and the projection of center of gravity is located inside the support area such that the robot is statically stable. The foot placements in the right part projects

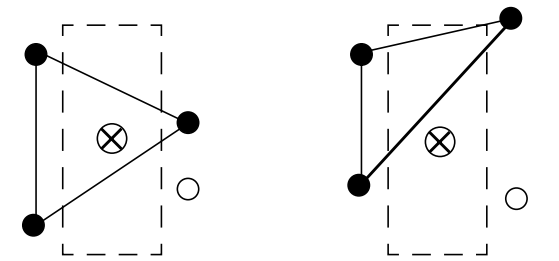


*Figure 2.2. Support polygon, statically stable and unstable cases. The center of gravity is the slightly larger circle, marked with 'X'. The smaller circles are the feet and are filled if they support the robot.*

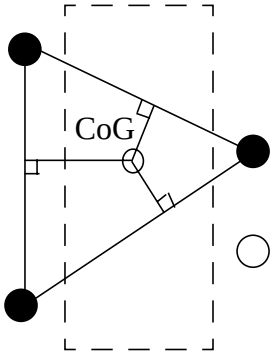


*Figure 2.3. Distances from the center of gravity to the different edges of the support area for a quadruped with three legs in support. The stability margin is defined as the shortest of these distances*

the center of gravity outside the support area, which leads to instability due to a tipping moment caused by gravity. In order for a quadruped to be statically stable while walking, a creeping gait has to be used which gives a lower bound on duty factor of 0.75. Statically stable gaits for quadrupeds are generally quite slow, but the advantage is that they can be executed arbitrarily slow or even stop while being stable at all times. The stability margin provides some indication of the ability to resist disturbances while walking statically stable. The stability margin is defined as the shortest distance from the vertical projection of the CoG of the vehicle onto a horizontal plane, to the boundary of the support area. and is defined as positive if the center of gravity is within the support polygon and negative otherwise (figure 2.3).

Dynamic stability is often referred to as active stability, and implies that balance is only achieved through motion, thereby in general, demanding more active strategies. If a walker is not statically stable it will start to fall. Balance is then resumed by placing a foot (or feet) such that the fall is braked and the motion of the body is changed. As shown by McGeer (1990), dynamic walking can be achieved by passive biped-like mechanisms, walking down a small incline, without any actuation except the influence of gravity. Dynamic stability is therefore sometimes described as controlled falling as it allows the body to fall freely for shorter periods of time, including periods of flight, until a new foot is set down. The advantage with dynamically stable gaits is that they are generally faster than statically stable gaits.

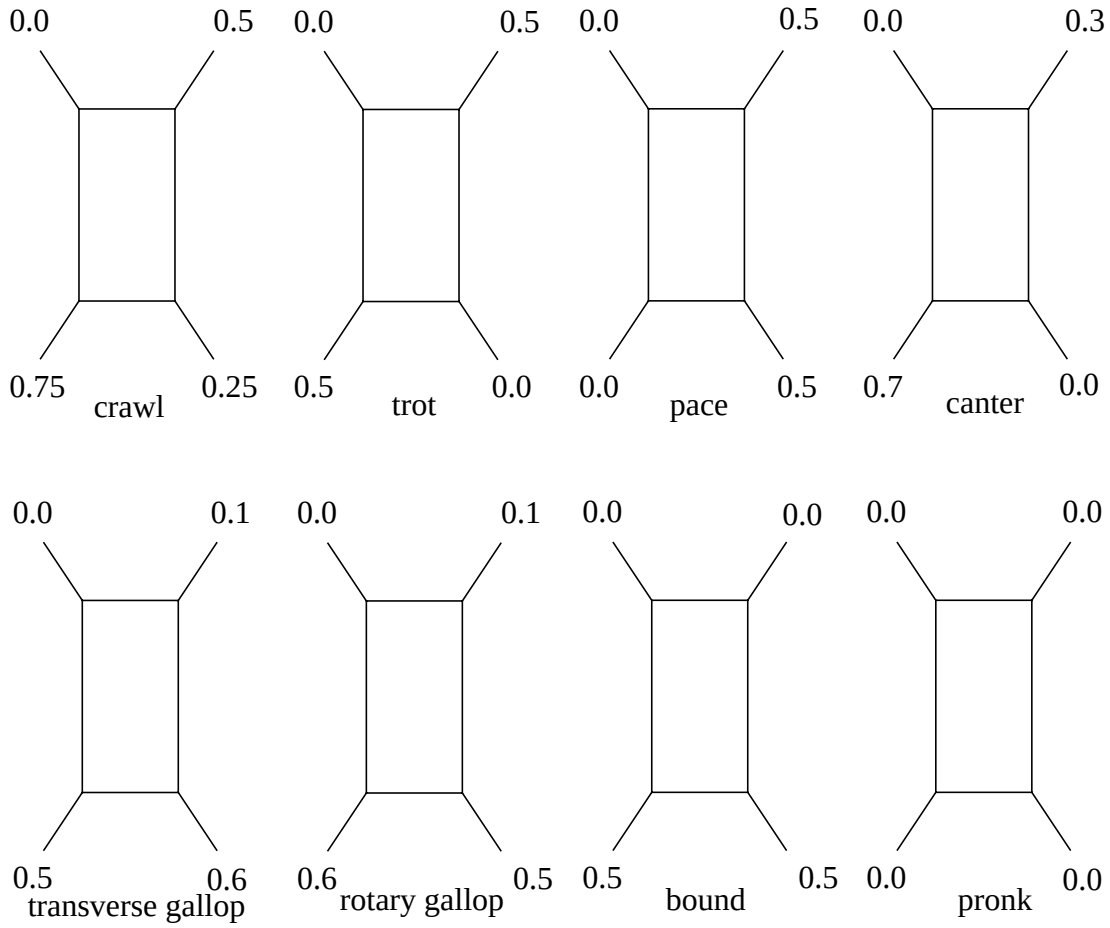


*Figure 2.4. Relative phase for different quadrupedal gaits (from Alexander, 1984).*

## 2.4. Gaits of quadrupeds

As discussed previously, the gaits of quadrupeds can be divided into creeping gaits, faster walking gaits, and running gaits. This is based on the classification that creeping gaits have duty factor greater than 0.75, faster walking gaits have duty factor between 0.5 and 0.75, and running gaits have duty factor less than 0.5. The gaits that are used by quadrupedal animals have often been given names, where some commonly known examples are crawl, trot and gallop. The typical relative phase for some of the most common quadrupedal gaits, are shown in figure 2.4. However, often different gait event sequences are reserved the same gait name, although they should be different gaits, according to the mathematical model. In the following discussion, some of the gaits that are used by mammals are described, starting with the slowest gaits. Gait diagrams are used to show the

development of the gait as a function of time. Each frame in the gait diagram is taken at an event of the gait, solid circles will denote foot in ground contact, open circles will denote a leg that has just been lifted, and dashed circles denote the position where a foot will be set down next.

For a very slow walk, for instance a predator stalking its prey, a mammal will use a creeping gait. The advantage with creeping gaits is that they are generally statically stable and hence can be executed arbitrarily slow. Of all 5040 different possible gaits for quadrupeds, there are only 6 that allow the animal to have three legs in ground contact at all times. McGhee, and Frank (1968) showed, under somewhat restrictive conditions, that three of these six gaits were statically instable and one, the crawl gait, maximizes the stability margin. The crawl gait is a regular alternating gait and the most common walking gait used by quadrupedal animals. In a crawl gait the placing of a hind leg is followed by lifting of the front leg on the same side. The front leg is then set down again before the hind leg on the other side is lifted, and the sequence continuous, as shown in the gait diagram (A) of figure 2.5. A necessary condition for the crawl gait, in order to always have three legs on the ground, is that a leg in the air must be set down before the next one is lifted. The gait event sequence for crawl gait is then

$$\{\varphi_1, \psi_4, \varphi_4, \psi_2, \varphi_2, \psi_3, \varphi_3, \psi_1\} \tag{2.2}$$

The crawl gait is an alternating gait, meaning that there is a 0.5 phase difference between a left and right pair legs, i.e. there is half a cycle time difference between setting down a left and right leg pair. If it is further assumed that the gait is regular, i.e. that all the legs have the same duty factor, then the timing of the events can be defined using only two parameters, the duty factor $\beta$ and the relative phase of one of the hind legs. For instance, if the relative phase of leg 3 is equal to $\varphi$, the relative phases for all the legs are

$$\varphi_1 = 0 \qquad \varphi_2 = 0.5 \qquad \varphi_3 = \varphi \qquad \varphi_4 = \varphi - 0.5 \tag{2.3}$$

In order for the gait to be statically stable, the duty factor has to fulfill $0.75 \leq \beta \leq 1$ and the relative phase of leg 3 has to fulfill $1.5 - \beta \leq \varphi \leq \beta$, in order to have always three legs in ground contact at all times.

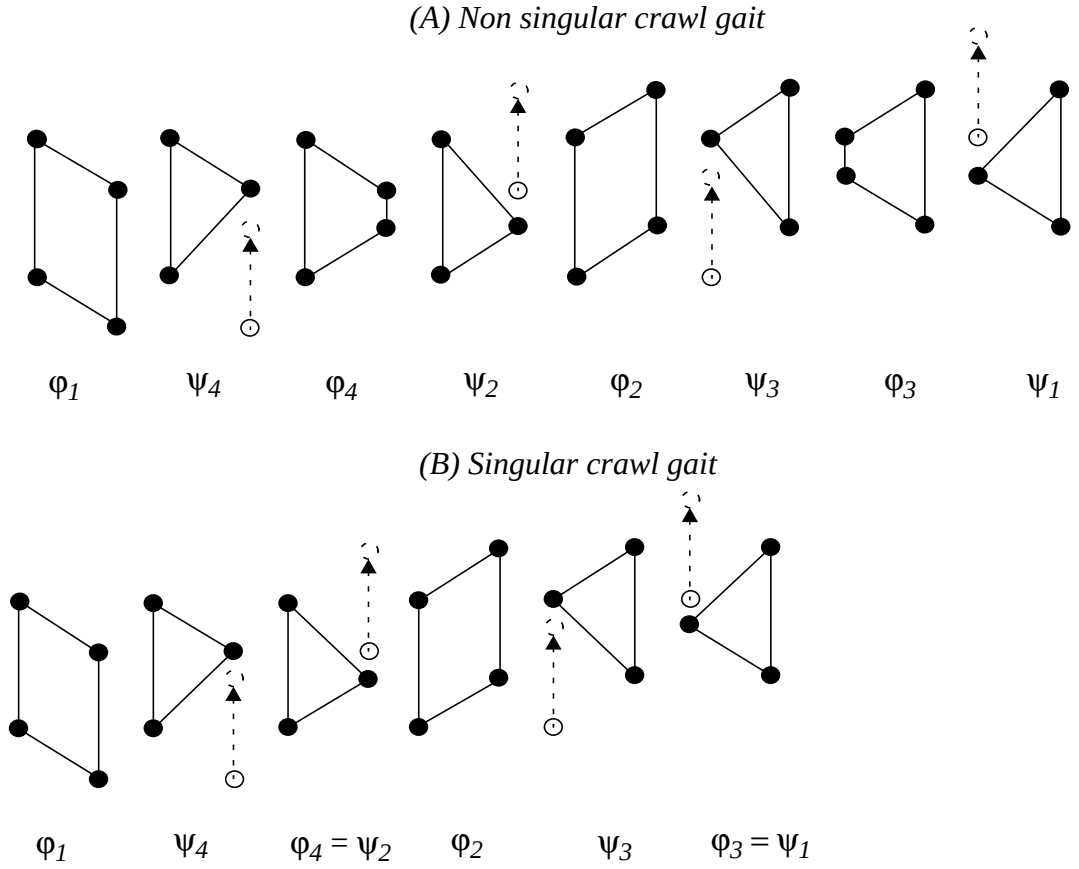


*Figure 2.5. Gait diagram for (A) non singular, and (B) singular, quadruped crawl gait.*

The results of McGhee, and Frank (1968) showed that a singular crawl gait, in which a front leg is lifted at the same instant as the hind leg on the same side is set down, maximizes the stability margin. The resulting relative phase is

$$\varphi_1 = 0 \qquad \varphi_2 = 0.5 \qquad \varphi_3 = \beta \qquad \varphi_4 = \beta - 0.5 \tag{2.4}$$

which is equivalent with setting $\varphi = \beta$ in equation (2.3). A gait diagram for such a gait is shown in figure 2.5.(B), where for example, it is shown for the event $\varphi_4 = \psi_2$ that leg 4 is set down at the same instant as leg 2 is lifted.

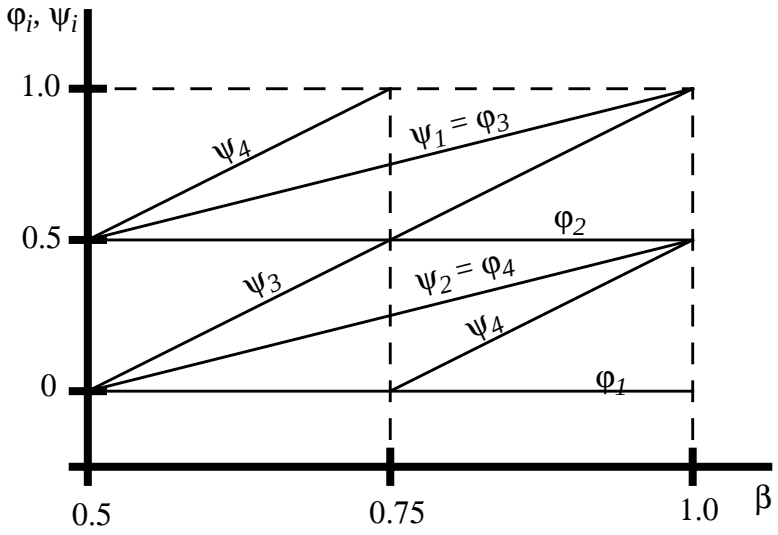


*Figure 2.6. Relationship between the gait event sequence and duty factor according to Inagaki, and Kobayashi (1993).*

As the speed increases, the duty factor will decrease and fall outside the creeping gait region. The transition from walking to running gaits can be continuous, for example, a cat will have a continuous transition from crawl gait to trot gait (Wadden, 1998). Inagaki, and Kobayashi (1993) proposed a rule for the relative phase of a quadruped to have a smooth transition from crawl gait to trotting. This rule is identical to the one McGhee, and Frank (1968) proposed in equation (2.4). When the duty factor is decreased from 0.75 to 0.5, the gait will smoothly transfer from crawl to trot, as shown in figure 2.6. The gait event sequence for a duty factor between 0.5 to 0.75 is then

$$\{\varphi_1, \psi_2, \varphi_4, \psi_3, \varphi_2, \psi_1, \varphi_3, \psi_4\} \tag{2.5}$$

The gait event sequence will be different but the order in which the legs are placed will be the same. The main difference is that the hind legs are lifted before a front leg in the air is set down, as shown in the gait diagram in figure 2.7. The trot gait will then appear as the limit of the gait event sequence for a duty factor equal to 0.5, at which the events are given as $\varphi_1 = \varphi_4 = \psi_2 = \psi_3 = 0$ and $\varphi_2 = \varphi_3 = \psi_1 = \psi_4 = 0.5$. A trot gait is usually defined as an alternating gait

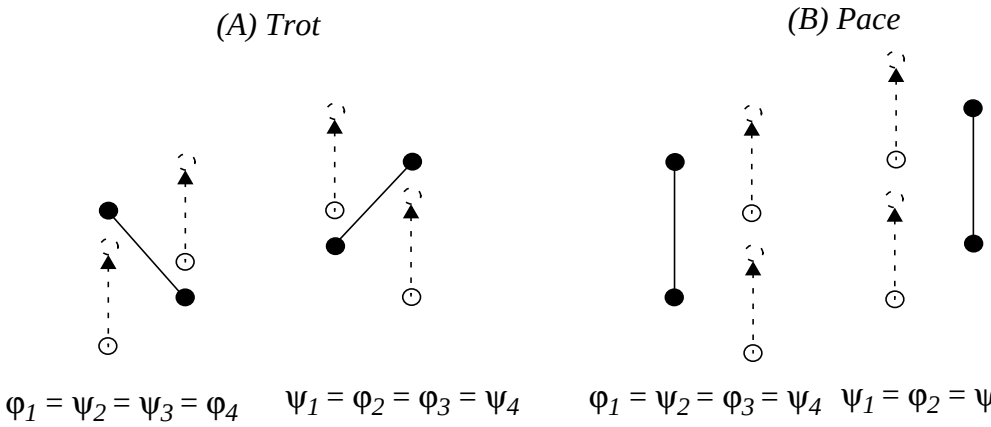


*Figure 2.8. Gait diagram for (A) quadruped trot gait, (B) pace gait, for duty factor* $\beta = 0.5$*. In a trot, the diagonal legs move synchronously, while in pace, legs on the same side of the body are moved synchronously.*

with duty factor ranging from 0.3- 0.5 and has relative phase

$$\varphi_1 = 0 \qquad \varphi_2 = 0.5 \qquad \varphi_3 = 0.5 \qquad \varphi_4 = 0 \tag{2.6}$$

The trot gait will therefore switch between two diagonal supporting legs as shown in the gait diagram (A) in figure 2.8. Another gait in the same speed range as trot is pace, in which ipsilateral legs step at the same time on one side of the body and then the other as shown in (B) in figure 2.8.

For quadrupedal animals there are a variety of running gaits. Trotting, pace and canter are examples of slower running gaits with duty factor ranging between 0.3-

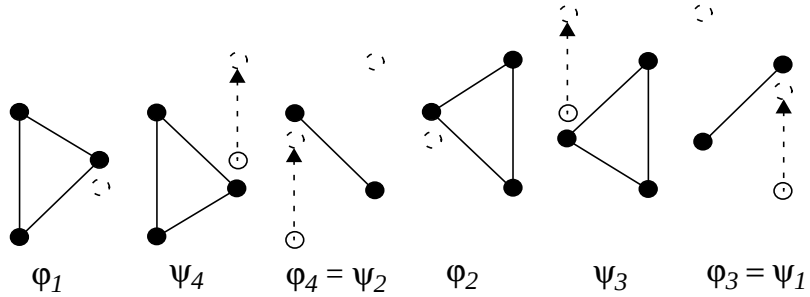


*Figure 2.7. Gait diagram for the gait rule proposed by Inagaki and Kobayashi (1993), with duty factor* $0.5 < \beta < 0.75$.

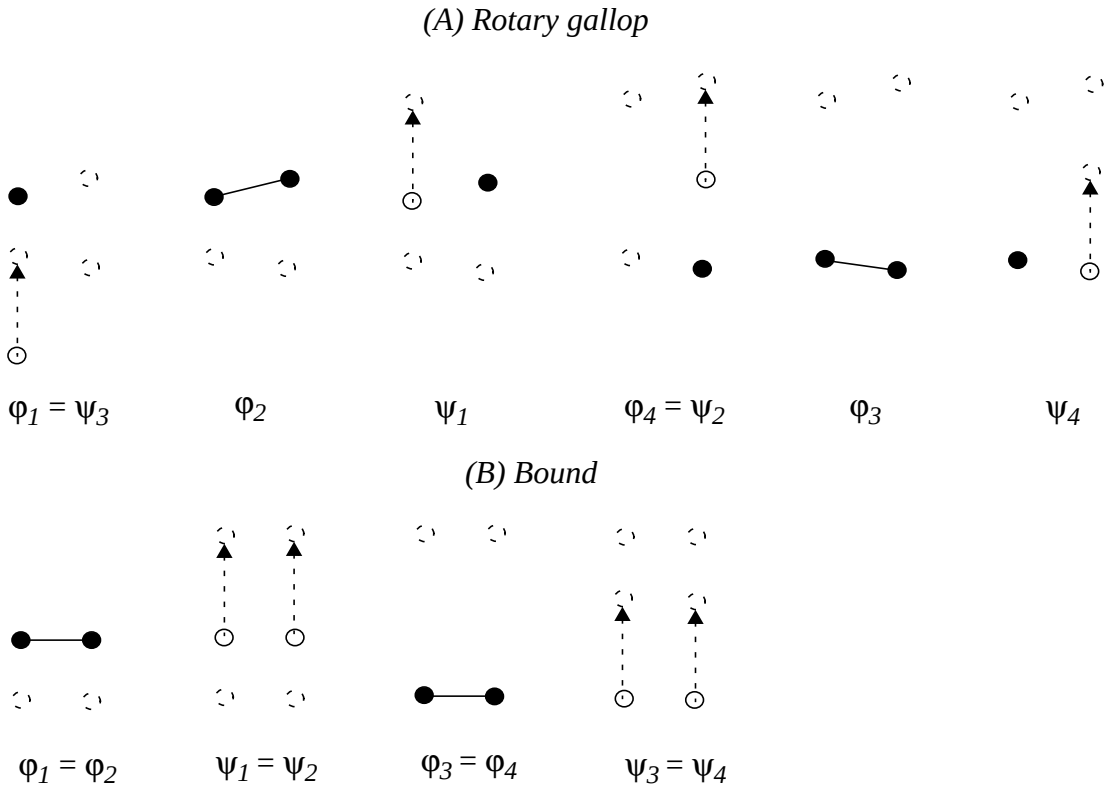


*Figure 2.9. Gait diagram for (A) rotary gallop, (B) bound, for* $\beta = 0.4$.

0.5. With increasing speed animals will switch to gallop which is usually executed for duty factors that are less than 0.4, as is shown in figure 2.9. The main difference between the running gaits is that trotting and pace are alternating gaits whereas galloping is a non alternating gait. Non alternating gaits usually make significant use of bending of the back whereas alternating gaits do not (McMahon, 1985).

# 3. KINEMATICS OF LEGGED ROBOTS

Kinematics is the study of the geometry of a mechanical system, where the motion of the system can be described in terms of the velocity and acceleration of all its components. The components can be connected through different types of joints, which limit how the components can move relative to each other. The interconnection of the components implies that the motion of the components relative to each other is constrained. Newtonian mechanics state that the forces acting on a system change the motion of the system. The forces can be divided into constraint forces, that limit (or constrain) the motion, and generalized forces, that cause the motion. Kinematics describe the interconnection of the components and the constraints without regard to the constraining forces and defines the motion of the interconnected bodies through space without regard to the generalized forces that cause a motion. The relationship between force and motion, i.e. the dynamics of the system, will be the subject of section 4.

It is assumed here that each component of the mechanical system can be treated as a rigid body. A rigid body can be defined as a component for which the distance between any two points in the component is fixed, i.e. the points can not move relative each other. The generalized coordinates (or configuration coordinates) determine the geometric configuration of the mechanical system. This means that any point in the mechanism can be specified by giving the values of the generalized coordinates. The generalized coordinates can be chosen in different ways where the choice is dependent on, for example, which coordinates are of interest, for instance due to placement of sensors, or simplification of the equations. The mini-

mum number of generalized coordinates that specify the configuration of the mechanism is called the geometric degree of freedom. A kinematic motion of the mechanism is determined by specifying all the generalized coordinates as function of one single variable, for example time, and thereby generating a curve for the motion of all points in the mechanism. The coordinates have to be given relative to a frame, usually a cartesian coordinate system, that is fixed relative to the earth. This frame will be called, interchangeably, the world frame or the inertial frame, depending on the context. Additional frames are defined for each of the components such that the orientation of a specific frame relative to a specific component is fixed, i.e. the frame will rotate with the component relative the world frame.

The focus will be on the forward kinematics, i.e. given the values of the generalized coordinates the configuration of the mechanism is specified. This is generally a straight forward problem as the generalized coordinates are chosen, in most cases, such that the positions of the points, in the mechanism, are functions of the generalized coordinates. An often more difficult problem is the inverse kinematics, where, given the position of a point in the mechanism, the generalized coordinates for that point are found. In many cases this can give multiple solutions, as a different set of values for the generalized coordinates can give the same position of a point. The subject of inverse kinematics will not be addressed as it will not be used in the work presented here, and therefore is beyond the scope of this thesis.

This chapter will derive the kinematic relationships needed for the work presented later on. As such it will not be very rigorous. Systematic approaches for formulating the kinematics exist, such as Denavit, and Hartenberg (1955). A survey of kinematics can be found in Lind (1993), and Lennartsson (1999). Further reading can be found in standard text books, such as Lesser (1995), Isidori (1995), and Murray, et al. (1994)

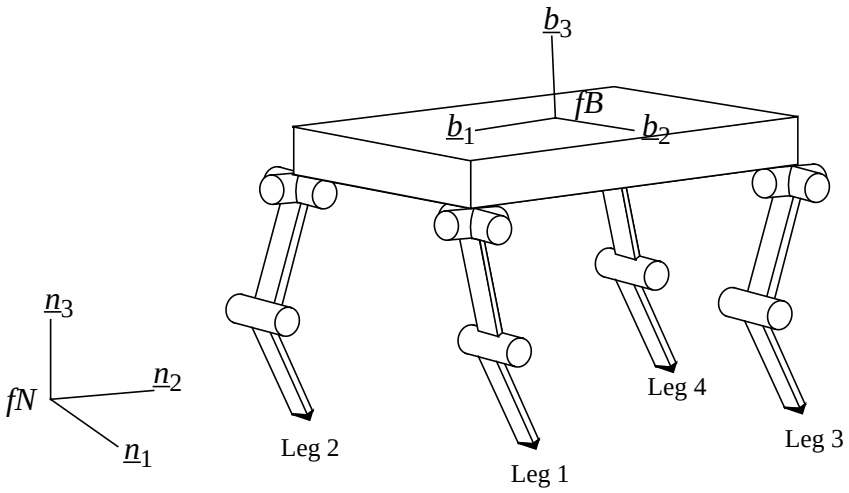


*Figure 3.1. Configuration of WARP1. The cylinders represent rotational joints where the rotational axis is along the longitudinal axis of the cylinders.*

## 3.1. Kinematics of the body

The structure of the quadruped robot WARP1 is described in section 1.1. First the motion of the body through space and the generalized coordinates associated with it will be defined. The discussion is, however, general for the motion of any free component. The motion of a single component through three dimensional space has a geometric degree of freedom of six and can be described with a set of six generalized coordinates. Three coordinates are needed to define the position of an index point of the component, and three coordinates to define its orientation. Several frames are needed to define the motion of all the different parts of the robot. The frames are all given by a chain of simple rotations, as shown in figure 3.2. This means that a right handed rotation around one axis of a frame will define a new frame, and the next frame will be defined by a single rotation around any of the axis of this new frame.

A fixed *world frame*, *fN*, is defined having its third axis parallel but opposite to the gravity vector, i.e. pointing straight up. The index point for the world is denoted by *N*, and placed at an arbitrary but fixed position in the world. A *body frame fB* is defined, with fixed orientation relative to the body of the robot, with axis 1 pointing along the longitudinal axis of the body in the forward direction, axis 2 in the lateral direction, to the left of the body, and axis 3 upwards, as shown in figure 3.1. The

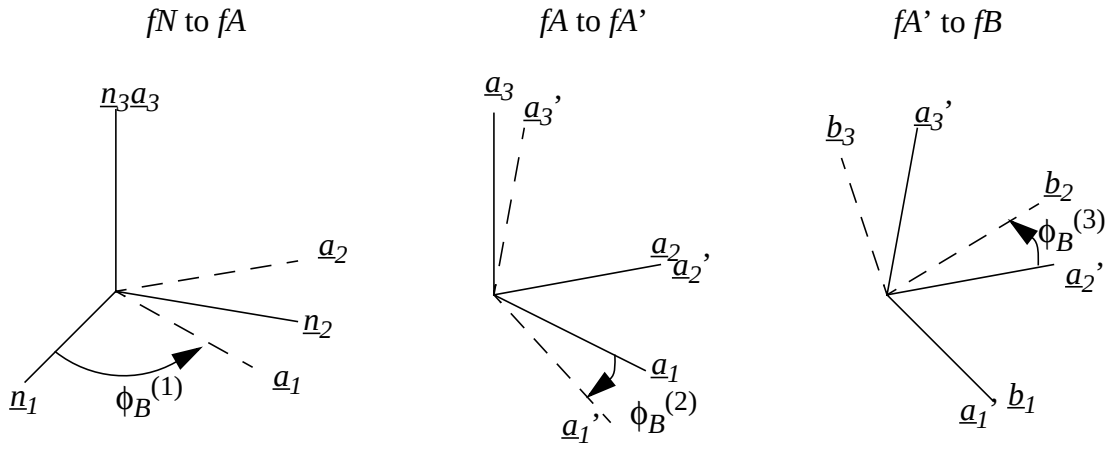


*Figure 3.2. Chain of simple rotations, from frame fN to frame fB.*

orientation of *fB* relative to *fN* is defined by a chain of three simple rotations which define a rotation matrix ${}^{N}\boldsymbol{R}^{B}(\underline{\phi}_B)$, where $\underline{\phi}_B \in \Re^3$ is the vector of generalized coordinates associated with the rotations, as shown in figure 3.2. The first rotation, $\phi_B^{(1)}$, is the yaw of the robot, i.e. the rotation around the third axis of *fN*, which defines a new frame *fA*, which will be called the *attitude frame*, for reasons that are explained later on (see also Rehbinder 2001). The second rotation, $\phi_B^{(2)}$, is the pitch of the robot, i.e. the rotation around the second axis of *fA*, which defines frame *fA*'. Finally, the third rotation $\phi_B^{(3)}$ is the roll of the robot, i.e. the rotation around the first axis of frame *fA*'. The rotation matrix from *fB* to *fN* is then given by

$$ {}^{N}\boldsymbol{R}^{B}(\underline{\phi}_B) = \begin{bmatrix} c\phi_B^{(1)} & -s\phi_B^{(1)} & 0 \\ s\phi_B^{(1)} & c\phi_B^{(1)} & 0 \\ 0 & 0 & 1 \end{bmatrix} \begin{bmatrix} c\phi_B^{(2)} & 0 & s\phi_B^{(2)} \\ 0 & 1 & 0 \\ -s\phi_B^{(2)} & 0 & c\phi_B^{(2)} \end{bmatrix} \begin{bmatrix} 1 & 0 & 0 \\ 0 & c\phi_B^{(3)} & -s\phi_B^{(3)} \\ 0 & s\phi_B^{(3)} & c\phi_B^{(3)} \end{bmatrix} \tag{3.1} $$

where $c\phi_B^{(j)} = \cos(\phi_B^{(j)})$ and $s\phi_B^{(j)} = \sin(\phi_B^{(j)})$, which results in

$$ {}^{N}\boldsymbol{R}^{B} = \begin{bmatrix} c\phi_B^{(1)}c\phi_B^{(2)} & c\phi_B^{(1)}s\phi_B^{(2)}s\phi_B^{(3)} - s\phi_B^{(1)}c\phi_B^{(3)} & c\phi_B^{(1)}s\phi_B^{(2)}c\phi_B^{(3)} + s\phi_B^{(1)}s\phi_B^{(3)} \\ s\phi_B^{(1)}c\phi_B^{(2)} & s\phi_B^{(1)}s\phi_B^{(2)}s\phi_B^{(3)} + c\phi_B^{(1)}c\phi_B^{(3)} & s\phi_B^{(1)}s\phi_B^{(2)}c\phi_B^{(3)} - c\phi_B^{(1)}s\phi_B^{(3)} \\ -s\phi_B^{(2)} & c\phi_B^{(2)}s\phi_B^{(3)} & c\phi_B^{(2)}c\phi_B^{(3)} \end{bmatrix} \tag{3.2} $$

The index point for the robot's body is chosen as its center of mass, and denoted as point *B*. The generalized coordinates, associated with the translation of the body, are chosen as the components of the position vector from the index point of the world, point *N*, to the index point of the body, point *B*, expressed in the world frame *fN*, that is

$$\underline{x}_B = {}^N\underline{r}^{NB} \tag{3.3}$$

where $\underline{x}_B \in \Re^3$ is the vector of generalized coordinates associated with the translation. The generalized coordinates for the position of the body are, therefore, the cartesian position of the index point of the body in the world frame. The position and orientation of the body is then defined by six generalized coordinates, defined as a vector

$$\underline{q}_B = \left[\underline{x}_B^T \ \underline{\phi}_B^T\right]^T \in \Re^6 \tag{3.4}$$

Given these relations for the position and orientation of the body, and the generalized coordinates associated with it, the motion of the body through space can be derived, and the position of any point in the body specified. Given a point *H* in the body (which might for instance be the position of a hip joint), the position vector from point *B* to *H* is constant when expressed in *fB*, i.e. the vector ${}^B\underline{r}^{BH}$ is constant. The position of point *H* relative to the world origin is

$$\underline{r}^{NH} = \underline{r}^{NB} + \underline{r}^{BH} \tag{3.5}$$

Given this relation it is of interest to derive the motion of point *H*. Straight forward derivation of equation (3.5), expressed in *fN*, gives

$$\frac{{}^N d}{dt}\underline{r}^{NH} = \frac{{}^N d}{dt}\underline{r}^{NB} + \frac{{}^N d}{dt}\underline{r}^{BH} \tag{3.6}$$

where the frame information in front of the derivative operator indicates that the derivation is done on the vector expressed in the world frame *fN*. As the vector $\underline{r}^{BH}$, expressed in *fB*, is a constant vector, its derivative is zero. Equation (3.6) can there-

fore be rewritten as

$$\frac{{}^{N}d}{dt}\underline{r}^{NH} = \frac{{}^{N}d}{dt}\underline{r}^{NB} + \frac{{}^{N}d}{dt}({}^{N}\boldsymbol{R}^{BB}\underline{r}^{BH}) = {}^{N}\underline{\dot{r}}^{NB} + {}^{N}\dot{\boldsymbol{R}}^{BB}\underline{r}^{BH} \tag{3.7}$$

In order to have all the vectors expressed in the world frame, equation (3.7) is rewritten as

$$\frac{{}^{N}d}{dt}\underline{r}^{NH} = {}^{N}\underline{\dot{r}}^{NB} + {}^{N}\dot{\boldsymbol{R}}^{BB}\boldsymbol{R}^{NN}\underline{r}^{BH} \tag{3.8}$$

The first term in equation (3.8) is the velocity of the index point *B*, expressed in *fN*

$${}^{N}\underline{v}^{NB} = \frac{{}^{N}d}{dt}\underline{r}^{NB} = {}^{N}\underline{\dot{r}}^{NB} \tag{3.9}$$

while the second term is the velocity of point *H* relative to point *B* due to the angular velocity of the body. The angular velocity of the body, i.e. the angular velocity between *fN* and *fB*, expressed in *fN*, is found by the relation

$${}^{N}\boldsymbol{\Omega}^{B}(\underline{\phi}_{B}, \dot{\underline{\phi}}_{B}) = {}^{N}\dot{\boldsymbol{R}}^{BB}\boldsymbol{R}^{N} \tag{3.10}$$

where ${}^{N}\boldsymbol{\Omega}^{B}$ is the anti-symmetric dual matrix of the angular velocity vector ${}^{N}\underline{\omega}^{B}$,

$${}^{N}\boldsymbol{\Omega}^{B} = \begin{bmatrix} 0 & -\omega_3 & \omega_2 \\ \omega_3 & 0 & -\omega_1 \\ -\omega_2 & \omega_1 & 0 \end{bmatrix} \tag{3.11}$$

and where $\omega_j$ are the components of the angular velocity vector, expressed in *fN*

$${}^{N}\underline{\omega}^{B} = \begin{bmatrix} \omega_1 & \omega_2 & \omega_3 \end{bmatrix}^{T} \tag{3.12}$$

The velocity of point *H* is then given by

$$\underline{v}^{NH} = \underline{v}^{NB} + {}^{N}\underline{\omega}^{B} \times \underline{r}^{BH} = \underline{v}^{NB} + {}^{N}\boldsymbol{\Omega}^{B}\underline{r}^{BH} \tag{3.13}$$

Generally a linear relationship exists between the velocity and angular velocity of a body and the derivatives of its generalized coordinates. The velocity of the body

center of mass is given by

$$ {}^{N}\underline{v}^{NB} = \dot{\underline{x}}_B \tag{3.14} $$

which clearly is a linear relationship. Insertion of equation (3.2) into equation (3.10) results in a linear relationship between the angular velocity vector and the derivatives of the generalized coordinates for the rotation.

$$ {}^{N}\underline{\omega}^{B} = {}^{N}\Phi^{B}(\underline{\phi}_B)\dot{\underline{\phi}}_B \tag{3.15} $$

where the matrix ${}^{N}\Phi^{B}$ is given by

$$ {}^{N}\Phi^{B}(\underline{\phi}_B) = \begin{bmatrix} 0 & -s\phi_B^{(1)} & c\phi_B^{(1)}c\phi_B^{(2)} \\ 0 & c\phi_B^{(1)} & 0 \\ 1 & 0 & -s\phi_B^{(2)} \end{bmatrix} \tag{3.16} $$

when expressed in frame *fN*. If the angular velocity is expressed in frame *fB*, it results in

$$ {}^{N}\Phi^{B}(\underline{\phi}_B) = \begin{bmatrix} -s\phi_B^{(2)} & 0 & 1 \\ c\phi_B^{(2)}s\phi_B^{(3)} & c\phi_B^{(3)} & 0 \\ c\phi_B^{(2)}c\phi_B^{(3)} & -s\phi_B^{(3)} & 0 \end{bmatrix} \tag{3.17} $$

## 3.2. Kinematics of the legs

The frames for the linkages of the legs are defined by a chain of simple rotations from *fB*. Each linkage *j*, of leg *i* has a frame $fL_{i,j}$ attached to it, and the index point $L_{i,j}$ is placed at the center of mass of the link. The generalized coordinates are chosen as the rotation of the joints of leg *i*, as shown in figure 3.3, and defined as a vector $\underline{\theta}_i$, where in the case of WARP1, $\underline{\theta}_i \in \Re^3$, as the legs have three degrees of freedom with respect to the body. The first joint of leg *i* is defined by rotation $\theta_i^{(1)}$ around the first axis of *fB*, i.e. a rotation around the longitudinal axis of the robot, which defines the frame $fL_{i,1}$. The second joint is defined by rotation $\theta_i^{(2)}$ around the second axis of the $fL_{i,1}$, which defines frame $fL_{i,2}$. Finally, the third joint is defined by rotation $\theta_i^{(3)}$ around the second axis of $fL_{i,2}$, which defines frame $fL_{i,3}$. Adding this new sets of generalized coordinates to those defined for the body,

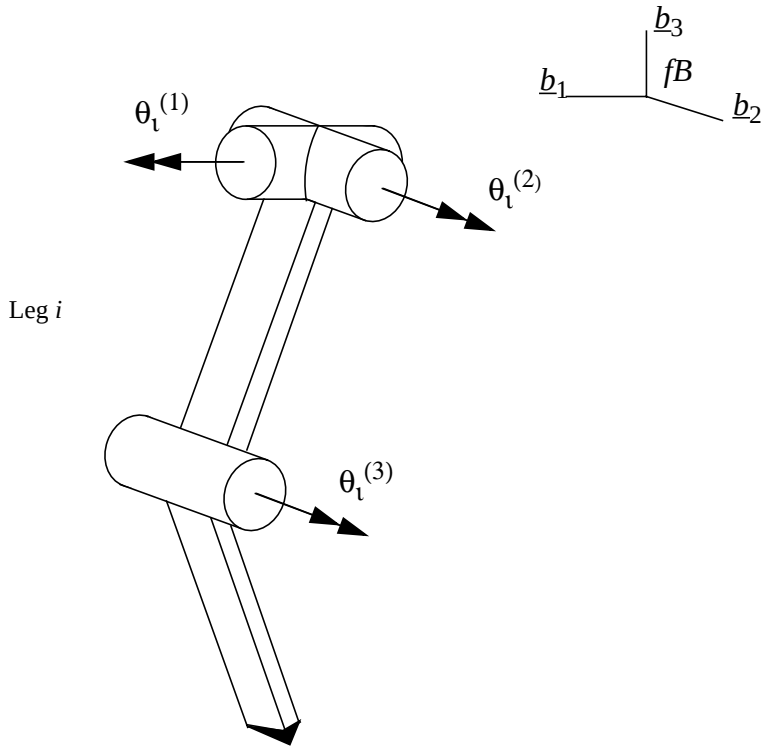


*Figure 3.3. The generalized coordinates chosen to define the position of the linkages of leg i, relative to the body.*

results in a vector of generalized coordinates chosen for the whole robot as

$$\underline{q} = \left[\underline{x}_B^T \ \underline{\phi}_B^T \ \underline{\theta}_1^T \ \underline{\theta}_2^T \ \underline{\theta}_3^T \ \underline{\theta}_4^T\right]^T \in \Re^{18} \tag{3.18}$$

The rotation matrix from frame $fL_{i,j}$ to $fB$ is denoted as ${}^{B}\boldsymbol{R}_{i,j}^{L}$, and rotation matrix between $fL_{i,j}$ to $fL_{i,j-1}$ is denoted as ${}_{i,j-1}^{L}\boldsymbol{R}_{i,j}^{L}$. The angular velocity of each link, relative the world frame, is defined by the rotation matrix and its derivative, expressed in $fN$, as

$${}^{N}\Omega_{i,j}^{L}(\underline{\phi}_B, \dot{\underline{\phi}}_B, \underline{\theta}_i^{(1\to j)}, \dot{\underline{\theta}}_i^{(1\to j)}) = {}^{N}\dot{\boldsymbol{R}}_{i,j}^{L} \cdot {}^{L}\boldsymbol{R}_{i,j}^{N} = {}^{N}\Omega^{B} + {}^{B}\Omega_{i,j}^{L} \tag{3.19}$$

where ${}^{N}\Omega_{i,j}^{L}$ is an anti-symmetric matrix of the components of the angular velocity vector ${}^{N}\underline{\omega}_{i,j}^{L}$, and ${}^{B}\Omega_{i,j}^{L}$ is an anti-symmetric matrix of the components of the angu-

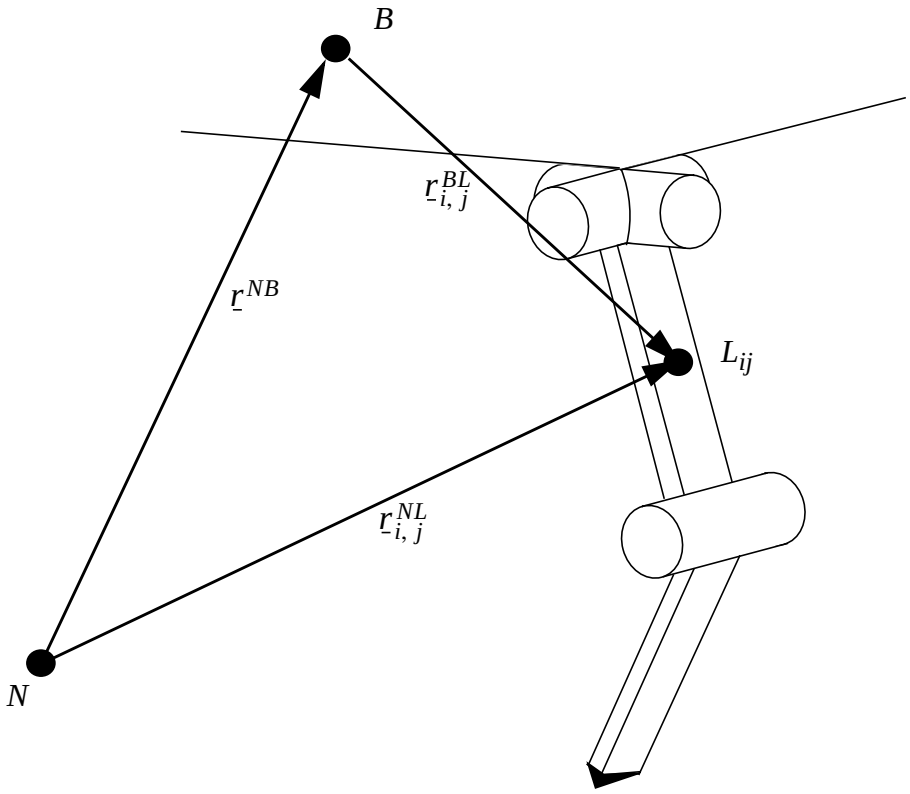


*Figure 3.4. Relationship between the position vectors of link j of leg i.*

lar velocity vector ${}^{B}\underline{\omega}^{L}_{i,j}$, given by

$$ {}^{B}\Omega^{L}_{i,j}(\underline{\phi}_B, \dot{\underline{\phi}}_B, \underline{\theta}_i^{(1\to j)}, \dot{\underline{\theta}}_i^{(1\to j)}) \;=\; {}^{N}\boldsymbol{R}^{B} \cdot {}^{B}\dot{\boldsymbol{R}}^{L}_{i,j} \cdot {}^{L}\boldsymbol{R}^{B}_{i,j} \cdot {}^{B}\boldsymbol{R}^{N} \tag{3.20} $$

The angular velocity vector between $fL_{i,j}$ and $fL_{i,j-1}$ is denoted ${}^{L}_{i,j-1}\underline{\omega}^{L}_{i,j}$ and is only a function of the derivative of the generalized coordinate defining the rotation between the frames, i.e. it is only function of $\dot{\theta}_i^{(j)}$.

The position vector $\underline{r}^{BL}_{i,j}$ is the vector from index point *B* to the index point $L_{i,j}$, i.e. the index point of link *j* of leg *i*, as shown in figure 3.4. The position of the center of mass of link *j* of leg *i* relative to *N* can be written as

$$ \underline{r}^{NL}_{i,j}(\underline{x}_B, \underline{\phi}_B, \underline{\theta}_i^{(1\to j)}) \;=\; \underline{r}^{NB} + \underline{r}^{BL}_{i,j} \tag{3.21} $$

The position vector of $L_{i,j}$ relative to *B*, when expressed in *fB*, is only a function of

the joint coordinates $\underline{\theta}_i^{(1 \to j)}$, i.e.

$$ {}^{N}\underline{r}_{i,j}^{BL}(\underline{\phi}_B, \underline{\theta}_i^{(1 \to j)}) = {}^{N}\boldsymbol{R}^{B}(\underline{\phi}_B) \cdot {}^{B}\underline{r}_{i,j}^{BL}(\underline{\theta}_i^{(1 \to j)}) \tag{3.22} $$

The velocity of the index point of each linkage is then

$$ \underline{v}_{i,j}^{NL}(\dot{\underline{x}}_B, \underline{\phi}_B, \dot{\underline{\phi}}_B, \underline{\theta}_i^{(1 \to j)}, \dot{\underline{\theta}}_i^{(1 \to j)}) = \underline{v}^{NB} + \underline{v}_{i,j}^{BL} + {}^{N}\underline{\omega}^{B} \times \underline{r}_{i,j}^{BL} \tag{3.23} $$

where $\underline{v}_{i,j}^{BL}$ is the velocity of $L_{i,j}$ relative to $B$, i.e.

$$ \underline{v}_{i,j}^{BL} = \frac{{}^{B}d}{dt}\underline{r}_{i,j}^{BL} \tag{3.24} $$

## 3.3. Motion of the feet relative to the body

The motion of the body is determined by the motion of the feet in ground contact, and the stability of the robot is dependent on where the feet are placed relative to the center of mass of the robot. This section will therefore look at the relation between the position and motion of the body, relative to a foot that is in ground contact.

If the point $P_i$ is the position of the foot of leg $i$, as shown in figure 3.5, then let $\underline{r}_i^{NP}$ be the position of the foot of leg $i$ relative to point $N$, where

$$ \underline{r}_i^{NP} = \underline{r}^{NB} + \underline{r}_i^{BP} \tag{3.25} $$

and the velocity is

$$ \underline{v}_i^{NP} = \underline{v}^{NB} + \underline{v}_i^{BP} + {}^{N}\underline{\omega}^{B} \times \underline{r}_i^{BP} \tag{3.26} $$

The velocity of the foot relative to the body is given by

$$ {}^{B}\underline{v}_i^{BP} = \frac{{}^{B}d}{dt}\underline{r}_i^{BP} = \frac{\partial^{B}\underline{r}_i^{BP}}{\partial\underline{\theta}_i} \cdot \frac{d\underline{\theta}_i}{dt} = {}^{B}J_i^{P}(\underline{\theta}_i) \cdot \dot{\underline{\theta}}_i \tag{3.27} $$

where ${}^{B}\boldsymbol{J}_i^{P}$ is the Jacobian which, in this case, is a $3 \times 3$ matrix. Let point $H_i$ denote

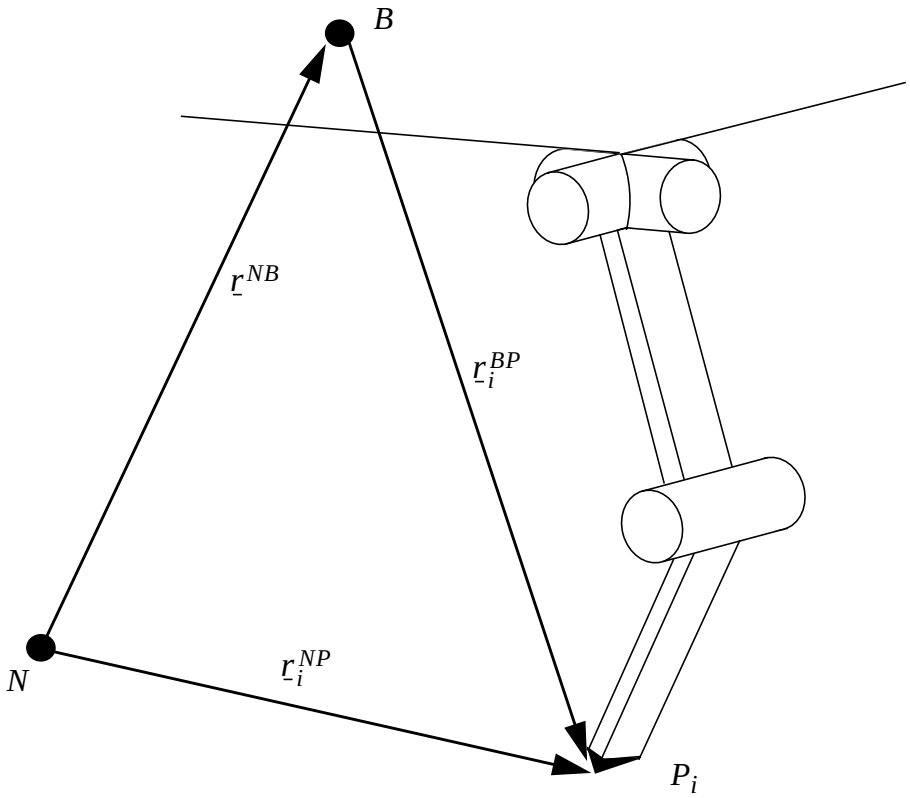


*Figure 3.5. Relationship between the position vectors for foot i.*

the position of the hip of leg *i*, i.e. the position of the first joint of leg *i*, then

$$\underline{r}_i^{BP} = \underline{r}_i^{BH} + \underline{r}_i^{HP} \tag{3.28}$$

As $\underline{r}_i^{BH}$ is a constant when expressed in *fB*, then

$${}^B\underline{v}_i^{BP}(\underline{\theta}_i, \dot{\underline{\theta}}_i) = \frac{\partial {}^B\underline{r}_i^{BP}}{\partial \underline{\theta}_i} \cdot \dot{\underline{\theta}}_i = \frac{\partial {}^B\underline{r}_i^{HP}}{\partial \underline{\theta}_i} \cdot \dot{\underline{\theta}}_i = {}^B\underline{v}_i^{HP}(\underline{\theta}_i, \dot{\underline{\theta}}_i) \tag{3.29}$$

The Jacobian for leg *i* is then

$${}^B J_i^P(\underline{\theta}_i) = \frac{\partial {}^B\underline{r}_i^{BP}}{\partial \underline{\theta}_i} = \frac{\partial {}^B\underline{r}_i^{HP}}{\partial \underline{\theta}_i} \tag{3.30}$$

If the foot is in support and therefore stationary on the ground, assuming that the foot doesn't slip and that the ground is completely rigid, then the velocity of the foot relative the world coordinate system is zero, i.e. if $\underline{v}_i^{NP} = \underline{0}$. The velocity of the foot relative to the body is then found by setting equation (3.26) equal to zero

and isolating the relative velocity, i.e.

$$\underline{v}_i^{BP} = -\underline{v}^{NB} - {}^N\underline{\omega}^B \times \underline{r}_i^{BP} \tag{3.31}$$

As $\underline{v}^{NB}$ and ${}^N\underline{\omega}^B$ are the velocity and angular velocity of the body, equation (3.31) gives the velocity of a foot, in support, relative to the body. If the robot body maintains a constant orientation, it can be seen that the motion of the foot relative to the body, is simply opposite to the motion of the body. Otherwise, the motion of the foot will be dependent also on where it is placed relative to the body.

If the foot is stationary on the ground, equation (3.25) gives a coupling between the generalized coordinates which makes several of them redundant, meaning that the geometric degree of freedom of the system is less than 18. For example, if the position of the foot is expressed in *fN*, the coupling can be written as

$$\underline{x}_B = {}^N\underline{r}_i^{NP} - {}^N\underline{r}_i^{BP}(\underline{\phi}_B, \underline{\theta}_i) \tag{3.32}$$

where the vector ${}^N\underline{r}_i^{NP}$ is a constant. However, since the assumptions that the foot is stationary on ground and that the ground is totally rigid are not completely true, this coupling will be ignored in the derivation of the equations of motion. Furthermore, the foot contact is not a point for WARP1, which has an oval club foot, so the contact point of the foot will move during the contact phase.

# 4. THE EQUATIONS OF MOTION FOR LEGGED ROBOTS

Dynamics is the study of how mechanical systems move under the influence of force. The force may be a function of position, velocity and time, and acts on the mechanical system to change its state of motion. The resulting motion will depend upon the kinematics of the system and the mass distribution. The equations of motion describe the dynamics of the system and give the relationship between the forces and the generalized coordinates. The forward dynamics describe how the system moves under the influence of force, while the inverse dynamics describe what force will make a mechanical system move in a predetermined manner.

Several methods have been developed for deriving the equations of motion, where the most commonly used in engineering are Newton-Euler, Lagrange equations, and Kane's equations. An overview can be found in Lind (1993), and Lennartsson (1999). The methods are all equivalent but there is a large difference in how the methods proceed. The Newton-Euler method sets up the mechanical system as free bodies and includes constraint forces to describe the connections between components. Lagrange equations and Kane's equations are more based on kinematics, where the constraint forces are eliminated by use of D'Alembert's principle, in which the forces are projected onto certain directions. Otherwise the two last methods are quite different. Lagrange equations is an analytic approach, in which an operator, called the Euler-Lagrange operator, is applied on the difference between kinetic and potential energy. Kane's method uses kinematic differential equations for velocity transformations and partial velocities to identify the directions that the forces are projected onto. Further reading can be found in standard textbooks on mechanics, such as Lesser (1995).

In this section the equations of motion will be derived using Lagrange equations. For a short introduction see Appendix A. Section 4.1. will describe the equations of motions of a robot with rigid joints, and is loosely based on Koo, and Yoon (1999). Section 4.2. will include joint dynamics in the equations of motion, including speed reduction gear, elasticity in the transmission and dynamics of DC-motors.

## 4.1. Equations of motion for the quadruped robot WARP1

The first step when using the Lagrange equations is to form the Lagrangian, denoted as $L$, which is the difference of the kinetic and potential energy, denoted $T$ and $P$ respectively, of the system, i.e. the Lagrangian is $L = T - P$. Mechanical systems, such as robots, have two important properties: The potential energy is only a function of the generalized coordinates, i.e. the potential energy can be expressed as $P(\underline{q})$, and the kinetic energy is a quadratic function of the derivatives of the generalized coordinates (Ortega, and Spong, 1988). The kinetic and potential energy are now formed by summing together the contributions of each component of the robot. The motion of the components of the robot was defined in section 3. For shortness of notation let $\underline{r}_B = \underline{r}^{NB}$, $\underline{r}_{ij} = \underline{r}_{ij}^{NL}$, $\underline{v}_B = \underline{v}^{NB}$, $\underline{v}_{ij} = \underline{v}_{ij}^{NL}$, $\omega_B = {}^N\underline{\omega}^B$ and $\omega_{ij} = {}^N\underline{\omega}_{ij}^L$.

The kinetic energy for each component is composed of two parts, one due to translation and one due to rotation. The kinetic energy for the robot's body is then

$$T_B = \frac{1}{2} m_B \underline{v}_B^T \underline{v}_B + \frac{1}{2} \underline{\omega}_B^T \boldsymbol{I}_B \omega_B \tag{4.1}$$

where $m_B$ and $\boldsymbol{I}_B$ are the mass and the inertia matrix of the robot's body, respectively. In the same manner the kinetic energy for the links of leg $i$ is

$$T_i = \frac{1}{2} \sum_{j=1}^{3} \{ m_{ij} \underline{v}_{ij}^T \underline{v}_{ij} + \underline{\omega}_{ij}{}^T \boldsymbol{I}_{ij} \underline{\omega}_{ij} \} \tag{4.2}$$

where $m_{ij}$ and $\boldsymbol{I}_{ij}$ are the mass and the inertia matrix, respectively, for link $j$ of leg $i$. The total kinetic energy of the whole robot is then

$$T(\underline{q}, \dot{\underline{q}}) = T_B(\underline{q}_B, \dot{\underline{q}}_B) + \sum_{i=1}^{4} T_i(\underline{q}, \dot{\underline{q}}) \tag{4.3}$$

As discussed in section 3., there exists a relationship between the velocities and angular velocities, and the derivatives of the generalized coordinates. The total kinetic energy can then be formulated on matrix form as a quadratic function of the derivatives of the generalized coordinates, as discussed above, that is

$$T(\underline{q}, \underline{\dot{q}}) = \frac{1}{2}\underline{\dot{q}}^T \boldsymbol{D}(\underline{q})\underline{\dot{q}} \tag{4.4}$$

where the matrix $\boldsymbol{D}$ is the inertia matrix, which is a symmetric and positive definite matrix, and $\underline{q}$ is the vector of generalized coordinates defined in equation (3.18). See Appendix B for details on how the inertia matrix is formed.

The potential energy $P$ is in this case the gravitational potential energy $P_G$, which is only a function of the generalized coordinates

$$P(\underline{q}) = P_G(\underline{q}) = \underline{\gamma}^T \left\{ m_B \underline{r}_B + \sum_{i=1}^{4} \sum_{j=1}^{3} m_{ij} \cdot \underline{r}_{ij} \right\} \tag{4.5}$$

where $\underline{\gamma}$ is the vector of gravitational acceleration, which is, when expressed in *fN*, ${}^N\underline{\gamma} = \begin{bmatrix} 0 & 0 & -a_g \end{bmatrix}^T$, where $a_g$ is the constant acceleration of gravity.

The Lagrangian is now formed by $L = T - P$, where $T$ and $P$ are given by equations (4.4) and (4.5), respectively. Applying the Euler-Lagrange operator on the Lagrangian gives

$$\left( \frac{d}{dt} \frac{\partial}{\partial \underline{\dot{q}}} - \frac{\partial}{\partial \underline{q}} \right) L = \left( \frac{d}{dt} \frac{\partial}{\partial \underline{\dot{q}}} - \frac{\partial}{\partial \underline{q}} \right) (T(\underline{q}, \underline{\dot{q}}) - P(\underline{q})) = \underline{f} \tag{4.6}$$

where $\underline{f}$ is the vector of generalized forces, which are the projection of the forces acting on the system along the directions of the generalized coordinates. Applying the operator in a straightforward manner results in

$$\boldsymbol{D}(\underline{q})\underline{\ddot{q}} + \dot{\boldsymbol{D}}(\underline{q})\underline{\dot{q}} - \frac{\partial}{\partial \underline{q}} \left( \frac{1}{2} \underline{\dot{q}}^T \boldsymbol{D}(\underline{q}) \underline{\dot{q}} \right) + \frac{\partial}{\partial \underline{q}} P(\underline{q}) = \underline{f} \tag{4.7}$$

The left hand side is usually divided into different parts depending on the nature of the forces, into inertial forces, centrifugal and coriolis forces and gravitational

forces. The equation of motion is then expressed as

$$\boldsymbol{D}(\underline{q})\ddot{\underline{q}} + \underline{c}(\underline{q}, \dot{\underline{q}}) + \underline{g}(\underline{q}) = \underline{f} \tag{4.8}$$

The first term in equation (4.8), $\boldsymbol{D}(\underline{q})\ddot{\underline{q}}$ is the inertial force which is an acceleration dependent force. The second term $\underline{c}(\underline{q}, \dot{\underline{q}})$ is the vector of centrifugal and coriolis forces, which has quadratic terms of the derivatives of the generalized coordinates. Terms of the form $(\dot{q}^{(i)})^2$ are called centrifugal terms whereas terms of the form $\dot{q}^{(i)} \cdot \dot{q}^{(j)}, i \neq j$, are called coriolis terms. The third term is the vector of gravity forces, $\underline{g}$, defined as

$$\underline{g}(\underline{q}) = \frac{\partial}{\partial \underline{q}} P_G(\underline{q}) \tag{4.9}$$

It is shown in Appendix B that the inertia matrix has a special structure. Equation (4.8) can be expressed as

$$\begin{bmatrix} \boldsymbol{D}_x & \boldsymbol{D}_{x\phi}^T & \boldsymbol{D}_{x\theta 1}^T & \boldsymbol{D}_{x\theta 2}^T & \boldsymbol{D}_{x\theta 3}^T & \boldsymbol{D}_{x\theta 4}^T \\ \boldsymbol{D}_{x\phi} & \boldsymbol{D}_{\phi} & \boldsymbol{D}_{\phi\theta 1}^T & \boldsymbol{D}_{\phi\theta 2}^T & \boldsymbol{D}_{\phi\theta 3}^T & \boldsymbol{D}_{\phi\theta 4}^T \\ \boldsymbol{D}_{x\theta 1} & \boldsymbol{D}_{\phi\theta 1} & \boldsymbol{D}_{\theta 1} & \boldsymbol{0} & \boldsymbol{0} & \boldsymbol{0} \\ \boldsymbol{D}_{x\theta 2} & \boldsymbol{D}_{\phi\theta 2} & \boldsymbol{0} & \boldsymbol{D}_{\theta 2} & \boldsymbol{0} & \boldsymbol{0} \\ \boldsymbol{D}_{x\theta 3} & \boldsymbol{D}_{\phi\theta 3} & \boldsymbol{0} & \boldsymbol{0} & \boldsymbol{D}_{\theta 3} & \boldsymbol{0} \\ \boldsymbol{D}_{x\theta 4} & \boldsymbol{D}_{\phi\theta 4} & \boldsymbol{0} & \boldsymbol{0} & \boldsymbol{0} & \boldsymbol{D}_{\theta 4} \end{bmatrix} \begin{bmatrix} \ddot{\underline{x}}_B \\ \ddot{\underline{\phi}}_B \\ \ddot{\underline{\theta}}_1 \\ \ddot{\underline{\theta}}_2 \\ \ddot{\underline{\theta}}_3 \\ \ddot{\underline{\theta}}_4 \end{bmatrix} + \begin{bmatrix} \underline{c}_x \\ \underline{c}_\phi \\ \underline{c}_{\theta 1} \\ \underline{c}_{\theta 2} \\ \underline{c}_{\theta 3} \\ \underline{c}_{\theta 4} \end{bmatrix} + \begin{bmatrix} \underline{g}_x \\ \underline{g}_\phi \\ \underline{g}_{\theta 1} \\ \underline{g}_{\theta 2} \\ \underline{g}_{\theta 3} \\ \underline{g}_{\theta 4} \end{bmatrix} = \begin{bmatrix} \underline{f}_x \\ \underline{f}_\phi \\ \underline{f}_{\theta 1} \\ \underline{f}_{\theta 2} \\ \underline{f}_{\theta 3} \\ \underline{f}_{\theta 4} \end{bmatrix} \tag{4.10}$$

where all the submatrices of the inertia matrix are of size $3 \times 3$, and the subvectors of the vector of centrifugal and coriolis forces, gravity and generalized forces are of size $3 \times 1$.

The vector $f$ is the vector of generalized forces acting along each generalized coordinate. It will be assumed that only external forces and moments act along the generalized coordinates associated with the body, along the directions of $\underline{x}_B$ and $\underline{\phi}_B$, i.e. $\underline{f}_x$ and $\underline{f}_\phi$ are the external force and moment acting on the body. The forces acting in the direction of the joints are torques and can be defined as the sum of three parts: applied torques, $\underline{\tau}_a$, i.e. output of the actuators at the joints, dissipative or frictional torques, $\underline{\tau}_f$, and external torques, $\underline{\tau}_e$, such as, due to the reaction forces

from the ground. The vector of generalized forces for each leg can be expressed as, for $i$ = 1...4,

$$\underline{f}_{\theta,\,i} = \underline{\tau}_{a,\,i} + \underline{\tau}_{f,\,i} + \underline{\tau}_{e,\,i} \tag{4.11}$$

where $\underline{\tau}_{a,i}$ and $\underline{\tau}_{f,i}$, for $i$ = 1...4, are the vectors of applied and frictional torques, respectively, acting on the joints of leg $i$. It is further assumed that the frictional torque at a joint is only a function of the derivative of the generalized coordinate at that joint, i.e. the frictional torque at joint $j$ of leg $i$ is $\underline{\tau}_{f,\,i}^{(j)}(\dot{\underline{\theta}}_i^{(j)})$.

The external forces will be assumed to be mainly due to the interaction with the ground through the feet, i.e. due to the ground reaction forces. In order to map the reaction force $\underline{R}_i$ acting on foot $i$, to external torques $\underline{\tau}_{e,i}$ at the joints, the preservation of the instantaneous power flow, from foot to the body, can be used. If the force and velocity vector of the foot are expressed in *fB*, then the instantaneous power flow for leg $i$ is

$$\underline{\tau}_{ei}^{T} \cdot \dot{\underline{\theta}}_i = {}^{B}\underline{R}_i^{T} \cdot {}^{B}\underline{v}_i^{BP} = {}^{B}\underline{R}_i^{T} \cdot {}^{B}\boldsymbol{J}_i^{P} \cdot \dot{\underline{\theta}}_i \tag{4.12}$$

where ${}^{B}\boldsymbol{J}_i^{P}$ is the Jacobian of the velocity of the foot relative to the body, defined in equation (3.30) in section 3.3. Equation (4.12) gives the relation between the torque and the reaction force from the ground as

$$\underline{\tau}_{ei} = ({}^{B}\boldsymbol{J}_i^{P})^{T} \cdot {}^{B}\underline{R}_i \tag{4.13}$$

## 4.2. Equations of motion including joint dynamics

In this section the equations of motions will be derived for the robot, given that the joints are actuated by rotary DC-motor, gear reduction and an elastic transmission. Elasticity arises naturally in transmissions in the gears and the shafts, but this effect is often negligible if the joint is sufficiently rigid. However, if the joint is relatively weak, the elasticity can have a seriously deteriorating effect on the performance of the robot if the elasticity is not taken into account in the control design.

The complete model for an elastic joint can be extremely complicated. To simplify matters, it is assumed that the rotor and gear inertia are symmetric about the axis

of rotation. This results in that the translational position and velocity of the rotor are independent of its angular position and velocity. The potential gravitational energy and translational kinetic energy of the rotor can then be included in the total energy of the link that the motor is attached to (Spong, 1987; Tomei, 1991).

The joints of WARP1 are actuated by DC-motors, and have transmissions that consist of a harmonic drive and a wire-pulley system. Both the flexspline of the harmonic drive and the wires give rise to a noticeable elasticity in the transmission. In figure 4.1 it is shown how the joints are modelled. The DC-motor stator is rigidly attached to one link, and the rotor is attached to the next link through the transmission. The inertia of the rotor and transmission are lumped together into a single inertia of the rotor. The transmission has reduction ratio of $n$, and an elasticity with stiffness of $k$, where all the elasticity is assumed to be on the joint side of the gear. The variable $\theta$ is the angle of link $j$ relative to link $j$-1, i.e. it is the generalized coordinate for the joint as before, but where the indices have been dropped for clarity. Two new angles are defined, $\theta_R$ is the angular position of the rotor relative to link $j$-1, and $\theta_M$ is the is the angular position of the output shaft of the gear, relative to link $j$-1. The two new variables are related through $\theta_R = n\theta_M$, i.e. the rotor will rotate $n$ times faster than the output shaft of the gear. A frame $fR$ is defined as rotating with the rotor, which has an angular velocity ${}^N\underline{\omega}^R$ relative to the inertial frame $fN$,

$$ {}^N\underline{\omega}^R = \underline{\omega}_{i,\,j-1} + \underline{\omega}_R \tag{4.14} $$

where $\underline{\omega}_{i,\,j-1}$ was defined in section 3.2. and $\underline{\omega}_R$ is the angular velocity of $fR$ relative to $fL_{i,j-1}$. The rotational kinetic energy of the rotor, $T_R$, is then

$$ T_R = \frac{1}{2}({}^N\underline{\omega}^R)^T \boldsymbol{I}_R {}^N\underline{\omega}^R = \frac{1}{2}\{\underline{\omega}^T_{i,\,j-1}\boldsymbol{I}_R\underline{\omega}_{i,\,j-1} + 2\underline{\omega}^T_{i,\,j-1}\boldsymbol{I}_R\underline{\omega}_R + \underline{\omega}^T_R\boldsymbol{I}_R\underline{\omega}_R\} \tag{4.15} $$

where $\boldsymbol{I}_R$ is the inertia matrix of the rotor. If the angular velocity $\underline{\omega}_R$ is expressed in $fR$ then the angular velocity of the output shaft $\underline{\omega}_M$ related through $\underline{\omega}_R = n \cdot \underline{\omega}_M$.

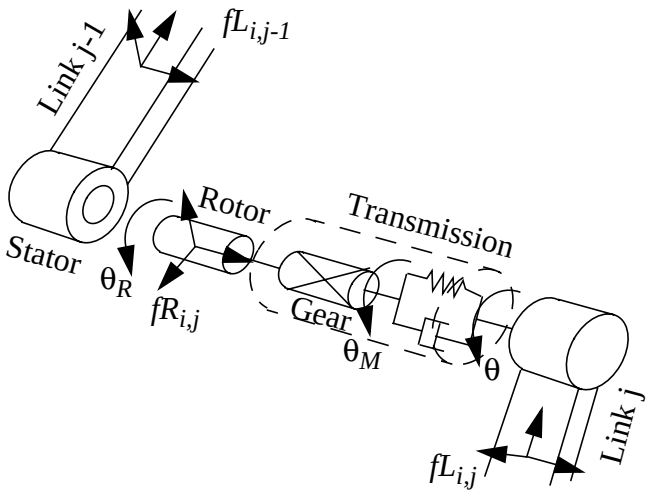


*Figure 4.1. Model of an elastic joint.*

The rotational kinetic energy of equation (4.15) is then

$$T_R = \frac{1}{2}\{\underline{\omega}_{i,j-1}^T \boldsymbol{I}_R \underline{\omega}_{i,j-1} + 2n\underline{\omega}_{i,j-1}^T \boldsymbol{I}_R \underline{\omega}_M + n^2 \underline{\omega}_M^T \boldsymbol{I}_R \underline{\omega}_M\} \tag{4.16}$$

where all angular velocity vectors are of the same order of magnitude.

Spong (1987) proposed to use an approximation if the rotor inertia is relatively small and the reduction ratio is large. The assumption is that the kinetic energy of the rotor is due mainly to its own rotation, or equivalently, that the motion of the rotor is a pure rotation with respect to an inertial frame. If the inertia of the rotor is very small and the gear reduction ratio is large $n^2 >> n$, i.e. if the first two terms in equation (4.16) are negligible relative to the square of the gear ratio, then the kinetic energy of a rotor due to its rotation is approximated by

$$T_R \approx \frac{1}{2} n^2 J \dot{\theta}_M^2 \tag{4.17}$$

where $J$ is the inertia of the rotor around its axis of rotation. The term $n^2 J$ is often called the reflected inertia of the rotor. The total approximate rotational kinetic energy due to the rotors is then

$$T_M = \frac{1}{2}\sum_{i,j}\{n_{i,j}^2 J_{i,j}(\dot{\theta}_{Mi}^{(j)})^2\} = \frac{1}{2}\sum_{i=1}^{4} \dot{\underline{\theta}}_{Mi}^T \boldsymbol{J}_i \dot{\underline{\theta}}_{Mi} \tag{4.18}$$

where the indices, *i* and *j*, refer to joint *j* of leg *i*, $\theta_{Mi}$ is a vector of generalized coordinates associated with the angular position of the rotors of leg *i*, and $\boldsymbol{J}_i$ is the diagonal matrix of the reflected inertias of the rotors

$$\boldsymbol{J}_i = \begin{bmatrix} n_{i,1}^2 J_{i,1} & 0 & 0 \\ 0 & n_{i,2}^2 J_{i,2} & 0 \\ 0 & 0 & n_{i,3}^2 J_{i,3} \end{bmatrix} \tag{4.19}$$

The total kinetic energy of the system is then

$$T(\underline{q}, \dot{\underline{q}}) = \frac{1}{2}\dot{\underline{q}}^T \boldsymbol{D}(\underline{q})\dot{\underline{q}} + \frac{1}{2}\sum_{i=1}^{4} \dot{\underline{\theta}}_{Mi}^T \boldsymbol{J}_i \dot{\underline{\theta}}_{Mi} \tag{4.20}$$

where the inertia matrix has been modified to include the translational kinetic energy of the rotors, as discussed in the beginning of this section.

The potential energy consists of two terms in this case, the gravitational potential energy, and the elastic potential energy stored in the springs, i.e. the total potential energy is $P = P_G + P_K$, where $P_G$ from equation (4.5) has been modified to include the mass of the rotors. The elastic potential energy stored in the springs is

$$P_K = \sum_{i,j} \int \tau_{k,i}^{(j)}(\bar{\theta}_i^{(j)}) d\bar{\theta}_i^{(j)} \tag{4.21}$$

where $\tau_{k,i}^{(j)}$ is the spring torque in joint *j* of leg *i*, which is a function of the twist of each spring, $\bar{\theta}_i^{(j)} = \theta_{Mi}^{(j)} - \theta_i^{(j)}$. If a linear elasticity is assumed, the energy stored in the spring is

$$P_K = \frac{1}{2}\sum_{i,j} k_{i,j}(\theta_{Mi}^{(j)} - \theta_i^{(j)})^2 = \frac{1}{2}\sum_{i=1}^{4} (\underline{\theta}_{Mi} - \underline{\theta}_i)^T \boldsymbol{K}_i (\underline{\theta}_{Mi} - \underline{\theta}_i) \tag{4.22}$$

where $k_{i,j}$ is the stiffness coefficient for joint *j* of leg *i*, and $\boldsymbol{K}_i$ is diagonal matrix of the stiffness coefficients of leg *i*,

$$\boldsymbol{K}_i = \begin{bmatrix} k_{i,1} & 0 & 0 \\ 0 & k_{i,2} & 0 \\ 0 & 0 & k_{i,3} \end{bmatrix} \tag{4.23}$$

Applying the Euler-Lagrange operator results in the equations of motion for the robot with joint dynamics. The external forces act only on the joint coordinates, as before, but the applied and friction torques are now acting on the motor coordinates. The resulting equations of motion are

$$\begin{bmatrix} \boldsymbol{D}_x & \boldsymbol{D}_{x\phi}^T & \boldsymbol{D}_{x\theta 1}^T & \boldsymbol{D}_{x\theta 2}^T & \boldsymbol{D}_{x\theta 3}^T & \boldsymbol{D}_{x\theta 4}^T \\ \boldsymbol{D}_{x\phi} & \boldsymbol{D}_{\phi} & \boldsymbol{D}_{\phi\theta 1}^T & \boldsymbol{D}_{\phi\theta 2}^T & \boldsymbol{D}_{\phi\theta 3}^T & \boldsymbol{D}_{\phi\theta 4}^T \\ \boldsymbol{D}_{x\theta 1} & \boldsymbol{D}_{\phi\theta 1} & \boldsymbol{D}_{\theta 1} & \boldsymbol{0} & \boldsymbol{0} & \boldsymbol{0} \\ \boldsymbol{D}_{x\theta 2} & \boldsymbol{D}_{\phi\theta 2} & \boldsymbol{0} & \boldsymbol{D}_{\theta 2} & \boldsymbol{0} & \boldsymbol{0} \\ \boldsymbol{D}_{x\theta 3} & \boldsymbol{D}_{\phi\theta 3} & \boldsymbol{0} & \boldsymbol{0} & \boldsymbol{D}_{\theta 3} & \boldsymbol{0} \\ \boldsymbol{D}_{x\theta 4} & \boldsymbol{D}_{\phi\theta 4} & \boldsymbol{0} & \boldsymbol{0} & \boldsymbol{0} & \boldsymbol{D}_{\theta 4} \end{bmatrix} \begin{bmatrix} \ddot{\underline{x}}_B \\ \ddot{\underline{\phi}}_B \\ \ddot{\underline{\theta}}_1 \\ \ddot{\underline{\theta}}_2 \\ \ddot{\underline{\theta}}_3 \\ \ddot{\underline{\theta}}_4 \end{bmatrix} + \begin{bmatrix} \underline{c}_x \\ \underline{c}_\phi \\ \underline{c}_{\theta 1} \\ \underline{c}_{\theta 2} \\ \underline{c}_{\theta 3} \\ \underline{c}_{\theta 4} \end{bmatrix} + \begin{bmatrix} \underline{g}_x \\ \underline{g}_\phi \\ \underline{g}_{\theta 1} \\ \underline{g}_{\theta 2} \\ \underline{g}_{\theta 3} \\ \underline{g}_{\theta 4} \end{bmatrix} - \begin{bmatrix} \underline{0} \\ \underline{0} \\ \underline{\tau}_{k,1} \\ \underline{\tau}_{k,2} \\ \underline{\tau}_{k,3} \\ \underline{\tau}_{k,4} \end{bmatrix} = \begin{bmatrix} \underline{f}_x \\ \underline{f}_\phi \\ \underline{\tau}_{e,1} \\ \underline{\tau}_{e,2} \\ \underline{\tau}_{e,3} \\ \underline{\tau}_{e,4} \end{bmatrix} \tag{4.24}$$

$$\begin{bmatrix} \boldsymbol{J}_1 & \boldsymbol{0} & \boldsymbol{0} & \boldsymbol{0} \\ \boldsymbol{0} & \boldsymbol{J}_2 & \boldsymbol{0} & \boldsymbol{0} \\ \boldsymbol{0} & \boldsymbol{0} & \boldsymbol{J}_3 & \boldsymbol{0} \\ \boldsymbol{0} & \boldsymbol{0} & \boldsymbol{0} & \boldsymbol{J}_4 \end{bmatrix} \begin{bmatrix} \ddot{\underline{\theta}}_{M1} \\ \ddot{\underline{\theta}}_{M2} \\ \ddot{\underline{\theta}}_{M3} \\ \ddot{\underline{\theta}}_{M4} \end{bmatrix} + \begin{bmatrix} \underline{\tau}_{k,1} \\ \underline{\tau}_{k,2} \\ \underline{\tau}_{k,3} \\ \underline{\tau}_{k,4} \end{bmatrix} = \begin{bmatrix} \underline{\tau}_{a,1} \\ \underline{\tau}_{a,2} \\ \underline{\tau}_{a,3} \\ \underline{\tau}_{a,4} \end{bmatrix} - \begin{bmatrix} \underline{\tau}_{f,1} \\ \underline{\tau}_{f,2} \\ \underline{\tau}_{f,3} \\ \underline{\tau}_{f,4} \end{bmatrix} \tag{4.25}$$

where the vectors of spring torques are defined by

$$\underline{\tau}_{k,i} = \boldsymbol{K}_i(\underline{\theta}_{Mi} - \underline{\theta}_i) \tag{4.26}$$

The applied torques on the rotors are proportional to the current in the motor,

$$\underline{\tau}_{a,i} = \boldsymbol{K}_{t,i}\underline{I}_i \tag{4.27}$$

where $\boldsymbol{K}_{t,i}$ is a diagonal matrix of terms $n_{i,j}k_{t,i,j}$ where $k_{t,i,j}$ is the torque constant of the motor, and $\underline{I}_i$ is the vector with currents for the motors of leg $i$. A simple model for the dynamics of a DC-motor is

$$u_{i,j} = l_{i,j}\dot{I}_i^{(j)} + r_{i,j}I_i^{(j)} + n_{i,j}k_{emf,i,j}\dot{\theta}_{Mi}^{(j)} \tag{4.28}$$

where $l_{i,j}$ is the inductance, $r_{i,j}$ the resistance and $k_{emf,i,j}$ the back electro-motive constant, respectively, for each motor in joint $j$ of leg $i$.

# 5. STABILITY OF STATICALLY BALANCED GAITS

A common assumption in statically stable walking is to neglect the effect of inertial forces acting on the robot. This is motivated by the relatively slow speed of statically stable gaits, in which case, gravitational forces are more dominating than motion dependent forces. The strategy is then to maintain the vertical projection of the center of gravity within the support area at all times, i.e. the area formed by the feet in ground contact, otherwise there would be an uncompensated moment acting around an edge of the support area that could cause the robot to tip over. However, if the vertical projection of the center of gravity is sufficiently close to an edge of the support area, a small momentum of the robot, an external force, or uncertainties in the exact position of the center of gravity, may be sufficient to tip the robot over. The loss of stability may cause a walking robot to fail to move as desired by the operator. A minor failure would be when the loss of stability results in a disruption of the gait in order to regain balance, for instance, by changing the timing or sequence in which the feet are lifted or set down, or by shifting the body in an unplanned manner. A more severe failure is when the robot tips over on its side, risking damage to itself and its surroundings. In order to reduce the risk of the robot losing stability while walking, a measure for the stability of the robot can be used in the gait and motion planning, in order to avoid or detect that the robot could become instable.

The aim of this chapter is to develop a stability measure, that can be used in planning a statically balanced motion for the robot. This measure will be based on determining the distance that the vertical projection of the center of gravity of the

robot, has to maintain relative to an edge of the support area. This distance is based on that the neglected inertial and external forces, acting on the robot, will not be able to tip the robot over. Section 5.1 will review some of the stability measures that have been proposed for walking robots. Section 5.2 will provide the basic theory necessary for the derivation of the stability measure. Section 5.3 will provide a basic relationship for the position of the vertical projection of the center of gravity of the robot, relative to an edge of the support area, in order for a robot to be statically balanced. The distance of the vertical projection of the center of gravity to an edge is proposed as a measure of the stability of the robot. Finally, sections 5.4 and 5.5 will show how the stability measure can be used in the motion planning and provide a simple example, respectively.

## 5.1. Stability measures

A natural (i.e. untripped or unforced) tipover of the vehicle will always occur about an edge of the support area, whereas tripped tipover of the vehicle occurs when one of the ground contact points encounters an obstacle or a sudden change in ground conditions (Papadopoulos, and Rey, 1996). McGhee, and Frank (1968) proposed to use the shortest distance from the vertical projection of the center of gravity onto a horizontal plane, to an edge of the convex polygon formed by the vertical projection of the feet contact points onto the same horizontal plane, that they call the *stability margin*. The stability margin is a measure of how large the neglected forces may be without the robot tipping over. However, the measure does not take into account top heaviness, i.e. the higher the position of the center of gravity of the robot, the greater the risk of tipping over. Furthermore, the shortest horizontal distance is only approximative when walking in uneven terrain, as then the edges of the support area, around which the robot would tip over, are not in a horizontal plane.

Messuri, and Klein (1985) proposed the *energy stability margin* (ESM), which is based on the minimum amount of work required to tip the robot over an edge of the support area. The ESM is defined as the difference between the current potential energy of the robot's center of gravity (CoG) and its maximum potential energy when the robot rotates rigidly around an edge on a circular path, i.e. $ESM = ma_G(h_{max} - h)$, where $m$ is the total mass of the robot, $h$ the vertical height of the center of gravity above the edge, and $h_{max}$ is the maximum height of

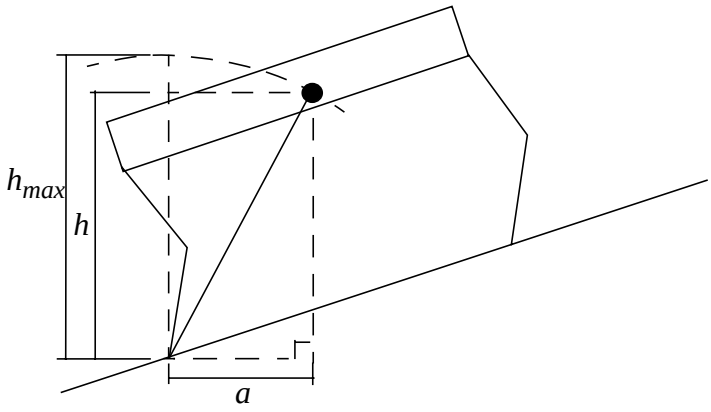


*Figure 5.1. The shortest horizontal distance (stability margin) (a) to an edge, and the ESM = $ma_G(h_{max}-h)$ stability measure.*

the center of gravity above the edge. The ESM is a function of the height, the distance to the edge, and the weight of the robot, where the last mentioned, results in that the ESM predicts that the robot is more stable the heavier it is. Hirose, et al. (2001) proposed to use the normalized ESM where the ESM is divided by the robot's weight, and is motivated by that the inertial and other forces, acting on the robot, will probably also increase with the weight of the robot. Nagy, et al. (1994) proposed, as an extension to the ESM, the *compliant static stability margin* (CSSM) in which the compliance of the robot and the ground is taken into account. The motivation is that when the robot starts to rotate around an edge, the whole weight of the robot is transferred to the two legs forming the edge. The compliance of the ground, or the legs, would then lower the maximum height of the CoG which means that the actual work needed to tip over the robot is less than predicted by the ESM. Ghasempoor, and Sepheri (1995) proposed another extension to the ESM by including the effect of inertial and external forces. Papadopoulos, and Rey (1996) proposed a different approach, called the *force-angle stability margin*. This measure is based on the magnitude of the resultant force acting on the CoG, and the angle it makes with the shortest line connecting the edge and the CoG. If the angle is zero the resultant force is pointing at the edge, meaning that only the two feet forming the edge are supporting the forces acting on the robot.

Lin, and Song (1993), proposed the dynamic stability margin (DSM), which is based on the moments acting around an edge of support area, and normalized by

the weight of the robot. The dynamic stability margin is defined as

$$min\frac{M_i}{W} \tag{5.1}$$

where $W$ is the total weight of the robot and $M_i$ is the resultant moment about edge $i$ due to external, gravitational, and inertial forces and moments, where a negative $M_i$ will turn the robot over the edge, in which case the robot is instable. The DSM has the unit of length and must be positive in order for the robot to be stable.

For biped robots, and other robots, that rely more on dynamic stability, it is necessary to take into account the inertial forces acting on the robot. In order to plan a stable motion, the zero moment point (ZMP) has been used extensively (Vukobratovic, and Stepanenko, 1972; Shih, et al., 1990; Yamaguchi, et al., 1993; Yoneda, and Hirose, 1995; Ito, and Kawasaki, 2000; Kurazume, et al., 2001; Takeuchi, 2001). There exists, however, several different definitions of the ZMP, as discussed by Goswami (1999), and he argues that ZMP is in fact equivalent to the center of pressure (CoP), discussed in the next section, which has also been used in a similar fashion as the ZMP (Kang, et al., 1997; Hirai, et al.,1998; Nelson, and Quinn, 1998; Silva, and Machado, 2001). Nevertheless, the ZMP and CoP are not stability measures, but are used in order to plan the robot's motion trajectories, which must fulfill the condition that the ZMP (or the CoP), calculated from the motion dependent forces and gravity, is within the boundary of the support area. Otherwise, the ground reaction forces would not be able to support the robot and it would fall. Goswami (1999) proposed to use the *foot rotation indicator* (FRI) to provide a stability measure for the planning of motion trajectories for biped robots. The FRI is the point on the foot/ground contact surface where the net ground reaction force would have to act to keep the foot stationary. If the FRI moves outside the support area, it is an indication that the robot will start to fall. The distance from the FRI to the boundary of the support area is then a measure of the stability of the robot.

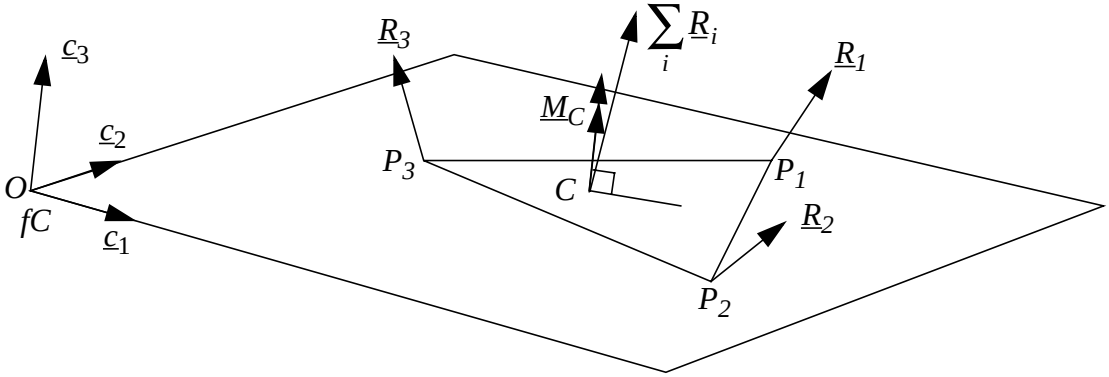


*Figure 5.2. The center of pressure (point C) for ground reaction forces acting at three points, $P_1$, $P_2$ and $P_3$, in a plane.*

## 5.2. The center of pressure

The basic assumptions for the following work is that the feet of the robot are point contacts, such that only a force and no moment is transmitted between the ground and a foot. Furthermore, the stability analysis will only deal with the rotational equilibriums, i.e. that the robot will tip over an edge of the support area, and not translational equilibrium, i.e. whether the robot is sliding, where the assumption is that the friction between the feet and ground is sufficient to prevent any sliding.

Let $\underline{F}_G$ and $\underline{M}_G$ be the resultant force and moment, respectively, acting at the CoG, due to the inertial and external forces and moments. The total resultant force, acting at the CoG, is then $\underline{F}_G + m\underline{\gamma}$, where $m$ is the total mass of the robot, and $\underline{\gamma}$ is the gravity vector. The moment balance equation for point $N$ is then

$$\sum_i \underline{r}_i^{NP} \times \underline{R}_i + \underline{r}^{NG} \times (\underline{F}_G + m\underline{\gamma}) + \underline{M}_G = \underline{0} \tag{5.2}$$

where point $G$ is the position of the CoG. The resultant force $\underline{F}_G$ acting at the CoG is given by

$$\underline{F}_G = -m_B \underline{a}^{NB} - \sum_{i,j} m_{i,j} \underline{a}_{i,j}^{NL} + \sum_i \underline{F}_{E,i} \tag{5.3}$$

where $\underline{F}_{E,i}$ is an external force acting on the robot, $\underline{a}^{NB}$ and $\underline{a}_{i,j}^{NL}$ are the accelera-

tion of the body and the linkages of the robot, respectively, given by

$$\underline{a}^{NB} = {}^{N}\frac{d^2\underline{r}^{NB}}{dt^2} \qquad \underline{a}^{NL}_{i,j} = {}^{N}\frac{d^2\underline{r}^{NL}_{i,j}}{dt^2} \tag{5.4}$$

The resulting moment $\underline{M}_G$ acting at the CoG is

$$\underline{M}_G = -{}^{N}\frac{d\underline{H}_G}{dt} + \sum_i (\underline{M}_{E,i} + \underline{r}^{GE}_i \times \underline{F}_{E,i}) \tag{5.5}$$

where $\underline{M}_{E,i}$ is the external moment acting on the robot, the point $E_i$ is where the external force $\underline{F}_{E,i}$ acts, and $\underline{H}_G$ is the angular momentum around the CoG,

$$\underline{H}_G = \boldsymbol{I}_B {}^{N}\underline{\omega}^{B} + \sum_{i,j} \boldsymbol{I}_{i,j} {}^{N}\underline{\omega}^{L}_{i,j} + \sum_{i,j} \underline{r}^{GL}_{i,j} \times m_{i,j}\underline{v}^{NL}_{i,j} \tag{5.6}$$

As mentioned in section 5.1, the *center of pressure* (CoP) and the *zero moment point* have been used extensively to plan stable motion for walking robots. They are defined as points in a plane, which is usually called the ground, and assumed to be planar. To define a plane, let frame *fC* be defined such that the first and second axis, $\underline{c}_1$ and $\underline{c}_2$ respectively, lie in the plane where the CoP (or the ZMP) should be found, and the third axis, $\underline{c}_3$, is normal to the plane, as shown in figure 5.2. The plane does not necessarily have to be horizontal, but let its normal $\underline{c}_3$ be defined as pointing upwards, opposite the direction of the gravity vector, such that $\underline{c}_3 \cdot \underline{\gamma} < 0$. Furthermore, let *O* be defined as a stationary point in the plane.

Goswami (1999) defines the *center of pressure* (CoP) as the point in a plane where the resultant of the ground reaction forces acts. In other words, the CoP is the point where the resultant of the ground reaction forces $\sum \underline{R}_i$ should act to provide the same moment, around some point, as the sum of the moments of the ground reaction forces. To provide the same moment as the ground reaction forces, the resultant of the ground reaction forces can act anywhere along a line of action. The CoP is then the point where the line of action intersects the ground. The problem of finding the CoP can be formulated as

$$\begin{aligned} \underline{r}^{OC} \times \sum_i \underline{R}_i &= \sum_i \underline{r}^{OP}_i \times \underline{R}_i \\ \underline{c}_3 \cdot \underline{r}^{OC} &= 0 \end{aligned} \tag{5.7}$$

where the point *C* denotes the CoP. The solution to equation (5.7) for the position of the CoP relative to point *O*, using the property of the cross product that $\underline{x} \times (\underline{y} \times \underline{z}) = (\underline{x} \cdot \underline{z})\underline{y} - (\underline{x} \cdot \underline{y})\underline{z}$, is

$$\underline{r}^{OC} = \frac{1}{\left(\underline{c}_3 \cdot \sum_i \underline{R}_i\right)} \underline{c}_3 \times \left(\sum_i \underline{r}_i^{OP} \times \underline{R}_i\right) \tag{5.8}$$

The resultant moment due to the ground reaction forces around the CoP, i.e. around point *C*, is

$$\underline{M}_C = \sum_i \underline{r}_i^{CP} \times \underline{R}_i = \frac{\left(\left(\sum_i \underline{R}_i\right) \cdot \left(\sum_i \underline{r}_i^{OP} \times \underline{R}_i\right)\right)}{\left(\underline{c}_3 \cdot \sum_i \underline{R}_i\right)} \underline{c}_3 \tag{5.9}$$

The resulting moment has therefore only a component normal to the plane, i.e. the resulting moment at the CoP is only acting around the normal of the plane, as shown in figure 5.2.

Arakawa, and Fukuda (1997) define the ZMP as the point on the ground where the moment generated by the ground reaction forces and torques, only has a component that is orthogonal the ground, i.e. the moment at the ZMP only acts around the normal to the plane. However, as equation (5.9) shows, the CoP has exactly this property, in which case, according to the above definition of the ZMP, the ZMP and the CoP are equivalent, as stated in Goswami (1999).

In the case that all the feet are in the same plane as point *O*, i.e. if $\underline{c}_3 \cdot \underline{r}_i^{OP} = 0$, the CoP in equation (5.8) is equal to

$$\underline{r}^{OC} = \frac{1}{\left(\underline{c}_3 \cdot \sum_i \underline{R}_i\right)} \sum_i (\underline{c}_3 \cdot \underline{R}_i)\underline{r}_i^{OP} \tag{5.10}$$

which is the equation for the position of the CoP as put forth by Goswami (1999). In this case, the center of pressure will always be within or on the edge of the convex polygon formed by the feet in ground contact, and can not move outside it.

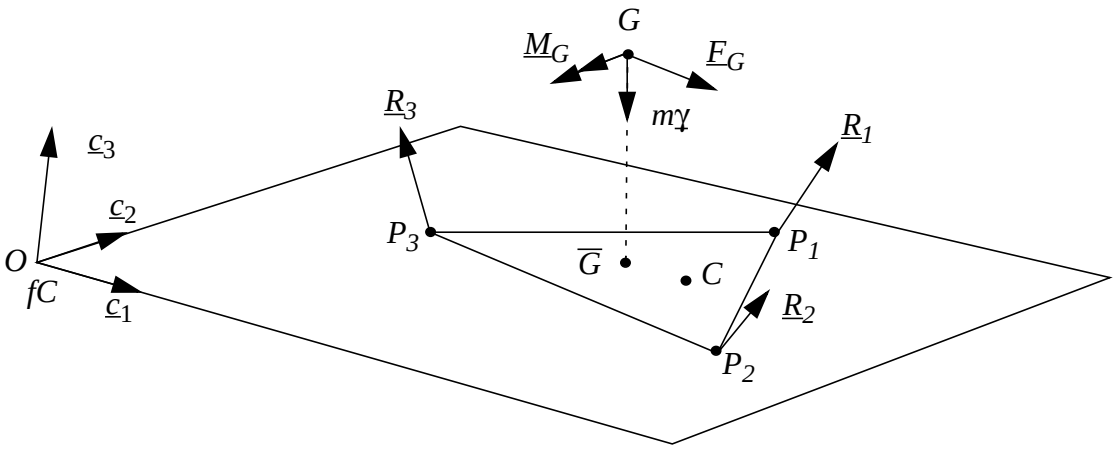


*Figure 5.3. The forces and moments acting at the center of gravity.*

This is a direct result of that the foot/ground contact is unilateral as a foot can only press on the ground but not pull, in other words, the ground reaction force normal to the ground can never be negative, $\underline{c}_3 \cdot \underline{R}_i \geq 0$. The CoP can in this case be seen as the weighed average of the foot positions, where the magnitude of the normal force, acting at each foot, is used as a weighing factor.

If there are no inertial or external forces acting on the robot, it can be shown that the CoP is equal to the vertical projection of the center of gravity onto the ground plane, i.e. the projection in the direction of the gravity vector. For shortness let PCoG denote the vertical projection of the center of gravity onto the ground plane. The moment balance equation for point *O* can be expressed as

$$\sum_i \underline{r}_i^{OP} \times \underline{R}_i = -\underline{r}^{OG} \times (\underline{F}_G + m\underline{\gamma}) - \underline{M}_G \tag{5.11}$$

and the force balance equation, in the direction of the normal $\underline{c}_3$ to the plane, can be expressed as

$$\underline{c}_3 \cdot \sum_i \underline{R}_i = -\underline{c}_3 \cdot (\underline{F}_G + m\underline{\gamma}) \tag{5.12}$$

Inserting the left hand side of equations (5.11) and (5.12) into equation (5.8), and using the relationship $\underline{r}^{OG} = \underline{r}^{O\overline{G}} + \underline{r}^{\overline{G}G}$, where point $\overline{G}$ is the position of PCoG,

the position of the CoP is

$$\underline{r}^{OC} = \underline{r}^{O\bar{G}} + \frac{\underline{c}_3 \times (\underline{M}_G + \underline{r}^{\bar{G}G} \times \underline{F}_G)}{(\underline{c}_3 \cdot (\underline{F}_G + m\underline{\gamma}))} \tag{5.13}$$

where the relation $\underline{r}^{\bar{G}G} \times \underline{\gamma} = \underline{0}$ has been used. Equation (5.13) shows that if the resultant force and moment, due to inertial and external forces, are equal to zero, i.e. if $\underline{M}_G = \underline{0}$ and $\underline{F}_G = \underline{0}$, then the CoP will equal the PCoG. For comparison, the CoP calculated using the ground reaction forces in equation (5.8), can be expressed as

$$\underline{r}^{OC} = \underline{r}^{O\bar{G}} + \frac{\underline{c}_3 \times \left( \sum_i \underline{r}_i^{\bar{G}P} \times \underline{R}_i \right)}{\left( \underline{c}_3 \cdot \sum_i \underline{R}_i \right)} \tag{5.14}$$

It should be noted that the denominator $\underline{c}_3 \cdot (\underline{F}_G + m\underline{\gamma})$ of the second term in equation (5.13) is always less than zero, i.e. $\underline{c}_3 \cdot (\underline{F}_G + m\underline{\gamma}) < 0$ is always true if the feet are in ground contact. This can be seen from the force balance equation for the forces normal to the plane in equation (5.12). If $\underline{c}_3 \cdot (\underline{F}_G + m\underline{\gamma}) > 0$, the sum of the ground reaction forces normal to the plane would have to be less than zero, i.e. $\underline{c}_3 \cdot \sum_i \underline{R}_i < 0$. That would, however, contradict the fact that the component of the ground reaction forces normal to the plane is always greater than or equal to zero. If $\underline{c}_3 \cdot (\underline{F}_G + m\underline{\gamma}) = 0$, the normal component of the ground reaction forces would also equal zero, in which case the CoP is not defined.

## 5.3. The center of pressure and stability

Generally, when there are four feet or more in support, it is not possible to define a plane such that all the feet, that are in ground contact, are in the same plane. The edges that the robot may tip over are therefore not in the same plane but will form the boundary of a more general surface. The *support surface* will be defined as the convex surface, which boundary is formed by the lines connecting the feet ground contact points, i.e. the surface is formed by the edges around which the robot can tip over. The form of the interior of the surface is unimportant, however, in order for the robot to be statically stable, the vertical projection of the center of gravity must cut the surface within its boundary.

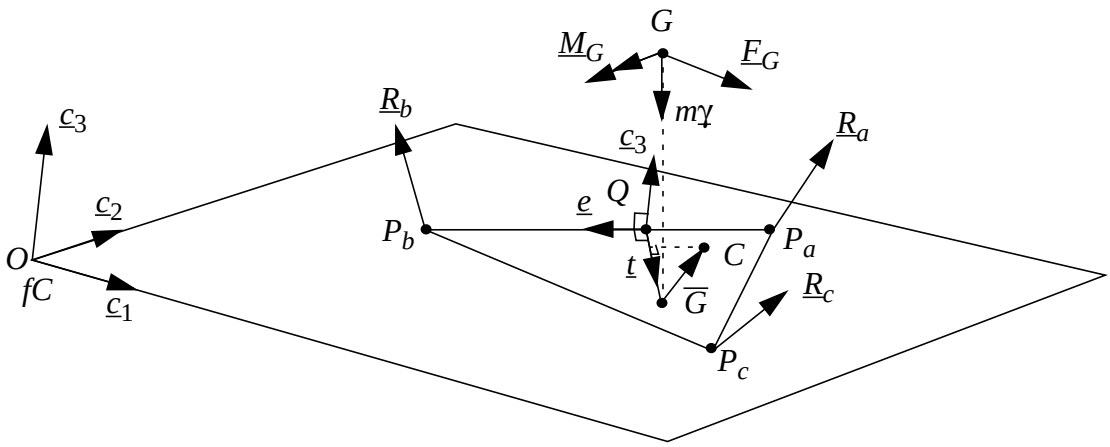


*Figure 5.4. The distance of the center of pressure from the edge formed by points $P_a$ and $P_b$.*

If the CoP is on an edge of the support surface, the forces acting on the robot are only being supported by the two feet that form the edge. In other words, the other feet are not really in ground contact and are not providing support to the robot. The robot would therefore be balancing on only two supporting legs, which violates the necessary condition for statically stable gaits to maintain at least three feet in ground contact at all times, and increases the risk of the robot tipping over. The criteria that will be proposed here for the stability of the robot, is that the CoP must be inside the boundary of the support surface and not on its boundary. The shortest distance from an edge of the support surface to the PCoG will be used as a measure of the stability of the robot, as it indicates how large the moment around the edge can be, due to inertial and external forces, without the CoP being on the boundary of the support surface

In order to examine the stability of the robot around a certain edge of the support surface, a plane in which the CoP should be found, is defined such that the two contact points forming the edge lie in the plane. In order to completely define the plane, a third point is needed and it is chosen as the contact point of a foot that is supposed to be in ground contact when walking statically stable. This plane will be referred to as the *ground plane*. Let the contact points be denoted as $P_a$, $P_b$, and $P_c$ in an anti-clockwise manner, as depicted in figure 5.4, where points $P_a$ and $P_b$ form the edge to be investigated. Let $\underline{e}$ be a unit vector, parallel with the edge, with a

direction such that a positive moment around the vector $\underline{e}$ will try to tip the robot over the edge, i.e. in the case shown in figure 5.4, $\underline{e} = \underline{r}^{P_aP_b} / \left\| \underline{r}^{P_aP_b} \right\|$.

The unit vector $\underline{c}_3$, normal to the ground plane can be found from

$$\underline{c}_3 = \frac{\underline{r}^{P_aP_b} \times \underline{r}^{P_aP_c}}{\left\| \underline{r}^{P_aP_b} \times \underline{r}^{P_aP_c} \right\|} \tag{5.15}$$

where it should noted that $\underline{c}_3$ points upwards, i.e. opposite to, but not necessarily parallel with the gravity vector, such that $\underline{c}_3 \cdot \underline{\gamma} < 0$. Furthermore, let $\underline{t}$ be a unit vector, orthogonal to the edge and to vector $\underline{c}_3$, pointing into the support surface,

$$\underline{t} = \underline{c}_3 \times \underline{e} \tag{5.16}$$

Finally, let point $Q$ be defined as the point on the edge closest to the PCoG, such that $\underline{r}^{Q\bar{G}} = \Lambda \underline{t}$, where $\Lambda$ is the distance from the edge to the PCoG and $\Lambda$ is positive if PCoG is inside the support surface, zero if PCoG is on the edge, and negative otherwise. From equation (5.13), the position of the CoP relative to the point $Q$ is

$$\underline{r}^{QC} = \underline{r}^{Q\bar{G}} + \frac{\underline{c}_3 \times (\underline{M}_G + \underline{r}^{\bar{G}G} \times \underline{F}_G)}{\underline{c}_3 \cdot (\underline{F}_G + m\underline{\gamma})} \tag{5.17}$$

If the CoP is to be within the support surface and not on the edge, the dot product of the vectors $\underline{r}^{QC}$ and $\underline{t}$ must be positive, i.e.

$$\underline{t} \cdot \underline{r}^{QC} = \Lambda + \frac{\underline{e} \cdot (\underline{M}_G + \underline{r}^{\bar{G}G} \times \underline{F}_G)}{\underline{c}_3 \cdot (\underline{F}_G + m\underline{\gamma})} > 0 \tag{5.18}$$

where the relationships $\underline{x} \cdot (\underline{y} \times \underline{z}) = (\underline{x} \times \underline{y}) \cdot \underline{z}$ and $\underline{e} = \underline{t} \times \underline{c}_3$ were applied. Equation (5.18) provides a constraint on the position of the PCoG relative to an edge, which in turn, provides a constraint on the motion of the CoG, that can be used in the motion planning for the robot.

An alternative approach to derive equation (5.18) is to use the moment balance equation around point $Q$, which is

$$\underline{M}_G + \underline{r}^{QG} \times (\underline{F}_G + m\underline{\gamma}) + \sum_i \underline{r}_i^{QP} \times \underline{R}_i = \underline{0} \tag{5.19}$$

Using that $\underline{r}^{QG} = \underline{r}^{Q\bar{G}} + \underline{r}^{\bar{G}G} = \Lambda\underline{t} + \underline{r}^{\bar{G}G}$ and $\underline{r}^{\bar{G}G} \times \underline{\gamma} = \underline{0}$, equation (5.19) can be rewritten as

$$\underline{M}_G + \underline{r}^{\bar{G}G} \times \underline{F}_G + \Lambda\underline{t} \times (\underline{F}_G + m\underline{\gamma}) + \sum_i \underline{r}_i^{QP} \times \underline{R}_i = \underline{0} \tag{5.20}$$

As point $Q$ is on the edge of the support surface, the moment balance equation around the edge can be found by projecting the moments around point $Q$ onto the vector $\underline{e}$, i.e. the vector along the edge. Using the relationships $\underline{x} \cdot (\underline{y} \times \underline{z}) = (\underline{x} \times \underline{y}) \cdot \underline{z}$ and $\underline{c}_3 = \underline{e} \times \underline{t}$, the dot product of $\underline{e}$ with equation (5.20) is

$$\underline{e} \cdot (\underline{M}_G + \underline{r}^{\bar{G}G} \times \underline{F}_G) + \Lambda\underline{c}_3 \cdot (\underline{F}_G + m\underline{\gamma}) + \sum_i (\underline{e} \times \underline{r}_i^{QP}) \cdot \underline{R}_i = 0 \tag{5.21}$$

The position of the feet relative to point $Q$ can, if all the feet lie in the ground plane, be expressed as

$$\underline{r}_i^{QP} = (\underline{e} \cdot \underline{r}_i^{QP})\underline{e} + (\underline{t} \cdot \underline{r}_i^{QP})\underline{t} \tag{5.22}$$

and the last term on the left hand side of equation (5.21) can be expressed as

$$\sum_i (\underline{e} \times \underline{r}_i^{QP}) \cdot \underline{R}_i = \sum_i (\underline{t} \cdot \underline{r}_i^{QP})(\underline{c}_3 \cdot \underline{R}_i) \tag{5.23}$$

For the two feet ground contact points, that form the edge, the foot positions fulfill that $(\underline{t} \cdot \underline{r}_i^{QP}) = 0$, as the feet lie on the edge, along the direction of vector $\underline{e}$. For the feet that do not form the edge, the foot position vector fulfills $(\underline{t} \cdot \underline{r}_i^{QP}) > 0$, as the support surface is convex and the vector $\underline{t}$ points into the support surface. The sum in equation (5.23) depends therefore only on the position and the normal component of the ground reaction forces of the feet that do not form the edge. In order for the robot to be statically stable, i.e. that the foot or the feet that do not form the edge are in ground contact, equation (5.23) has to fulfill that

$$\sum_i (\underline{t} \cdot \underline{r}_i^{QP})(\underline{c}_3 \cdot \underline{R}_i) > 0 \tag{5.24}$$

which in turn leads to, using equation (5.21), that

$$\underline{e} \cdot (\underline{M}_G + \underline{r}^{\bar{G}G} \times \underline{F}_G) + \Lambda \underline{c}_3 \cdot (\underline{F}_G + m\underline{\gamma}) < 0 \tag{5.25}$$

Using that $\underline{c}_3 \cdot (\underline{F}_G + m\underline{\gamma}) < 0$, it can be shown that equation (5.25) is equivalent with equation (5.18). Equation (5.25), and consequently equation (5.18), states that the projection of the sum of the moments around point *Q*, onto the vector $\underline{e}$, due to gravitational, inertial and external forces, has to be less than zero in order for the CoP not to be on the edge of the support surface. In other words, as expected, the moment around the edge has to be directed such that it will push the robot down on the feet that do not form the edge.

The approach is now to select the distance of the PCoG from the edge such that equation (5.18) is fulfilled, by choosing

$$\Lambda > \frac{\underline{e} \cdot (\underline{M}_G + \underline{r}^{\bar{G}G} \times \underline{F}_G)}{-\underline{c}_3 \cdot (\underline{F}_G + m\underline{\gamma})} \tag{5.26}$$

The term $\underline{e} \cdot (\underline{M}_G + \underline{r}^{\bar{G}G} \times \underline{F}_G)$ is the moment which could potentially tip the robot over the edge, i.e. the term is the potentially destabilizing moment. The term $\underline{c}_3 \cdot (\underline{F}_G + m\underline{\gamma}) < 0$ is the magnitude of the force acting normal to the ground plane, that is pushing the robot down onto the ground plane. The distance $\Lambda$ is the moment arm for the normal force around the edge, and by increasing $\Lambda$, the effect of the potentially destabilizing moment is reduced. The variable $\Lambda$ is therefore a measure of how large the potentially destabilizing moments around the edge may be without destabilizing the robot, and hence $\Lambda$ will be referred to as the *support stability indicator (SSI)*, and will be used in the subsequent chapters as a stability measure to plan a statically balanced motion for the robot, as will be explained in the next chapter.

Note that $\Lambda$ does not necessarily have to be larger than zero, i.e. the PCoG can be outside the support surface, while the CoP remains within, under certain force conditions. In that case the robot would be leaning into the forces acting on it, but still not risking to tip over. However, static stability demands that the PCoG should be within the support surface at all times, so the robot will not be statically stable if $\Lambda \leq 0$. Nevertheless, in some special circumstances, for instance when there are

large external forces acting on the robot, it might be necessary for the robot to move the PCoG out of the support surface in order to avoid tipping over.

## 5.4. The support stability margin

To use the support stability indicator in the motion planning, the *support stability margin* (SSM) is defined as a lower bound on the distance from the PCoG to an edge of the support surface, such that

$$\Lambda \geq \Lambda_m > \frac{\underline{e} \cdot (\underline{M}_G + \underline{r}^{\bar{G}G} \times \underline{F}_G)}{-\underline{c}_3 \cdot (\underline{F}_G + m\underline{\gamma})} \tag{5.27}$$

where $\Lambda_m$ denotes the SSM. The SSM is determined based on the magnitude of the forces and moments that the robot should be able to withstand, the height of the CoG above the ground plane and the attitude of the ground plane. To show how the SSM is dependent on the height of the CoG and the attitude of the ground plane, let frame *fC* be defined through a chain of simple rotations from world frame *fN*, such that the third axis of *fC* is normal to the ground plane. Let $\underline{\phi}_c \in \Re^3$ be a vector with the rotations between frame *fN* and *fC*, such that, the first rotation $\phi_c^{(1)}$ is around the third (vertical) axis of *fN*, the second rotation $\phi_c^{(2)}$ is around the second axis, and the third rotation $\phi_c^{(3)}$ is around the first axis. The corresponding rotation matrix between *fC* and *fN* will be denoted ${}^C\boldsymbol{R}^N(\underline{\phi}_c)$, and has the same structure as the transpose of the rotation matrix ${}^N\boldsymbol{R}^B$ in equation (3.2) in section 3.1. The gravity vector $\underline{\gamma}$ and the vector $\underline{r}^{\bar{G}G}$ can be expressed in *fN* as ${}^N\underline{\gamma} = \begin{bmatrix} 0 & 0 & -a_G \end{bmatrix}^T$ and ${}^N\underline{r}^{\bar{G}G} = \begin{bmatrix} 0 & 0 & h \end{bmatrix}^T$, respectively, where $a_G$ and $h$ are the acceleration of gravity and the height of the CoG above its vertical projection on the ground plane, respectively. The vectors can be expressed as

$$\underline{\gamma} = -a_G \underline{n}_3 \tag{5.28}$$

$$\underline{r}^{\bar{G}G} = h\underline{n}_3 \tag{5.29}$$

where $\underline{n}_3$ is the vector defining the third axis of *fN*, and is equal to the third column of the rotation matrix, ${}^C\boldsymbol{R}^N(\underline{\phi}_c)$, when expressed in *fC*,

$${}^C\underline{n}_3 = \begin{bmatrix} -s\phi_c^{(2)} & c\phi_c^{(2)}s\phi_c^{(3)} & c\phi_c^{(2)}c\phi_c^{(3)} \end{bmatrix}^T \tag{5.30}$$

where $c\phi_c^{(j)} = \cos\phi_c^{(j)}$ and $s\phi_c^{(j)} = \sin\phi_c^{(j)}$. The vector ${}^C\underline{n}_3$ is only a function of $\phi_c^{(2)}$ and $\phi_c^{(3)}$, which are the rotations that define the attitude of the ground plane relative to the gravity vector. Equation (5.26) can now be expressed as

$$\Lambda > \frac{\underline{e} \cdot \underline{M}_G + h(\underline{F}_G \times \underline{e}) \cdot \underline{n}_3}{ma_G(\underline{c}_3 \cdot \underline{n}_3) - (\underline{c}_3 \cdot \underline{F}_G)} \tag{5.31}$$

The dot product of vectors $\underline{n}_3$ and $\underline{c}_3$ has the property that

$$0 \leq (\underline{c}_3 \cdot \underline{n}_3) = {}^C n_3^{(3)} = c\phi_c^{(2)} c\phi_c^{(3)} \leq 1 \tag{5.32}$$

where $(\underline{c}_3 \cdot \underline{n}_3) = 1$ if the ground plane is horizontal.

The term including the resultant force acting at the CoG, $\underline{F}_G$, in the numerator can be expanded to

$$(\underline{F}_G \times \underline{e}) \cdot \underline{n}_3 = (\underline{F}_G \cdot \underline{c}_3)(\underline{t} \cdot \underline{n}_3) - (\underline{F}_G \cdot \underline{t})(\underline{c}_3 \cdot \underline{n}_3) \tag{5.33}$$

The term $(\underline{F}_G \cdot \underline{c}_3)$ is the force component acting normal to the ground plane and term $(\underline{F}_G \cdot \underline{t})$ is the force component acting along the direction of vector $\underline{t}$, tangential to the ground plane and orthogonal to the edge and vector $\underline{e}$.

The support stability margin will be based on a worst-case situation, which is when the resultant force and moment are directed such that they will try tipping the robot over. The worst case for the denominator of the right hand side of equation (5.31) is that the force acting normal to the ground plane is positive, i.e. if $(\underline{F}_G \cdot \underline{c}_3) > 0$. The worst case for the tangential part of the force is when it is directed opposite the vector $\underline{t}$, i.e. if $-(\underline{F}_G \cdot \underline{t}) > 0$. The worst case for the resultant moment is that $(\underline{M}_G \cdot \underline{e}) > 0$. The SSM will therefore be defined as

$$\Lambda_m = \frac{|\underline{M}_G|_{max} + h((\underline{n}_3 \cdot \underline{t})|\underline{F}_{G,n}|_{max} + {}^C n_3^{(3)}|\underline{F}_{G,t}|_{max})}{ma_G {}^C n_3^{(3)} - |\underline{F}_{G,n}|_{max}} \tag{5.34}$$

where the vectors $\underline{n}_3$ and $\underline{t}$ are known. The term $|\underline{M}_G|_{max}$ is the maximum moment acting around the edge, and the terms $|\underline{F}_{G,n}|_{max}$ and $|\underline{F}_{G,t}|_{max}$ are the maximum forces normal and tangential to the ground plane, respectively, and are set based on how large inertial and external forces the robot should be able to withstand. Instead

of using vertical height $h$ of the CoG above the ground plane, it is possible to use equation (5.29) to find the height of the CoG $h_n$, normal to the plane, using that

$$h_n = {}^{C}r^{\bar{G}G(3)} = h\,{}^{C}n_3^{(3)} \tag{5.35}$$

The support stability margin is then defined by

$$\Lambda_m = \frac{\left|\underline{M}_G\right|_{max} + h_n((\underline{n}_3 \cdot \underline{t})\left|\underline{F}_{G,n}\right|_{max} / {}^{C}n_3^{(3)} + \left|\underline{F}_{G,t}\right|_{max})}{ma_G\,{}^{C}n_3^{(3)} - \left|\underline{F}_{G,n}\right|_{max}} \tag{5.36}$$

The effect of the destabilizing forces and moments in the numerator of equations (5.35) and (5.36), is therefore dependent on the height of the CoG above the ground plane and the attitude of the ground plane. The restoring force, in the denominator of equations (5.35) and (5.36), is affected by the attitude of the ground plane, and has a maximum when the ground plane is horizontal.

The support stability margin will be used as a stability measure to plan a statically stable body motion for the robot, as will be described in chapter 6. Compared to the stability measures presented in section 5.1, the support stability indicator is more general than the shortest horizontal distance, proposed by McGhee, and Frank (1968), as the plane does not have to be horizontal and the height of the robot is taken into account. Compared to the energy stability margin of Messuri, and Klein (1985), the SSI is more conservative as it indicates when the feet, that are not forming the edge considered, will lose ground contact, whereas the ESM indicates when the robot will tip over on its side. For that reason the support stability indicator is more suitable than the ESM, as statically stable motion can only be planned if at least three legs are in ground contact. Compared to the foot rotation indicator (FRI) of Goswami (1999), the support stability indicator specifies where the CoG must be located to provide a restoring moment around an edge, making it suitable for planning body motion, whereas the FRI only indicates where the resultant of the ground reaction forces will have to act.

The SSM is somewhat related to the dynamic stability margin (DSM) of Lin, and Song (1993), shown in equation (5.1). The moment $M_i$ around an edge $i$, can be can

be expressed as

$$M_i = -\underline{e}_i \cdot (\underline{M}_G + \underline{r}^{QG} \times (\underline{F}_G + m\underline{\gamma})) \tag{5.37}$$

where the minus sign is due to the difference in the definition of the direction of the tipping moment around an edge, used in this chapter and that of Lin, and Song (1993). Using the results of section 5.3, equation (5.37) can be expressed as

$$M_i = -\underline{e}_i \cdot (\underline{M}_G + \underline{r}^{\bar{G}G} \times \underline{F}_G) - \Lambda_i \underline{c}_3 \cdot (\underline{F}_G + m\underline{\gamma}) \tag{5.38}$$

The condition that DSM should be larger than zero, in order for the robot to be stable, is then

$$\frac{M_i}{W} = \frac{-\underline{e}_i \cdot (\underline{M}_G + \underline{r}^{\bar{G}G} \times \underline{F}_G) - \Lambda_i \underline{c}_3 \cdot (\underline{F}_G + m\underline{\gamma})}{ma_G} > 0 \tag{5.39}$$

which is equivalent with the condition on $\Lambda$ in equation (5.26). However, as the SSM is coupled to the position of the CoG of the robot, it has an advantage over the DSM in the synthesis of a statically balanced walking.

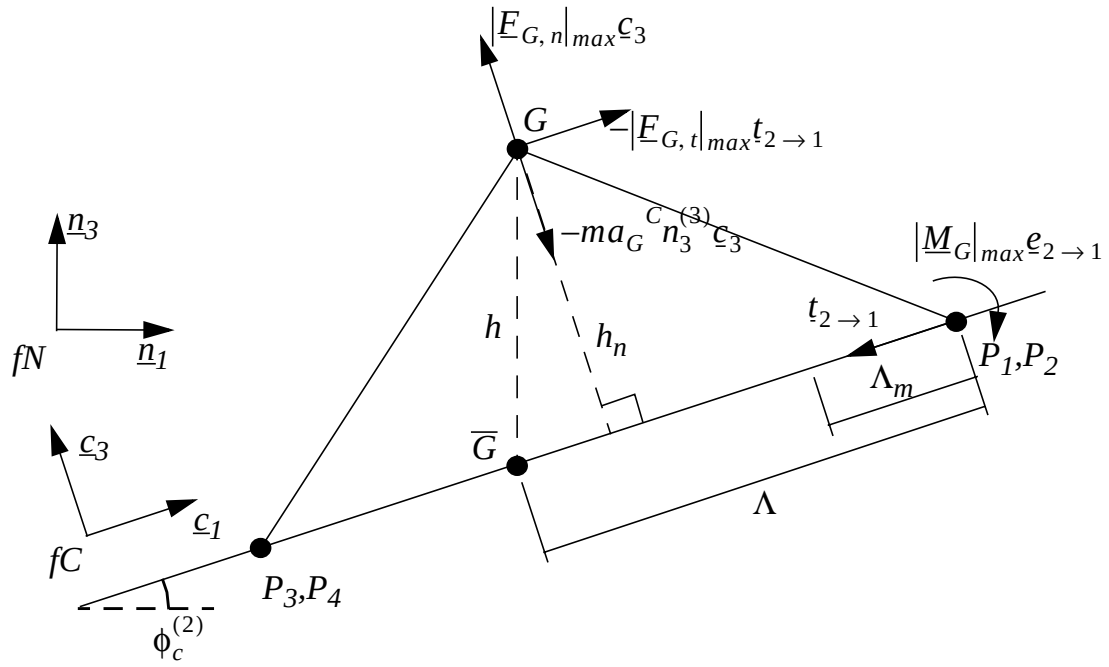


*Figure 5.5. Example of a robot standing on an incline, along with the worst case force and moment vectors*

## 5.5. Example of the support stability margin

To illustrate the properties of the SSM, two simple examples are shown in figure 5.5 and figure 5.6, which depicts a sideways view of the robot. The robot is standing with all four feet in ground contact, on an incline defined by a negative rotation around axis 2 of frame *fN*, i.e. the relationship between frame *fC* and *fN* is given by $\phi_c^{(2)} < 0$ and $\phi_c^{(1)} = \phi_c^{(3)} = 0$. The third axis of *fN* can be expressed in *fC* as ${}^{C}\underline{n}_3 = \left[-s\phi_c^{(2)} \;\; 0 \;\; c\phi_c^{(2)}\right]^T$, which in this case equals ${}^{C}\underline{n}_3 = \left[\left|s\phi_c^{(2)}\right| \;\; 0 \;\; \left|c\phi_c^{(2)}\right|\right]^T$, i.e. first and third elements of ${}^{C}\underline{n}_3$ are positive. The robot is standing such that front feet, the points $P_1$ and $P_2$, and hind feet, points $P_3$ and $P_4$, are at the same height, respectively. The support stability margin is derived for the edge connecting points $P_1$ and $P_2$ (figure 5.5), and the edge connecting points $P_3$ and $P_4$ (figure 5.6), i.e. the upper and lower edges of the support surface. The vector $\underline{t}_{2\to1}$ is orthogonal to the edge connecting points $P_1$ and $P_2$, and pointing into the support surface, and given by ${}^{C}\underline{t}_{2\to1} = \left[-1 \;\; 0 \;\; 0\right]^T$, and the vector $\underline{t}_{3\to4}$ is orthogonal to the edge connecting points $P_3$ and $P_4$, and given by ${}^{C}\underline{t}_{3\to4} = \left[1 \;\; 0 \;\; 0\right]^T$. The support stabil-

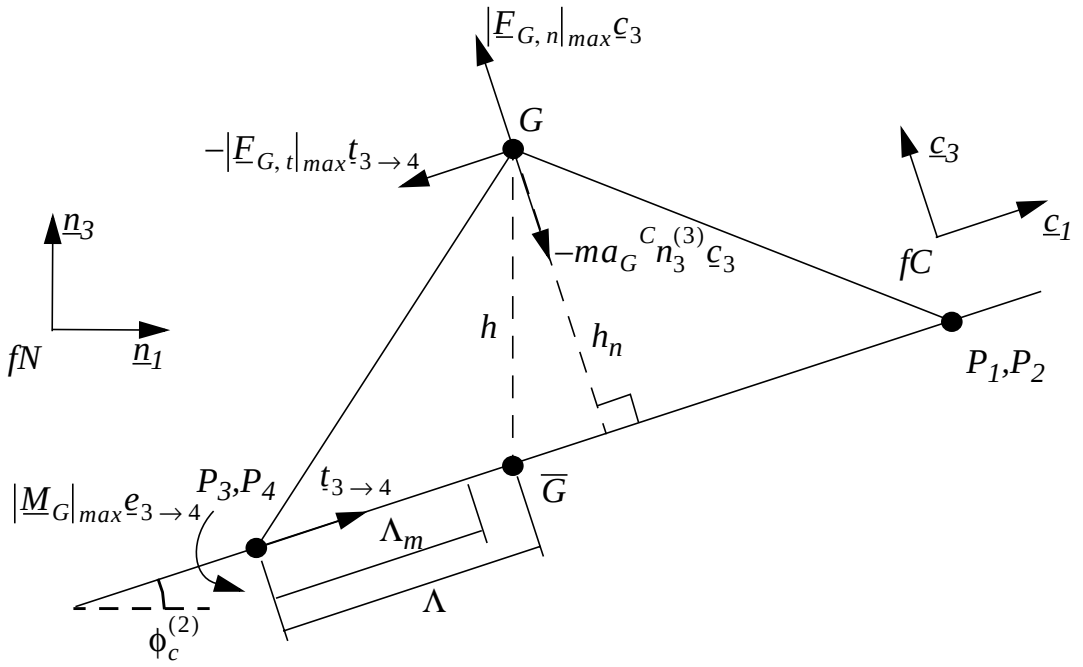


*Figure 5.6. Example of a robot standing on an incline, along with the worst case force and moment vectors*

ity margin for the edge connecting points $P_1$ and $P_2$, is then

$$\Lambda_{m(2\to1)} = \frac{|\underline{M}_G|_{max} + h_n(-|\underline{F}_{G,n}|_{max}|s\phi_c^{(2)}|/|c\phi_c^{(2)}| + |\underline{F}_{G,t}|_{max})}{ma_G c\phi_c^{(2)} - |\underline{F}_{G,n}|_{max}} \tag{5.40}$$

and the support stability margin for the edge connecting points $P_3$ and $P_4$, is

$$\Lambda_{m(3\to4)} = \frac{|\underline{M}_G|_{max} + h_n(|\underline{F}_{G,n}|_{max}|s\phi_c^{(2)}|/|c\phi_c^{(2)}| + |\underline{F}_{G,t}|_{max})}{ma_G c\phi_c^{(2)} - |\underline{F}_{G,n}|_{max}} \tag{5.41}$$

As expected, the necessary support stability margin for the lower edge (the edge connecting points $P_3$ and $P_4$) is larger than the support stability margin for the higher edge (the edge connecting points $P_1$ and $P_2$).

# 6. MOTION PLANNING BASED ON THE CENTER OF PRESSURE

In this chapter, a motion trajectory for the robot is planned by specifying a desired motion for the CoP based on the ground reaction forces and the position of the feet. The basic assumption is that the inertial and external forces are negligible, and only gravitational forces are acting on the robot, in which case the CoP will equal the PCoG. Thus, given the desired motion of the CoP, the motion of the CoG of the robot can be determined. The results of section 5.4 are used to determine stability margins for each edge of the support surface for the desired motion of the CoP, to account for the effect of the neglected forces and modelling errors. This chapter requires two main investigations, how the feet should be placed to form a support surface, and based on the position of the feet, how the supporting forces should be determined in order to have a smooth and balanced motion of the robot.

## 6.1. The supporting forces

For a given placement of the feet, the position of the CoP is determined by the distribution of the forces, acting on the robot, to the supporting feet. The motion of the CoP, while the same support area is maintained, depends then on how the distribution of the forces varies over time. This chapter will introduce a dimensionless variable for the component of the supporting force of each leg, normal to the ground plane, and relate the variable to the position and velocity of the CoP. Furthermore, boundaries on the variable will be found based on the support stability margin (SSM).

### 6.1.1. The support ratio

The *support ratio* is defined as a dimensionless variable for the ratio of normal force that each leg is supporting to the total normal force

$$\eta_i = \frac{\underline{c}_3 \cdot \underline{R}_i}{\underline{c}_3 \cdot \sum_i \underline{R}_i} \tag{6.1}$$

where $\eta_i$ denotes the support ratio for leg $i$. As seen by equation (6.1), the support ratio has the property that the sum of the support ratios is equal to one, i.e.

$$\sum_i \eta_i = 1 \tag{6.2}$$

The support ratio will be used as a design variable for the planning of the desired motion of the center of pressure, where instead of determining the normal force that each leg should support, the ratio of the total normal force, that each leg should support, is determined. Under the assumption that all the supporting feet are in the same plane, the position of the center of pressure in equation (5.10) can be expressed relative to point $N$ as

$$\underline{r}^{NC} = \sum_i \eta_i \underline{r}_i^{NP} \tag{6.3}$$

Using the support ratios, a simple expression for the velocity of the CoP can be derived. The velocity of the center of pressure is

$$\underline{v}^{NC} = \frac{{}^N d\underline{r}^{NC}}{dt} = \sum_i \dot{\eta}_i \underline{r}_i^{NP} \tag{6.4}$$

where it has been used that $\eta_i = 0$ for a leg in the air, and it is assumed that a foot in ground contact is stationary, i.e. using that ${}^N\dot{\underline{r}}_i^{NP} = 0$ for a leg in ground contact. The velocity of the CoP is independent of the point, relative to which the feet positions are given. For example if the point $P_j$ is the position of a supporting foot, the velocity of the CoP can be expressed as

$$\underline{v}^{NC} = \sum_i \dot{\eta}_i (\underline{r}^{NP_j} + \underline{r}^{P_j P_i}) = \sum_i \dot{\eta}_i \underline{r}^{P_j P_i} \tag{6.5}$$

using that $\sum \dot{\eta}_i = 0$. The velocity of the center of pressure is therefore only

dependent on how the feet are placed relative to each other, and on the derivatives of the support ratios. Thus, given a support area, the derivatives of the support ratios can be used to determine the motion of the CoP.

### 6.1.2. The support ratio and the support stability margin

When the robot is supported by three feet, the support ratios have a simple geometric relationship with the distance of the CoP from the edges of the support area. In section 6.3, this relationship will be used to derive a set of parameters for the support ratios, and to provide constraints on the parameters, based on the support stability margin.

Figure 6.1 shows the triangular support area just prior to that leg 2 is set down, i.e. just prior to event $\varphi_2$. For compactness let the value of the support ratio of leg $i$ at the time instant of the event $\varphi_2$, be denoted as $\eta_{i,\varphi_2} = \eta_i(\varphi_2 T)$. The position of the CoP at this time instant is then given by

$$\underline{r}_{\varphi_2}^{NC} = \sum_i \eta_{i,\varphi_2} \underline{r}_{i,\varphi_2}^{NP} \tag{6.6}$$

where $\underline{r}_{\varphi_2}^{NC}$ and $\underline{r}_{i,\varphi_2}^{NP}$ denote the position of the CoP and foot $i$, respectively, at the time instant $\varphi_2 T$. The support ratio for leg 2 is $\eta_{2,\varphi_2} = 0$, and furthermore, the support ratio for leg 1 can be expressed as $\eta_{1,\varphi_2} = 1 - \eta_{3,\varphi_2} - \eta_{4,\varphi_2}$, using equation (6.21). The position of the CoP can then be expressed as

$$\underline{r}_{\varphi_2}^{NC} = \underline{r}_{1,\varphi_2}^{NP} + \eta_{3,\varphi_2} \underline{r}_{\varphi_2}^{P_1P_3} + \eta_{4,\varphi_2} \underline{r}_{\varphi_2}^{P_1P_4} \tag{6.7}$$

The position of the CoP, at this time instant, can therefore be determined by the support ratios of leg 3 and 4, i.e. only two values for the support ratios are needed.

Let edge $i$ denote the edge of the triangular support area that is opposite the vertex point $P_i$, as shown in figure 6.1. Let $a_i$ denote the shortest distance of the CoP from edge $i$. Furthermore, let $\underline{t}_i$ denote a vector in the plane that is orthogonal to edge $i$, such that $\underline{t}_i = \underline{r}_{\varphi_2}^{Q_iP_i} / \left\| \underline{r}_{\varphi_2}^{Q_iP_i} \right\|$, where $Q_i$ is the point on edge $i$ closest to point $P_i$. Finally, let $d_i$ be defined as the shortest distance from point $P_i$ to edge $i$, i.e. $d_i = \left\| \underline{r}_{\varphi_2}^{Q_iP_i} \right\|$.

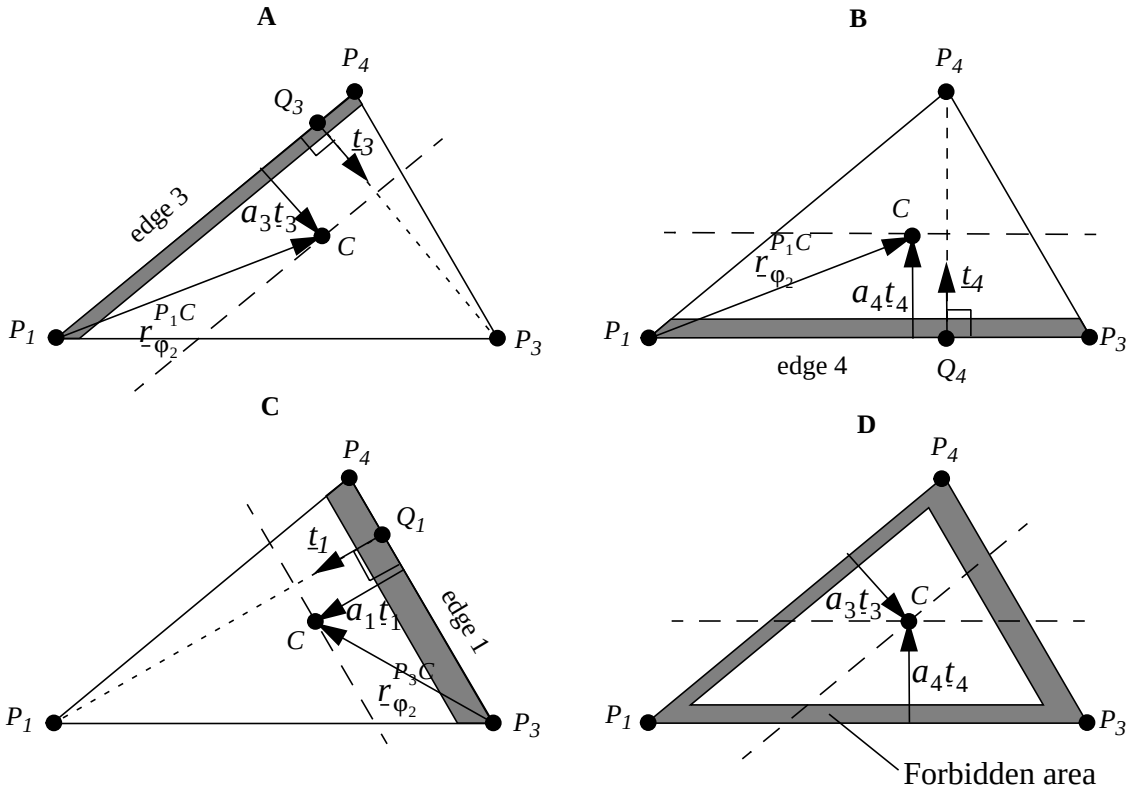


*Figure 6.1. The support area just prior to foot 2 being set down. The figure shows the distance of the CoP (point C) from edge 3 (***A***), edge 4 (***B***), and edge 1 (***C***). The CoP should be outside the shaded parts of the support areas, in order to maintain a certain SSM. In (***D***), the figures in (***A***-***C***) are combined.*

The distance of the CoP from edge *i* can be found by projecting the position vector, from any point on edge *i* to point *C*, onto vector $\underline{t}_i$. For instance, using one of the foot positions that form edge *i*, the shortest distance of the CoP from edge *i* is $a_i = \underline{t}_i \cdot \underline{r}_{\varphi_2}^{P_jC}$, where $j \neq i$. The distance of the CoP from the edges of the support area are then

$$\begin{aligned} a_3 &= \underline{t}_3 \cdot \underline{r}_{\varphi_2}^{P_1C} = \eta_{3,\varphi_2}(\underline{t}_3 \cdot \underline{r}_{\varphi_2}^{P_1P_3}) \\ a_4 &= \underline{t}_4 \cdot \underline{r}_{\varphi_2}^{P_1C} = \eta_{4,\varphi_2}(\underline{t}_4 \cdot \underline{r}_{\varphi_2}^{P_1P_4}) \\ a_1 &= \underline{t}_3 \cdot (\underline{r}_{\varphi_2}^{P_3P_1} + \underline{r}_{\varphi_2}^{P_1C}) = (1 - \eta_{3,\varphi_2} - \eta_{4,\varphi_2})(\underline{t}_1 \cdot \underline{r}_{\varphi_2}^{P_3P_1}) \end{aligned} \tag{6.8}$$

where $\underline{r}_{\varphi_2}^{P_1C}$ is given by, using equation (6.7)

$$\underline{r}_{\varphi_2}^{P_1C} = \underline{r}_{\varphi_2}^{NC} - \underline{r}_{1,\varphi_2}^{NP} = \eta_{3,\varphi_2}\underline{r}_{\varphi_2}^{P_1P_3} + \eta_{4,\varphi_2}\underline{r}_{\varphi_2}^{P_1P_4} \tag{6.9}$$

Furthermore, using that

$$\begin{aligned} d_3 &= (\underline{t}_3 \cdot \underline{r}_{\varphi_2}^{P_1P_3}) \\ d_4 &= (\underline{t}_4 \cdot \underline{r}_{\varphi_2}^{P_1P_4}) \\ d_1 &= (\underline{t}_1 \cdot \underline{r}_{\varphi_2}^{P_3P_1}) \end{aligned} \tag{6.10}$$

equation (6.8) can be expressed as

$$\begin{aligned} c_3 &= \eta_{3,\varphi_2} d_3 \\ c_4 &= \eta_{4,\varphi_2} d_4 \\ c_1 &= (1 - \eta_{3,\varphi_2} - \eta_{4,\varphi_2}) d_1 \end{aligned} \tag{6.11}$$

The support ratio $\eta_{3,\varphi_2}$ will determine that the CoP is somewhere on the dashed line that is parallel with edge 3 in figure 6.1(A), whereas the support ratio $\eta_{4,\varphi_2}$ will determine that the CoP is somewhere on the dashed line parallel with edge 4 in figure 6.1(B). The position of the CoP is then at the intersection of these two lines, as shown in figure 6.1(D).

As mentioned before, it is assumed that the position of the CoP is equal to the PCoG. The support stability margin, introduced in section 5.4, is then be used to set constraints on the support ratios. Given the support stability margin $\Lambda_{m,i}$ for edge *i*, the distance of the CoP from edge *i* has to fulfill that $a_i \geq \Lambda_{m,i}$. The support ratios are then subject to three inequality constraints

$$\begin{aligned} \eta_{3,\varphi_2} &\geq \Lambda_{m,3} / d_3 \\ \eta_{4,\varphi_2} &\geq \Lambda_{m,4} / d_4 \\ -\eta_{3,\varphi_2} - \eta_{4,\varphi_2} &\geq \Lambda_{m,1} / d_1 - 1 \end{aligned} \tag{6.12}$$

The effect of the support stability margin is to create a forbidden area for the CoP around the boundary of the support area, as shown by the shaded areas in figure 6.1, where the thickness of the forbidden area at edge *i* is equal to $\Lambda_{m,i}$. The support

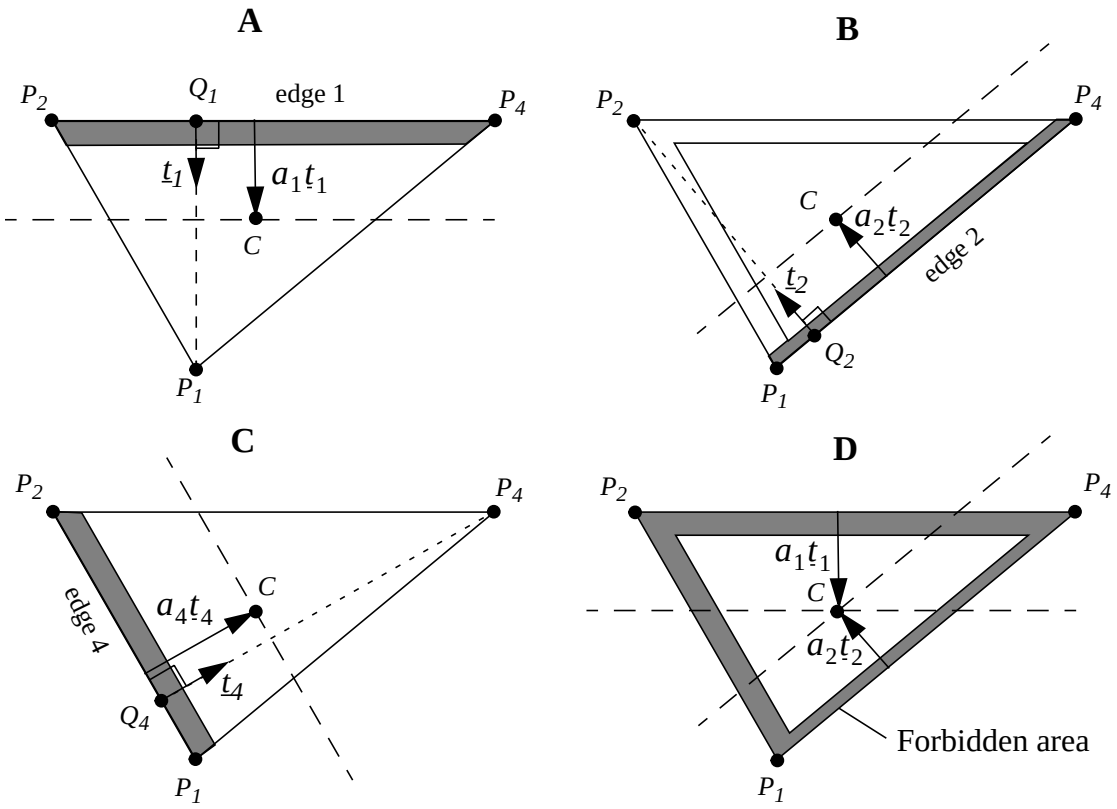


*Figure 6.2. The support area just prior to foot 3 being set down. The figure shows the distance of the CoP (point C) from edge 1 (***A***), edge 2 (***B***), and edge 4 (***C***). The CoP should be outside the shaded parts of the support areas, in order to maintain a certain SSM. In (***D***) the figures in (***A***-***C***) are combined.*

stability margin for each edge need not necessarily be equal. For instance, the support stability margin for a diagonal edge might be chosen smaller than the other edges motivated by the fact that, if the robot tips over a diagonal edge, the fall can be stopped by the leg that is in the air, by setting the foot down earlier than planned.

Figure 6.2 gives another example, where the support area is shown just prior to that foot 3 is set down, i.e. just prior to the event $\varphi_3$. In a similar fashion as in the previous example, the support ratio for leg 4 is expressed as $\eta_{4,\varphi_3} = 1 - \eta_{1,\varphi_2} - \eta_{2,\varphi_2}$, and the resulting inequality constraints on the support ratios for the event $\varphi_3$ are

$$\begin{aligned} \eta_{1,\varphi_3} &\geq \Lambda_{m,1}/d_1 \\ \eta_{2,\varphi_3} &\geq \Lambda_{m,2}/d_2 \\ -\eta_{1,\varphi_3} - \eta_{2,\varphi_3} &\geq \Lambda_{m,4}/d_4 - 1 \end{aligned} \tag{6.13}$$

The inequality constraints on the support ratios, with respect to the support stability margins and the support area, can in the same manner be determined for each event of the gait.

## 6.2. The foot placement

Ideally a mobile robot should move with the desired velocity set by the operator, where the operator is either a human or a higher level controller. However, in order to remain stable, it might be necessary for a walking robot to deviate from the desired velocity, for instance, by including lateral, longitudinal or vertical sway to its body motion. Nevertheless, the average velocity of the robot should be equal to the desired velocity set by the operator. To keep track of the desired motion of the robot, the *virtual vehicle*, which moves perfectly with the desired velocity relative to the ground plane, is introduced. The purpose of the virtual vehicle is to allow the operator to disregard the lifting and placing of the legs and how the balance should be maintained. Furthermore, from the motion of the virtual vehicle it can be determined where the feet should be placed in order for the robot to maintain the desired average velocity, and to provide the shape of the support area, that will be used in determining the support ratios, that will provide a desired motion of the CoP.

### 6.2.1. The virtual vehicle

A walking robot can be treated as an omnidirectional vehicle as it can move in any direction and turn. In this case, the desired velocities, that the operator can set, will be limited to translation in a plane and a rotation around the normal to that plane, i.e. to forward and sideway velocity and turning rate, which will then determine the motion of the virtual vehicle. Logically the desired velocity and angular velocity should be given in a frame situated such that the axis are in the longitudinal and lateral direction of the robot. However, as the body of the robot may vary its orientation during walking, i.e. the body may yaw, pitch or roll, this frame should not necessarily equal the body frame *fB*. Instead, the desired velocities are given in a frame *fD* attached to the virtual vehicle, with the third axis of the frame pointing upwards and the first axis pointing in the forward direction. Correspondingly, the index point for the virtual vehicle is denoted as point *D*. The desired velocity of the virtual vehicle, when expressed in the frame *fD*, is

$$ {}^{D}\underline{v}_{d}^{ND} = \begin{bmatrix} v_d^{(1)} & v_d^{(2)} & 0 \end{bmatrix}^T \tag{6.14} $$

The desired angular velocity ${}^{N}\underline{\omega}^{D}$ is in this case only the yaw rate for the virtual vehicle, i.e. rotation around the third axis of *fD*, and is when expressed in *fD*,

$$ {}^{N}\underline{\omega}_{d}^{D} = \begin{bmatrix} 0 & 0 & \omega_d \end{bmatrix}^{T} \tag{6.15} $$

The frame *fD* will represent a desired orientation of the of the body frame relative to the world frame *fN*. For instance, if it was desired to keep the body horizontal, the third axis, $\underline{d}_3$, of frame *fD*, would be parallel with the gravity vector, whereas if it was desired to keep the body parallel with the ground, the third axis of *fD* would be normal to the ground.

### 6.2.2. Foot placement relative to virtual vehicle

Given the desired velocity and angular velocity, the velocity of the feet in ground contact, relative to the virtual vehicle, can be found, using equation (3.31) in section 3.3, as

$$ \underline{v}_i^{DP} = -\underline{v}_d^{ND} - {}^{N}\underline{\omega}_d^{D} \times \underline{r}_i^{DP} \tag{6.16} $$

where $\underline{r}_i^{DP}$ and $\underline{v}_i^{DP}$ are the position and the velocity of foot *i* relative to the virtual vehicle, respectively. To simplify notation, the position of a foot relative to the virtual vehicle, when expressed in *fD*, is defined as

$$ {}^{D}\underline{r}^{DP} = \begin{bmatrix} r^{(1)} & r^{(2)} & r^{(3)} \end{bmatrix}^{T} \tag{6.17} $$

As the velocity of the foot, relative to the virtual vehicle, is the derivative of the relative position in frame *fD*, the relative velocity in frame *fD* is

$$ {}^{D}\underline{v}_i^{DP} = {}^{D}\frac{d}{dt}\underline{r}_i^{DP} = \begin{bmatrix} \dot{r}^{(1)} & \dot{r}^{(2)} & \dot{r}^{(3)} \end{bmatrix}^{T} \tag{6.18} $$

If all the vectors are expressed in frame *fD*, equation (6.16) can be written as a first order differential equation

$$ \begin{bmatrix} \dot{r}^{(1)} \\ \dot{r}^{(2)} \\ \dot{r}^{(3)} \end{bmatrix} = \begin{bmatrix} 0 & \omega_d & 0 \\ -\omega_d & 0 & 0 \\ 0 & 0 & 0 \end{bmatrix} \begin{bmatrix} r^{(1)} \\ r^{(2)} \\ r^{(3)} \end{bmatrix} - \begin{bmatrix} v_d^{(1)} \\ v_d^{(2)} \\ 0 \end{bmatrix} \tag{6.19} $$

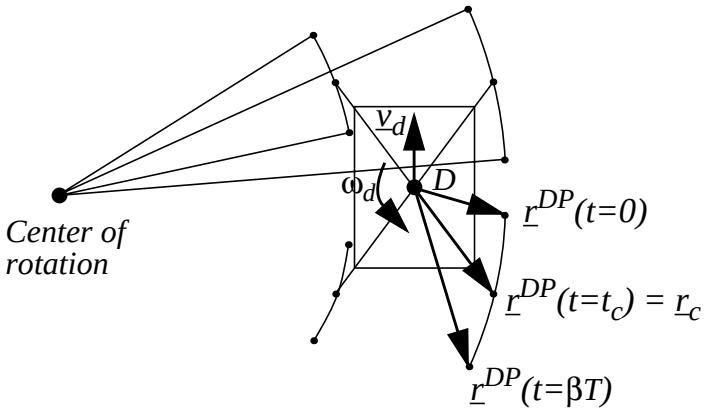


*Figure 6.3. The motion of the feet relative to the virtual vehicle when walking forward and turning*

which can be easily solved if it is assumed that all the desired velocities are constants. Let $t = 0$ be the time when the foot is set down on the ground and $\beta T$ is the duration of the support phase. The boundary condition for equation (6.19) is chosen as the position of the foot at time $t_c$, where $0 \le t_c \le \beta T$, such that

$$\underline{r}(t_c) = \underline{r}_c \tag{6.20}$$

The foot trajectory relative to the virtual vehicle during the support phase is then, for $0 \le t \le \beta T$

$$\begin{aligned} \begin{bmatrix} r^{(1)}(t) \\ r^{(2)}(t) \end{bmatrix} &= \begin{bmatrix} c\omega_d(t-t_c) & s\omega_d(t-t_c) \\ -s\omega_d(t-t_c) & c\omega_d(t-t_c) \end{bmatrix} \left( \begin{bmatrix} r_c^{(1)} \\ r_c^{(2)} \end{bmatrix} + \frac{1}{\omega_d} \begin{bmatrix} 0 & 1 \\ -1 & 0 \end{bmatrix} \begin{bmatrix} v_d^{(1)} \\ v_d^{(2)} \end{bmatrix} \right) \\ &\quad - \frac{1}{\omega_d} \begin{bmatrix} 0 & 1 \\ -1 & 0 \end{bmatrix} \begin{bmatrix} v_d^{(1)} \\ v_d^{(2)} \end{bmatrix} \\ r^{(3)}(t) &= r_c^{(3)} \end{aligned} \tag{6.21}$$

where $c\omega_d(t-t_c) = \cos\omega_d(t-t_c)$ and $s\omega_d(t-t_c) = \sin\omega_d(t-t_c)$. An example of the motion of the feet, relative to the virtual vehicle, is shown in figure 6.3. Equation (6.21) is the equation of a circle with center in $(-v_d^{(2)}/\omega_d, v_d^{(1)}/\omega_d)$ and

radius $\sqrt{(v_d^{(1)}/\omega_d - r_c^{(2)})^2 + (v_d^{(2)}/\omega_d + r_c^{(1)})^2}$. The stroke of the foot, i.e. the length of the trajectory that the foot travels, relative to the virtual vehicle, during the support phase, is

$$|\lambda| = \beta T \sqrt{(v_d^{(1)} - \omega_d r_c^{(2)})^2 + (v_d^{(2)} + \omega_d r_c^{(1)})^2} \tag{6.22}$$

The velocity of the foot relative to the virtual vehicle during the support phase is then

$$\begin{bmatrix} v^{(1)}(t) \\ v^{(2)}(t) \end{bmatrix} = \begin{bmatrix} c\omega_d(t-t_c) & s\omega_d(t-t_c) \\ -s\omega_d(t-t_c) & c\omega_d(t-t_c) \end{bmatrix} \left( \omega_d \begin{bmatrix} 0 & 1 \\ -1 & 0 \end{bmatrix} \begin{bmatrix} r_c^{(1)} \\ r_c^{(2)} \end{bmatrix} - \begin{bmatrix} v_d^{(1)} \\ v_d^{(2)} \end{bmatrix} \right) \tag{6.23}$$
$$v^{(3)}(t) = 0$$

which results in that the absolute velocity of the foot is constant, i.e.

$$|\underline{v}(t)| = \sqrt{(v_d^{(1)} - \omega_d r_c^{(2)})^2 + (v_d^{(2)} + \omega_d r_c^{(1)})^2} \tag{6.24}$$

If the angular velocity is zero, the trajectory of the foot relative to the virtual vehicle is a straight line,

$$\begin{bmatrix} r^{(1)}(t) \\ r^{(2)}(t) \end{bmatrix} = \begin{bmatrix} r_c^{(1)} - (t-t_c)v_d^{(1)} \\ r_c^{(2)} - (t-t_c)v_d^{(2)} \end{bmatrix} \tag{6.25}$$
$$r^{(3)}(t) = r_c^{(3)}$$

for $0 \le t \le \beta T$, which can be seen by letting $\omega_d \to 0$ in equation (6.21).

During one stride of a gait, all the legs are lifted and placed exactly once with a certain phase shift, as discussed in chapter 2. Let $t = 0$ at the beginning of the stride and $t = T$ at the end of the stride. The trajectories of the feet, during the support phase, can be found by shifting equation (6.21) by the time difference $\tau_i$

between when foot $i$ is set down and the start of the stride, i.e.

$$ {}^{D}\underline{r}_i^{DP}(t) = \underline{r}(t - \tau_i) \tag{6.26} $$

where $\underline{r}$ is given by equation (6.21). As the stride starts when foot 1 is set down, the time shift is $\tau_1 = 0$ and the foot trajectory for foot 1 is ${}^{D}\underline{r}_1^{DP}(t) = \underline{r}(t)$ for $0 \le t \le \beta T$. The time shift $\tau_i$ for the remaining legs are given by

$$ \tau_i = \begin{cases} (\psi_i - \beta)T & \text{for} \quad 0 \le t \le \psi_i T \\ \varphi_i T & \text{for} \quad \varphi_i T \le t \le T \end{cases} \tag{6.27} $$

for $i = 2 \ldots 4$. The foot trajectories, using equation (6.21), are

$$ \begin{aligned} \begin{bmatrix} {}^{D}r_i^{DP(1)}(t) \\ {}^{D}r_i^{DP(2)}(t) \end{bmatrix} &= \begin{bmatrix} c\omega_d(t - t_c) & s\omega_d(t - t_c) \\ -s\omega_d(t - t_c) & c\omega_d(t - t_c) \end{bmatrix} \begin{bmatrix} c\omega_d\tau_i & -s\omega_d\tau_i \\ s\omega_d\tau_i & c\omega_d\tau_i \end{bmatrix} \\ &\cdot \left( \begin{bmatrix} r_{i,c}^{(1)} \\ r_{i,c}^{(2)} \end{bmatrix} + \frac{1}{\omega_d} \begin{bmatrix} 0 & 1 \\ -1 & 0 \end{bmatrix} \begin{bmatrix} v_d^{(1)} \\ v_d^{(2)} \end{bmatrix} \right) - \frac{1}{\omega_d} \begin{bmatrix} 0 & 1 \\ -1 & 0 \end{bmatrix} \begin{bmatrix} v_d^{(1)} \\ v_d^{(2)} \end{bmatrix} \\ {}^{D}r_i^{DP(3)}(t) &= r_{i,c}^{(3)} \end{aligned} \tag{6.28} $$

for $i = 1 \ldots 4$, where $0 \le t \le \beta T$ for $i = 1$, $0 \le t \le \psi_i T$ and $\varphi_i T \le t \le T$ for $i = 2 \ldots 4$.

The solution to equation (6.19) may seem limited as it assumes constant desired velocities. However, the solution will be used to determine where the feet should be placed in the beginning of each step and not as a reference trajectory for the feet during the support phase. Furthermore, the solution will be used to determine the desired motion of the center of pressure in a feedforward manner, as will be explained in section 6.3.

### 6.2.3. Velocity of the CoP based on virtual vehicle

The velocity of the CoP calculated from the positions of the feet relative to the virtual vehicle, is

$$\underline{v}^{NC} = \sum_i \dot{\eta}_i \underline{r}_i^{DP} \tag{6.29}$$

which results in, using equation (6.28), that the velocity of the CoP, expressed *fD*, is

$$\begin{aligned}
\begin{bmatrix} {}^{D}v^{NC(1)}(t) \\ {}^{D}v^{NC(2)}(t) \end{bmatrix} &= \begin{bmatrix} c\omega_d(t-t_c) & s\omega_d(t-t_c) \\ -s\omega_d(t-t_c) & c\omega_d(t-t_c) \end{bmatrix} \\
&\cdot \sum_i \dot{\eta}_i \begin{bmatrix} c\omega_d\tau_i & -s\omega_d\tau_i \\ s\omega_d\tau_i & c\omega_d\tau_i \end{bmatrix} \left( \begin{bmatrix} r_{i,c}^{(1)} \\ r_{i,c}^{(2)} \end{bmatrix} + \frac{1}{\omega_d} \begin{bmatrix} 0 & 1 \\ -1 & 0 \end{bmatrix} \begin{bmatrix} v_d^{(1)} \\ v_d^{(2)} \end{bmatrix} \right) \\
{}^{D}v^{NC(3)}(t) &= \sum_i \dot{\eta}_i r_{c,i}^{(3)}
\end{aligned} \tag{6.30}$$

It can be shown that the average velocity of the CoP in one stride, using equation (6.30), is equal to the average velocity of the virtual vehicle. To show that, the velocity of the CoP relative to the virtual vehicle ${}^{D}\underline{v}^{DC}$ is used. If it is assumed that the stride starts at time $t = 0$, and the end of the stride is at time $t = T$, then the average velocity of the CoP relative to the virtual vehicle is

$$\frac{1}{T}\int_0^T {}^{D}\underline{v}^{DC} dt = \frac{1}{T}[{}^{D}\underline{r}^{DC}(T) - {}^{D}\underline{r}^{DC}(0)] \tag{6.31}$$

If the desired velocities and gait parameters are constant during the stride, the motion of the feet relative to the virtual vehicle and the support ratios are cyclic, i.e. ${}^{D}\underline{r}_i^{DP}(0) = {}^{D}\underline{r}_i^{DP}(T)$ and $\eta_i(0) = \eta_i(T)$. The position of the CoP relative to the virtual vehicle is therefore cyclic, i.e. ${}^{D}\underline{r}^{DC}(0) = {}^{D}\underline{r}^{DC}(T)$, which results in that equation (6.31) is equal to zero. The average velocity of the CoP, when the foot trajectories relative to the virtual vehicle are used, is therefore equal to the average velocity of the virtual vehicle, independent of the support ratios.

## 6.3. Support ratios for statically stable walking

The most crucial instants in the gait are when a leg is set down or lifted, i.e. at the events of the gait, as then there is an abrupt change in the support area. Following the discussion in section 6.1.2, it is possible to define a set of parameters for the support ratios and determine bounds for the parameters. For each event, there are two parameters needed and for them there are three inequality constraints. Therefore, for a whole stride cycle, i.e. for all eight events in the case that the gait is not singular, there are 16 parameters and 24 inequality constraints. The results of section 6.2 is used to determine the support area, in which the desired motion of the CoP will be found.

As the desired CoP will be used as the reference position for the PCoG of the robot, the trajectory for the $CoP_d$ should be continuous. The easiest approach is to let the support ratio for each leg be zero at the beginning and end of each support phase, and let the support ratio vary linearly between the events. This corresponds to that the vertical force that each foot should support varies linearly, if it is assumed that the total vertical force supported by the feet is constant and equal to the weight of the robot. Linearly varying vertical foot forces have been used in several papers, such as Yoneda, et al. (1994), Liu, and Wen (1997) and Zhou, and Low (1999). Furthermore, Klein, et al. (1983) show that if the inertial forces are ignored, the pseudo-inverse solution to the distribution of forces to each foot, will change linearly with vehicle motion when a given set of feet are in ground contact. Similarly Kumar, and Waldron (1988) also showed that the solution to the force distribution, using the zero interaction force constraint, results in linearly varying supporting forces.

The parameters chosen for the support ratios at each event are shown in figure 6.4, and an example of the support ratio for each leg, for a whole stride, is shown in figure 6.5. Note that for each event, there are only three feet that are supposed to be supporting the robot, in which case a plane can be determined such that all the foot contact points are in the same plane as the CoP. The vector of support ratio parameters is then

$$\underline{H} = \left[\bar{\eta}_{1,d} \cdots \bar{\eta}_{4,d}\ \bar{\eta}_{1,sd} \cdots \bar{\eta}_{4,sd}\ \bar{\eta}_{1,l} \cdots \bar{\eta}_{4,l}\ \bar{\eta}_{1,sl} \cdots \bar{\eta}_{4,sl}\right]^T \in \Re^{16\times 1} \quad (6.32)$$

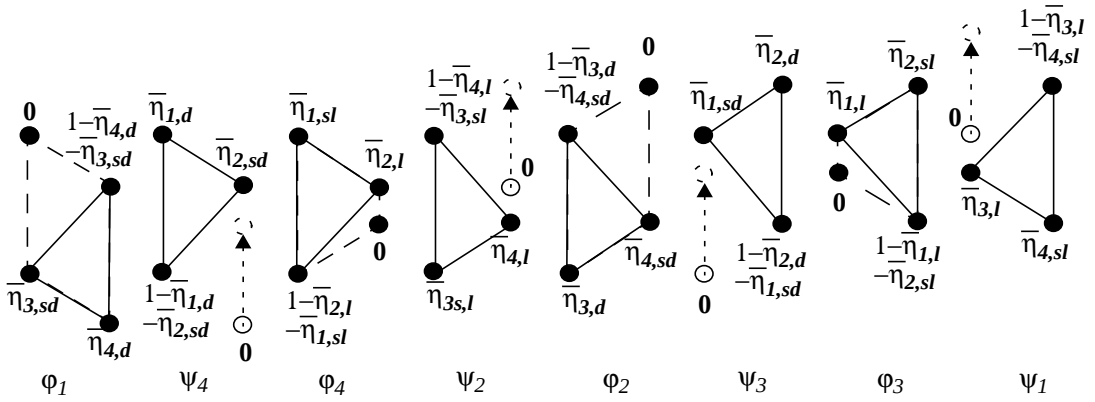


*Figure 6.4. Gait diagram for non singular quadruped crawl gait, and the choice of support ratio parameters used for each event. For events $\varphi_i$, the support area is shown just prior to that the foot is set down, where the dashed lines show the next support area.*

The parameter names are chosen such that they reflect the function they have. The parameters $\bar{\eta}_{i,\,d}$, for $i = 1 \ldots 4$ where $i$ is the number of the foot, determine how close to a diagonal edge the $\mathrm{CoP_d}$ should be at the events when a front leg is being set down and the diagonally opposite hind leg is being lifted, i.e. the events $\varphi_1$, $\psi_4$, $\varphi_2$, and $\psi_3$, where figure 6.1 is an example for the event $\varphi_2$. The parameters $\bar{\eta}_{i,\,sd}$ is then the second parameter for those events and determines how far sideways the $\mathrm{CoP_d}$ should be. The parameters $\bar{\eta}_{i,\,l}$ determine how far sideways the $\mathrm{CoP_d}$ should be when a hind leg is set down and the front leg on the same side is being lifted, i.e. for the events $\varphi_4$, $\psi_2$, $\varphi_3$, and $\psi_1$. Figure 6.2 shows an example for the event $\varphi_3$. The parameters $\bar{\eta}_{i,\,sl}$ is then the second parameter for those events and determines how close to the diagonal edge the $\mathrm{CoP_d}$ should be. The parameters for the support ratios for each event are listed in table 6.1.

Given the set of parameters for the support ratio and the inequality constraints associated with the support stability margin, the problem is to find values for the parameters. The approach chosen is to formulate the problem as a quadratic optimization problem to find values for the support ratios at each event of the gait, by minimizing the velocity of the CoP quadratically over one stride,

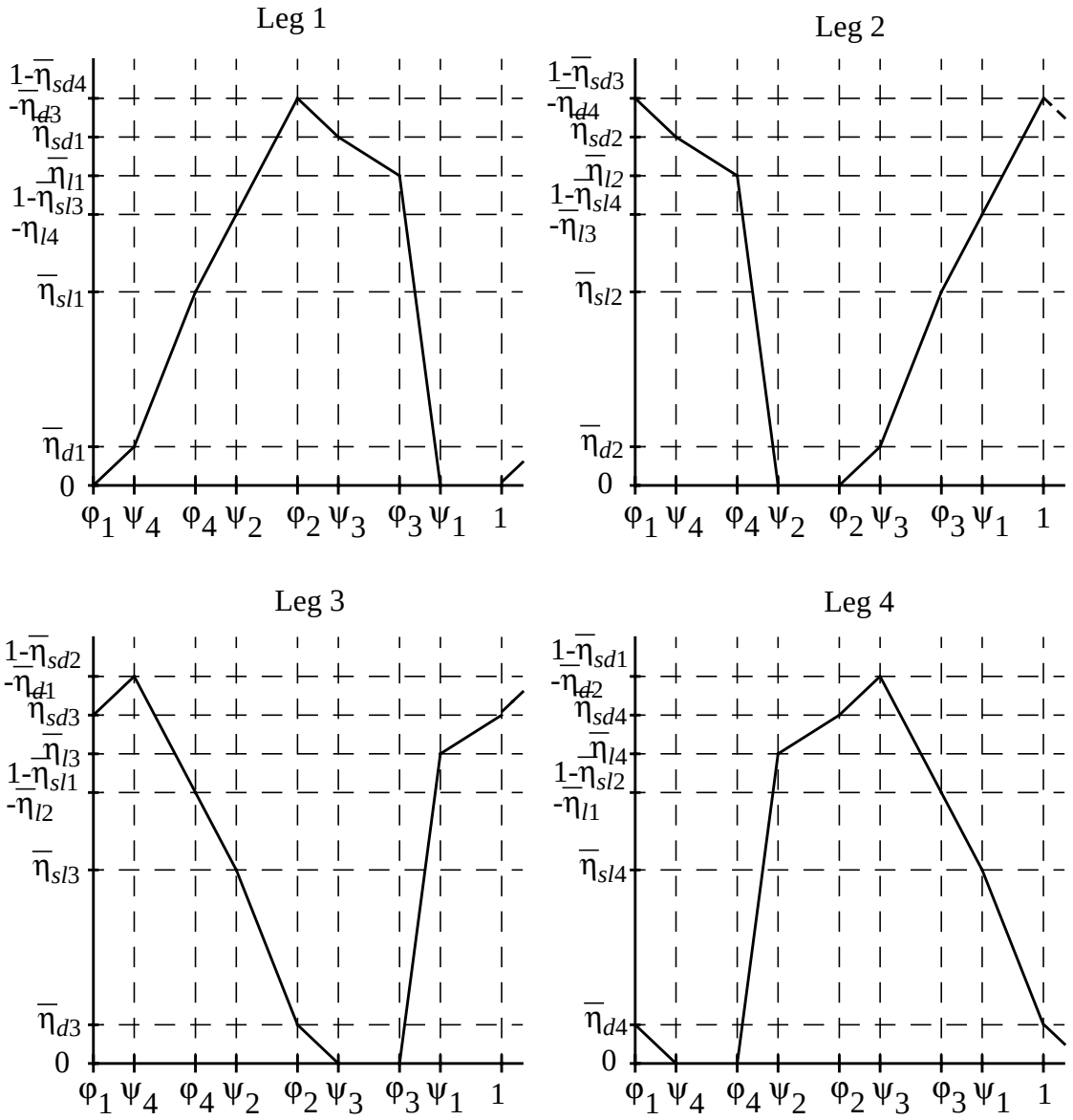


*Figure 6.5. Support ratios for all the legs for one stride with the support ratio parameters used.*

i.e. minimize the function

$$\frac{1}{2}\int_0^T (\underline{v}^{NC}(t))^T (\underline{v}^{NC}(t))dt \tag{6.33}$$

with respect to the vector of support ratio parameters in equation (6.32).

*Table 6.1:* The support ratios and the parameters for each event.

| | Events of the gait | | | | | | | |
|---|---|---|---|---|---|---|---|---|
| | $\varphi_1$ | $\psi_4$ | $\varphi_4$ | $\psi_2$ | $\varphi_2$ | $\psi_3$ | $\varphi_3$ | $\psi_1$ |
| $\eta_1$ | 0 | $\bar{\eta}_{1,d}$ | $\bar{\eta}_{1,sl}$ | $1-\bar{\eta}_{4,l}$ $-\bar{\eta}_{3,sl}$ | $1-\bar{\eta}_{3,d}$ $-\bar{\eta}_{4,sd}$ | $\bar{\eta}_{1,sd}$ | $\bar{\eta}_{1,l}$ | 0 |
| $\eta_2$ | $1-\bar{\eta}_{4,d}$ $-\bar{\eta}_{3,sd}$ | $\bar{\eta}_{2,sd}$ | $\bar{\eta}_{2,l}$ | 0 | 0 | $\bar{\eta}_{2,d}$ | $\bar{\eta}_{2,sl}$ | $1-\bar{\eta}_{3,l}$ $-\bar{\eta}_{4,sl}$ |
| $\eta_3$ | $\bar{\eta}_{3,sd}$ | $1-\bar{\eta}_{1,d}$ $-\bar{\eta}_{2,sd}$ | $1-\bar{\eta}_{2,l}$ $-\bar{\eta}_{1,sl}$ | $\bar{\eta}_{3,sl}$ | $\bar{\eta}_{3,d}$ | 0 | 0 | $\bar{\eta}_{3,l}$ |
| $\eta_4$ | $\bar{\eta}_{4,d}$ | 0 | 0 | $\bar{\eta}_{4,l}$ | $\bar{\eta}_{4,sd}$ | $1-\bar{\eta}_{2,d}$ $-\bar{\eta}_{1,sd}$ | $1-\bar{\eta}_{1,l}$ $-\bar{\eta}_{2,sl}$ | $\bar{\eta}_{4,sl}$ |

In each time period between two adjacent events, the feet are assumed stationary on the ground relative to the world origin, so the support area is fixed. With the assumption that the support ratios vary linearly between the events, the derivative of the support ratios are constant between two adjacent events, i.e. the derivatives of the support ratios are piece-wise constant. The velocity of the $\mathrm{CoP_d}$, when expressed in the world frame *fN*, ${}^{N}\underline{v}^{NC}$, will therefore be constant between two adjacent events, and consequently the quadratic of the velocity of the CoP, $(\underline{v}^{NC})^{T}(\underline{v}^{NC})$, is also constant between two adjacent events, independent of which frame the velocity of the CoP is expressed in.

The results of section 6.2 can be used in the optimization to determine the velocity of the CoP and the inequality constraints. The third component of the velocity of the CoP, when expressed in *fD*, is set to zero, so only the first two components of the velocity vector will be used in the optimization. To simplify the expressions, define $\tilde{\underline{r}}_i$ and $\tilde{\underline{v}}$ as

$$\tilde{\underline{r}}_i = \begin{bmatrix} c\omega_d\tau_i & -s\omega_d\tau_i \\ s\omega_d\tau_i & c\omega_d\tau_i \end{bmatrix} \left( \begin{bmatrix} r_{c,i}^{(1)} \\ r_{c,i}^{(2)} \end{bmatrix} + \frac{1}{\omega_d} \begin{bmatrix} 0 & 1 \\ -1 & 0 \end{bmatrix} \begin{bmatrix} v_d^{(1)} \\ v_d^{(2)} \end{bmatrix} \right) \tag{6.34}$$

and

$$\tilde{\underline{v}} = \sum_i \dot{\eta}_i \tilde{\underline{r}}_i \tag{6.35}$$

respectively. The terms $\tilde{\underline{r}}_i$ and $\tilde{\underline{v}}$ are constants between two adjacent events and change depending on the derivative of the support ratio and the term $\tau_i$, where $\tau_i$ is given by equation (6.27). The velocity of the CoP, using the position of the feet relative the virtual vehicle, as in equation (6.30), is

$$\begin{bmatrix} {}^{D}v^{NC(1)}(t) \\ {}^{D}v^{NC(2)}(t) \end{bmatrix} = \begin{bmatrix} c\omega_d\left(t - \frac{\beta T}{2}\right) & s\omega_d\left(t - \frac{\beta T}{2}\right) \\ -s\omega_d\left(t - \frac{\beta T}{2}\right) & c\omega_d\left(t - \frac{\beta T}{2}\right) \end{bmatrix} \tilde{\underline{v}} \tag{6.36}$$

The optimization problem in equation () can then be formulated as

$$\int_0^T \frac{1}{2}({}^{D}\underline{v}^{NC}(t))^T({}^{D}\underline{v}^{NC}(t))dt = \int_0^T \frac{1}{2}\tilde{\underline{v}}^T\tilde{\underline{v}}dt \tag{6.37}$$

For a non singular crawl gait, the stride cycle can be divided into eight time periods, separated by the events of the gait. Let $\underline{v}_j^{NC}$ denote the velocity of the CoP between events $j$ and $j$+1, for $j = 1\ldots8$, where the ninth event is when leg 1 is set down again, and define correspondingly $\tilde{\underline{v}}_j$. Let $t_j$ denote the time when event $j$ occurs, where $t_1 = 0$. The function to be minimized in equation (6.37) can be formulated as

$$\sum_{j=1}^{8} \int_{t_j}^{t_{j+1}} \frac{1}{2}\tilde{\underline{v}}_j^T\tilde{\underline{v}}_j dt = \sum_{j=1}^{8} \frac{1}{2}\tilde{\underline{v}}_j^T\tilde{\underline{v}}_j \Delta t_j \tag{6.38}$$

where $\Delta t_j = t_{j+1} - t_j$ is the time difference between events $j$ and $j$+1. The derivatives of the support ratios are constant between each event

$$\dot{\eta}_i(t) = \frac{\eta_i(t_{j+1}) - \eta_i(t_j)}{\Delta t_j}, \text{ for t} \in [t_j, t_{j+1}] \tag{6.39}$$

Equation (6.35) can then be expressed as

$$\tilde{\underline{v}}_j = \sum_i \frac{\eta_i(t_{j+1}) - \eta_i(t_j)}{\Delta t_j}\tilde{\underline{r}}_i, \text{ for t} \in [t_j, t_{j+1}] \tag{6.40}$$

Equation (6.40) can be expressed in matrix format as

$$\tilde{\underline{v}}_j = \boldsymbol{W}_j\underline{H} + \underline{b}_j \tag{6.41}$$

where $\boldsymbol{W}_j \in \Re^{2\times 16}$ and $\underline{b}_j \in \Re^{2\times 1}$ are functions of the desired velocity and angular velocity, the cycle time, the duty factor and the relative phase. For instance, if the time period between the first two events is used as an example, i.e. time period between $t_1 = \varphi_1 T = 0$ and $t_2 = \psi_4 T$. The support ratios for the first and second event can be found in figure 6.4 or figure 6.5, and results in that

$$\tilde{\underline{v}}_1 = \frac{\bar{\eta}_{d1}(\tilde{\underline{r}}_1 - \tilde{\underline{r}}_3) + \bar{\eta}_{d4}(\tilde{\underline{r}}_2 - \tilde{\underline{r}}_4) + (\bar{\eta}_{sd2} + \bar{\eta}_{sd3})(\tilde{\underline{r}}_2 - \tilde{\underline{r}}_3) + (\tilde{\underline{r}}_3 - \tilde{\underline{r}}_2)}{(\psi_4 - \varphi_1)T} \tag{6.42}$$

from which the matrix $\boldsymbol{W}_1$ and the vector $\underline{b}_1$ can be found. The vectors $\tilde{\underline{r}}_i$ are calculated from equation (6.34), where the term $\tau_i$ is given by equation (6.27), and is in this case, $\tau_1 = 0$ and $\tau_k = (\psi_k - \beta)T$ for $k = 2\ldots 4$.

Each event will provide three inequality constraints on the support ratio parameters, of the form

$$\boldsymbol{C}_j \underline{\underline{H}} \geq \underline{d}_j \tag{6.43}$$

where $\boldsymbol{C}_j \in \Re^{3\times 16}$ and $\underline{d}_j \in \Re^{3\times 1}$. Two examples of how the inequality constraints can be formulated for each event, are given by equations (6.12) and (6.13) in section 6.1.2. The support stability margin for each edge can be calculated from equations (5.34) or (5.36) in section 5.4.

The optimization problem can now be formulated in matrix format using

$$\boldsymbol{W} = \begin{bmatrix} \boldsymbol{W}_1 \\ | \\ \boldsymbol{W}_8 \end{bmatrix} \qquad \underline{b} = \begin{bmatrix} \underline{b}_1 \\ | \\ \underline{b}_8 \end{bmatrix} \qquad \Delta = \begin{bmatrix} \Delta t_1 I^{2\times 2} & & 0 \\ & \diagdown & \\ 0 & & \Delta t_8 I^{2\times 2} \end{bmatrix} \tag{6.44}$$

where $\boldsymbol{W} \in \Re^{16\times 16}$, $\underline{b} \in \Re^{16\times 1}$, and $\Delta \in \Re^{16\times 16}$, and using

$$\boldsymbol{C} = \begin{bmatrix} \boldsymbol{C}_1 \\ | \\ \boldsymbol{C}_8 \end{bmatrix} \qquad \underline{b} = \begin{bmatrix} \underline{d}_1 \\ | \\ \underline{d}_8 \end{bmatrix} \tag{6.45}$$

where $\boldsymbol{C} \in \Re^{24\times 16}$ and $\underline{d} \in \Re^{24\times 1}$. The quadratic optimization problem can then

be formulated in standard quadratic programming form as minimizing

$$min\frac{1}{2}\underline{H}^T\boldsymbol{W}^T\Delta\boldsymbol{W}\underline{H} + \underline{b}^T\Delta\boldsymbol{W}\underline{H} \tag{6.46}$$

with respect to the vector of support ratio parameters $\underline{H}$ and subject to the inequality constraints

$$\boldsymbol{C}\underline{H} \geq \underline{d} \tag{6.47}$$

where $\underline{d}$ is a function of the support stability margins and the height of the triangles formed by the feet in ground contact, as explained in section 6.1.2, based on the position of the feet relative the virtual vehicle. Quadratic optimization problems with inequality constraints can be solved using standard methods for quadratic programming, e.g. as described in Nahon, and Angeles (1992).

A singular gait occurs when there is a simultaneous lifting or placing of two or more legs. For instance, using the gait rule of Inagaki, and Kobayashi (1993), the relative phase of leg 3 is $\varphi_3 = \beta$, and the crawl gait becomes singular as a front leg is lifted at the same instance as the back leg on the same side is set down. In that case, while $\beta > 0.75$, there are only six distinct events in the gait as $\varphi_3 = \psi_1$ and $\varphi_4 = \psi_2$. Therefore, there are only six time periods in which the velocity of the $CoP_d$ can be calculated. In order to ensure that the trajectory of the $CoP_d$ is continuous, it becomes necessary to include two equality constraints, i.e. that the $CoP_d$ is constant just before and after the events when there is simultaneous lifting and placing. This corresponds to that the singular events are split in two events, one just prior to the singular event and one just after, although the time period between them is zero. Using the same set of support ratio parameters as in equation (6.32), the optimization problem can then be formulated in the same manner as in equation (6.46), with $\boldsymbol{W}$, $\Delta$, and $\underline{b}$ have been modified for six time periods, and subject to the constraints

$$\begin{aligned} \boldsymbol{C}\underline{H} &\geq \underline{d} \\ \underline{r}^{DC}(\varphi_3^-) &= \underline{r}^{DC}(\varphi_3^+) \\ \underline{r}^{DC}(\varphi_4^-) &= \underline{r}^{DC}(\varphi_4^+) \end{aligned} \tag{6.48}$$

The support ratio, and consequently the supporting forces, will not be continuous, in this case, at the events where simultaneous lifting and placing occurs. Furthermore, if the duty factor is equal to 0.75, there will only be four distinct events in each stride, which can be solved by adding constraints based on continuity of the $CoP_d$ trajectory for each of the events. An advantage with selecting a singular gait is that the equality constraints can be used to eliminate some of the support ratio parameter, thereby reducing the amount of calculation in the optimization.

## 6.4. Kinematic simulations

A kinematic simulation of WARP1 was done to demonstrate the trajectory of the $CoP_d$. Figure 6.6 shows a gait diagram when the robot walks straight forward with desired velocity $v_d^{(1)} = 0.1$, duty factor $\beta = 0.85$ and relative phase for leg 3, $\varphi_3 = 0.8$. As this is a kinematic simulation, support stability margin was set such that the desired CoP should maintain a certain distance from the edges of the support surface. The straight dashed line is the motion of the virtual vehicle and the swaying trajectory is the motion of the $CoP_d$. Figure 6.7 shows the corresponding support ratios for the four legs, where it can be observed, not unexpectedly, that the support ratio for the left and right front feet and the hind feet, respectively, are identical except that they are half a cycle out of phase. Furthermore, the support ratios for a front leg and a hind leg are mirror images of each other.

Figure 6.8 shows the robot turning at a rate of 0.05 rad/s while it is walking forward with a speed of 0.1 m/s. Figure 6.9 shows the corresponding support ratios, where it can be observed that leg 2 and 4, which are the right hand leg pair, support more of the weight than the left hand pair. An observation from figure 6.9 is that the support ratios for feet on the same side are mirror images of each other.

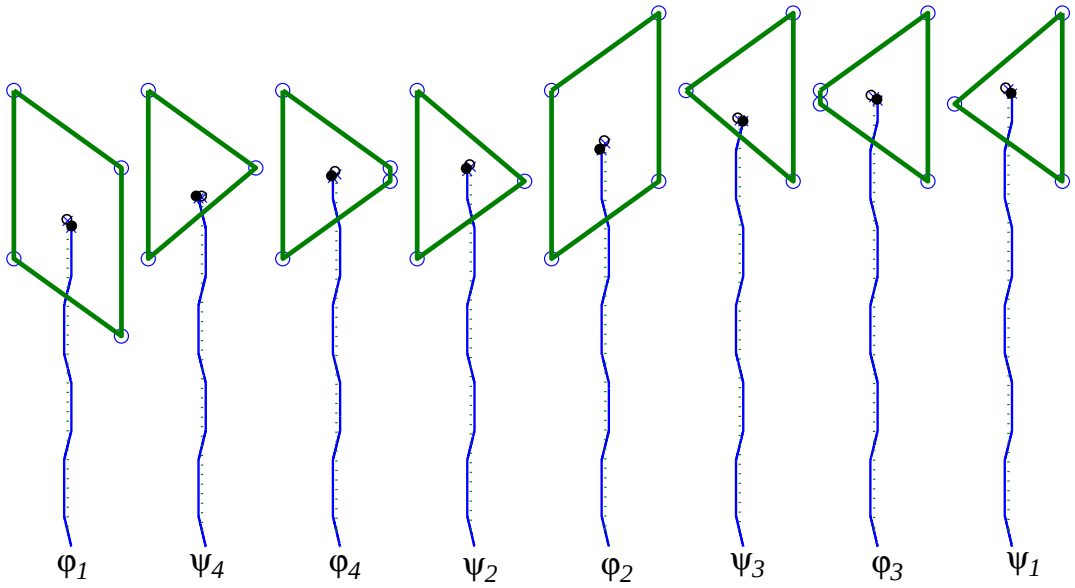


*Figure 6.6. Gait diagram for one stride of quadruped crawl gait. The polygons are the support patterns, the straight dashed line is the trajectory of the of the virtual vehicle when moving with forward velocity of 0.1 m/s, and the swaying line is the desired motion of the CoP*

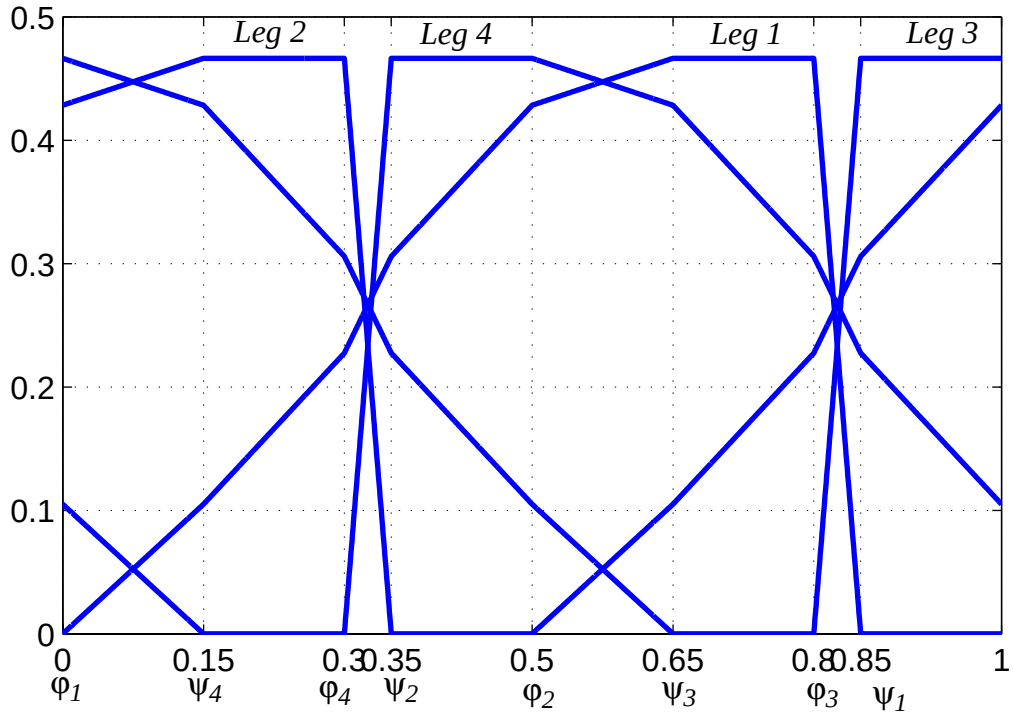


*Figure 6.7. Support ratios for each leg with desired forward velocity of 0.1 m/s*

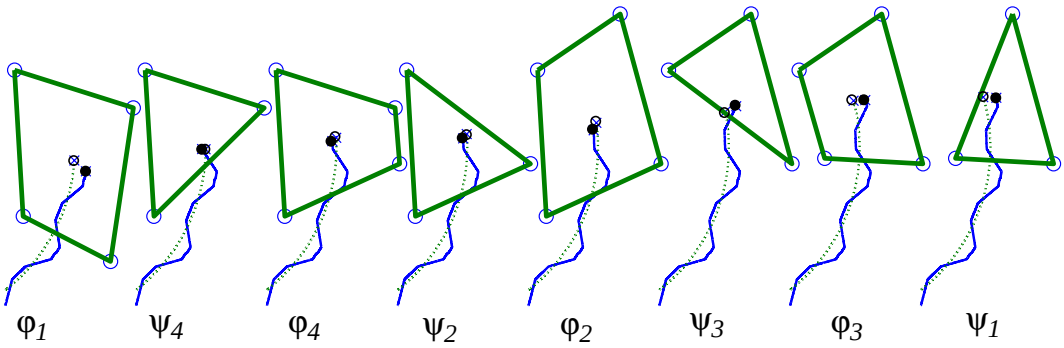


*Figure 6.8. Gait diagram for one stride of quadruped crawl gait. The polygons are the support patterns, the dotted line is the trajectory of the of the virtual vehicle when moving with forward velocity of 0.1 m/s and turning rate of 0.05 rad/s, and the swaying solid line is the desired motion of the CoP*

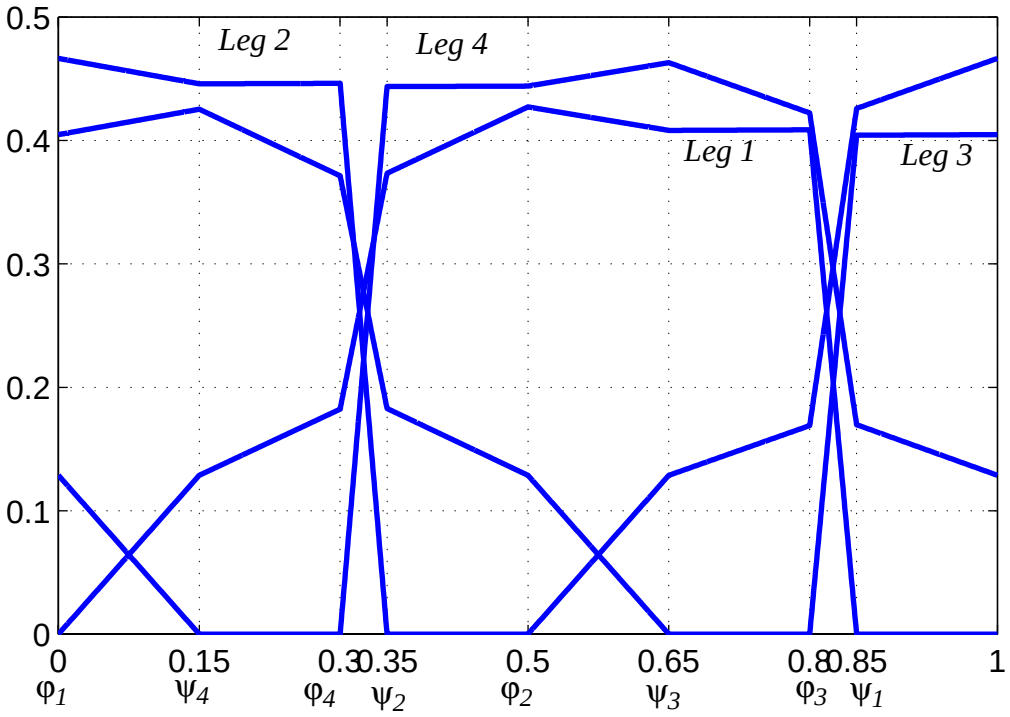


*Figure 6.9. Support ratios for each leg when the desired forward velocity is 0.1 m/s and the turning rate is 0.05 rad/s*

# 7. SYNTHESIS OF A CONTROLLER FOR A STATICALLY BALANCED CRAWL GAIT FOR WARP1

In this chapter the findings of chapters 5 and 6 are used to develop and implement a controller for statically balanced crawl gait for the quadruped robot WARP1. The main emphasis of the chapter is on the control of the motion of the body by coordinating the legs. The body controller will provide position, velocity and force references to the supporting legs. However, the synthesis of a controller for walking robots requires the treatment of several other issues than just the body control, such as the control of the gait, legs and each individual joint, and methods for signal processing. These issues will not be presented specifically in this chapter, but in a simplified manner when appropriate. For further references, the control of the joints is presented in Ridderström, et al. (2000), the control of the legs in Hardarson, et al. (1999), and Ridderström, et al. (2000), and the estimation of the attitude of the robot in Rehbinder (2001).

The assumptions made about the terrain are that the ground is rigid, not to steep and relatively smooth, i.e. there are no steps or holes, and the support surface, formed by the supporting feet at each time instant, can adequately be approximated by a plane. During walking, the robot will keep its body parallel with the ground, while maintaining a constant distance between the body and the ground, i.e. the robot will follow the contours of the terrain. The frame *fD*, i.e. the frame in which the motion planning will be done, will therefore have its third component $\underline{d}_3$ normal to the ground.

The implementation of the controller will be described in section 7.1. The body of the robot has six degrees of freedom, three for translation and three for orientation, that have to be controlled by coordinating the legs. The algorithm, presented in section 6.3, defines how two of the degrees of freedom should be controlled, the desired translation in the ground plane. Furthermore, the desired turning rate, around the normal to the ground plane, is set by the operator. The remaining three degrees freedom are the height of the body above the ground plane and the attitude, i.e. the pitch and roll of the body. In this implementation, the height of the robot's body and its attitude are fixed relative to the ground plane, simply by setting the reference height of all the hip joints equal to the desired height of the body. However, in the case of more uneven terrain, it might be necessary to actively control the remaining three degrees of freedom, i.e. the height and the attitude of the body, to avoid too much tilt to the body or to increase the stability. For that purpose, the length of the legs can be varied to give a desired height and attitude of the robot without significantly affecting the algorithm presented here.

Section 7.2 will provide experimental results. The experiments were designed to illustrate some of the properties of using the support stability margin for the planning of body motion. Tests for different velocities are shown and, furthermore, tests when the robot is walking on an incline.

Certain assumptions and simplifications are done in the implementation, some due to limitations in what can realistically be implemented, due to lack of sensed signals or computational power available on the robot, and others that leave room for future refinements. The most notable approximation is that the position of the CoG is not known exactly, and it is dependent on the position of the legs which are relatively heavy. Instead, a fixed point $B$, i.e. the index point for the robot body, is used as an approximation for the CoG, and $\overline{B}$ denotes the vertical projection of point $B$ onto the ground plane.

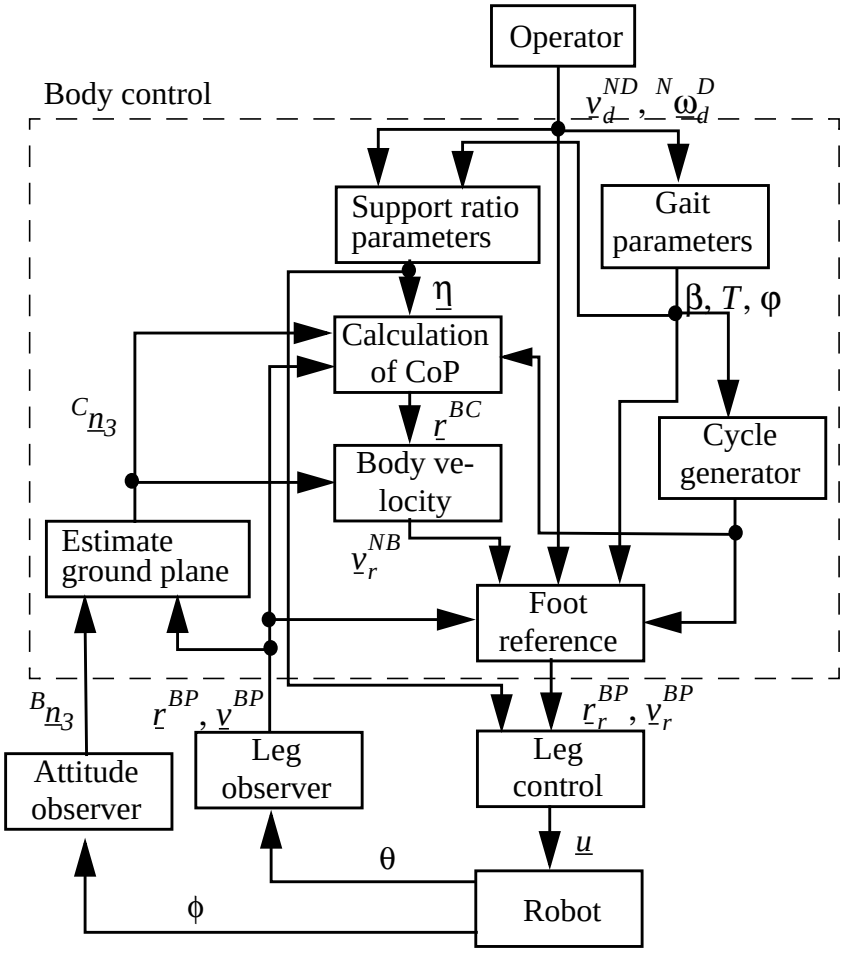


*Figure 7.1. Control structure for implementing a statically balanced gait*

## 7.1. Body control

The control structure for the robot is shown in figure 7.1. The main components of the controller are the control of the gait parameters, motion planning for the robot, and generation of foot references. The body control can be divided into a feedforward part and a feedback part. In the feedforward part, the gait parameters and the support ratio parameters are calculated depending on the desired velocity set by the operator. In the feedback part, the sensed position of the feet and the attitude of the robot body are used to create velocity references for the body and the feet. The walk is driven by a cycle generator with a cycle time *T*, where *T* is the duration of one stride. The cycle generator functions as a clock which is reset at the beginning of each stride, i.e. when foot 1 is set down. The lifting and placing of the feet occur

at fixed instants relative to the start of the stride, based on the relative phase of the legs and the output of the cycle generator.

### 7.1.1. Estimation of the ground plane

A plane is defined by the normal vector to the plane and a point in the plane. As the CoP is constrained to be in the ground plane, the problem is to find the normal vector $\underline{c}_3$. The ground plane can be described by

$$\underline{c}_3 \cdot (\underline{r}^{BO} - \underline{r}^{BC}) = 0 \tag{7.1}$$

where *O* is a point in the plane. Preferably, the ground plane should be chosen such that all the supporting feet are in the ground plane, i.e. such that $\underline{c}_3 \cdot (\underline{r}_i^{BP} - \underline{r}^{BC}) = 0$ where foot *i* is a supporting foot. In the case when the robot is in three legged support, the normal to the ground plane can easily be calculated by selecting one of the foot contact points, i.e. one of the vertices of the triangle formed by the feet. The normal vector is then the crossproduct of the two vectors along the edges connecting the selected foot with the other two feet in ground contact, i.e.

$$\underline{c}_3 = \frac{\underline{r}^{P_iP_j} \times \underline{r}^{P_iP_k}}{\left\| \underline{r}^{P_iP_j} \times \underline{r}^{P_iP_k} \right\|} \tag{7.2}$$

where *j* and *k* are chosen such that $\underline{c}_3 \cdot \underline{\gamma} < 0$. However, in the case of four legged support it is generally not possible to determine a plane that includes all the contact points of the feet. Furthermore, it is desired that the transition between different ground planes, when the feet are being lifted and repositioned, should be smooth, at least in the case of a nonsingular crawl gait. The approach is to use the support ratios to weigh together all the possible normal vectors that can be calculated for each foot.

The attitude estimation node on WARP1, described in Rehbinder (2001), estimates the pitch and roll angles of the body by estimating the third axis of frame *fN*, i.e. it estimates the vector ${}^{B}\underline{n}_3$, based on the sensed direction of the gravity vector. However, in order to calculate the support stability margin and the vertical projection of point *B*, the third axis of *fN* has to be expressed in frame *fC*.

In this implementation, the positions of the feet are known in the body frame *fB*, in which case, the estimate of the normal vector is in frame *fB*, i.e. the estimate is ${}^{B}\underline{c}_3$. The ground frame *fC* will now be defined by a chain of two simple rotations relative to *fB*, such that the first rotation $\phi_{bc}^{(1)}$ is around the second axis of *fB* and the second rotation $\phi_{bc}^{(2)}$ is around the first axis of the resulting frame. The rotation matrix between frames *fB* and *fC* is

$$ {}^{C}\boldsymbol{R}^{B}(\underline{\phi}_{bc}) = \begin{bmatrix} c\phi_{bc}^{(1)} & 0 & -s\phi_{bc}^{(1)} \\ s\phi_{bc}^{(1)}s\phi_{bc}^{(2)} & c\phi_{bc}^{(2)} & c\phi_{bc}^{(1)}s\phi_{bc}^{(2)} \\ s\phi_{bc}^{(1)}c\phi_{bc}^{(2)} & -s\phi_{bc}^{(2)} & c\phi_{bc}^{(1)}c\phi_{bc}^{(2)} \end{bmatrix} \tag{7.3} $$

The rotations $\underline{\phi}_{bc}$ are found from the relation ${}^{C}\boldsymbol{R}^{B}(\underline{\phi}_{bc})\,{}^{B}\underline{c}_3 = \begin{bmatrix} 0 & 0 & 1 \end{bmatrix}^T$, which results in

$$ \begin{aligned} \phi_{bc}^{(1)} &= \operatorname{atan}({}^{B}c_3^{(1)} / {}^{B}c_3^{(3)}) \\ \phi_{bc}^{(2)} &= \operatorname{asin}(-{}^{B}c_3^{(2)}) \end{aligned} \tag{7.4} $$

The vector ${}^{C}\underline{n}_3$, needed for the planning of the body motion and calculation of the CoP, is then simply given by

$$ {}^{C}\underline{n}_3 = {}^{C}\boldsymbol{R}^{B}(\underline{\phi}_{bc})\,{}^{B}\underline{n}_3 \tag{7.5} $$

The position of the desired CoP, relative to the body, is calculated from the sensed position of the feet relative to the body and the support ratios as

$$ \underline{r}_d^{BC} = \sum_i \eta_i \underline{r}_i^{BP} \tag{7.6} $$

The $\mathrm{CoP_d}$ is the desired position for the vertical projection of point *B* onto the ground plane, and the position of the $\mathrm{CoP_d}$ relative to point $\overline{B}$ is

$$ \underline{r}_d^{\bar{B}C} = \underline{r}_d^{BC} + \underline{r}^{\bar{B}B} = \underline{r}_d^{BC} + h\underline{n}_3 \tag{7.7} $$

using that $\underline{r}^{\bar{B}B} = h\underline{n}_3$, where *h* is the vertical height difference between points $\overline{B}$ and *B*. The height *h* can be calculated using that ${}^{C}r_d^{\bar{B}C(3)} = 0$, as points $\overline{B}$ and *C*

are, by definition, in the same plane. Equation (7.7) can then be expressed in *fC* as

$$ {}^{C}\underline{\bar{r}}_{d}^{BC} = \begin{bmatrix} {}^{C}r_{d}^{BC(1)} - {}^{C}r_{d}^{BC(3)} {}^{C}n_{3}^{(1)} / {}^{C}n_{3}^{(3)} \\ {}^{C}r_{d}^{BC(2)} - {}^{C}r_{d}^{BC(3)} {}^{C}n_{3}^{(2)} / {}^{C}n_{3}^{(3)} \\ 0 \end{bmatrix} \tag{7.8} $$

The term ${}^{C}r^{BC(3)}$ is the height of point *B* above the ground plane, along the normal to the plane, and will be defined, as in equation (5.35) in section 5.4, by

$$ h_n = -{}^{C}r_{d}^{BC(3)} = h\,{}^{C}n_{3}^{(3)} \tag{7.9} $$

The height $h_n$ of point *B* above the plane is therefore the weighted average of the position of the feet, using the support ratios as a weighing factor. This is similar to the estimate of body height used in Yoneda, et al. (1994).

### 7.1.2. Calculation of support ratio

The calculation of the support ratio parameters is done by solving the quadratic optimization problem in equations (6.46) and (6.47) in section 6.3. However, it was soon noticed in simulations, that the parameters $\bar{\eta}_{i,d}$, for $i = 1 \ldots 4$, equaled or were very close to the inequality constraint, i.e. the solution resulted in $\bar{\eta}_{i,d} \cong \Lambda_{m,i} / d_i$ . Furthermore, the remaining parameters fulfilled their inequality constraints with large margin. To reduce the amount of calculation when implementing the algorithm on the robot, a simpler solution was used, where the number of parameters is reduced to 12, by setting

$$ \bar{\eta}_{i,d} = \Lambda_{m,i} / d_i \tag{7.10} $$

and neglecting the remaining inequality constraints. The solution to the quadratic optimization problem is then the pseudo-inverse

$$ \underline{H}' = -(\boldsymbol{W}^T \Delta \boldsymbol{W})^{-1} \boldsymbol{W}^T \Delta \underline{b} \tag{7.11} $$

where $\underline{H}'$ is the new vector of support ratio parameters

$$ \underline{H}' = \left[ \bar{\eta}_{1,sd} \ \ldots \ \bar{\eta}_{4,sd} \ \bar{\eta}_{1,l} \ \ldots \ \bar{\eta}_{4,l} \ \bar{\eta}_{1,sl} \ \ldots \ \bar{\eta}_{4,sl} \right]^T \in \Re^{12 \times 1} \tag{7.12} $$

and $\boldsymbol{W}$ and $\underline{b}$ have been modified to include $\bar{\eta}_{i,d}$. It should be noted that the simplification used in the calculation of the support ratio parameters is not general for all robots and is possible mainly because WARP1 is relatively wide, i.e. the distance between the left and right legs is relatively large.

Further reduction of the number of support ratio parameters were also tested by utilizing the symmetry in support ratios between the different legs, observed in kinematic simulations in section 6.4. For instance, if the anti symmetry in the support ratios between the front and hind legs on the same side is used, the number of support ratio parameters to be calculated can be reduced to six. This is done by setting, for example, $\bar{\eta}_{l,l} = \bar{\eta}_{1,l} = \bar{\eta}_{3,l}$ and $\bar{\eta}_{r,l} = \bar{\eta}_{2,l} = \bar{\eta}_{4,l}$, where $l$ and $r$ denote the left and right legs, respectively, resulting in a vector of support ratio parameters

$$\underline{H}'' = \left[\bar{\eta}_{l,sd}\ \bar{\eta}_{r,sd}\ \bar{\eta}_{l,l}\ \bar{\eta}_{r,l}\ \bar{\eta}_{l,sl}\ \bar{\eta}_{r,sl}\right]^T \in \Re^{6\times 1} \tag{7.13}$$

The uncertainty in the position of the CoG has to be taken into account in the selection of the support stability margin in equation (5.27), along with the estimate of the neglected inertial and external forces. Furthermore, as the robot will maintain a certain desired height normal to the ground plane, equation (5.36) in section 5.4 is used rather than equation (5.34). If the position of the CoG is known relative to point B, the stability margin using point B instead of point G results in

$$\Lambda_m = \frac{|\underline{M}_G|_{max} - {}^C r^{BC(3)}((\underline{n}_3 \cdot \underline{t})|\underline{F}_{G,n}|_{max} / {}^C n_3^{(3)} + |\underline{F}_{G,t}|_{max})}{m a_G {}^C n_3^{(3)} - |\underline{F}_{G,n}|_{max}} - (\underline{t} \cdot \underline{r}^{\bar{B}\bar{G}}) \tag{7.14}$$

where

$$\underline{r}^{\bar{B}\bar{G}} = \underline{r}^{BG} - \frac{(\underline{c}_3 \cdot \underline{r}^{BG})}{{}^C n_3^{(3)}} \underline{n}_3 \tag{7.15}$$

However, if the position the CoG is only estimated, the second term on the right hand side of equation (7.14) can be replaced by the estimated maximum error between PCoG and $\bar{B}$.

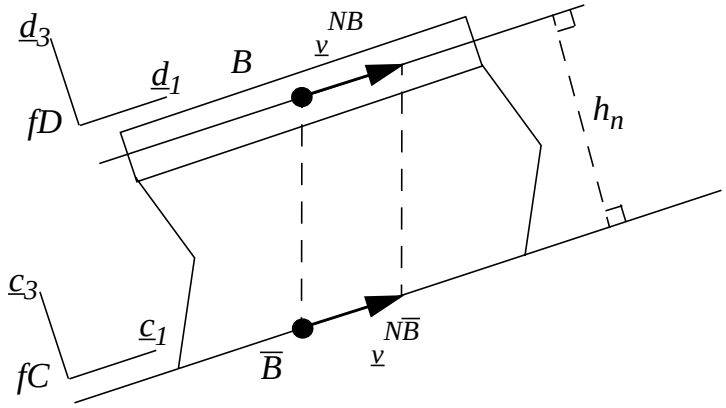


*Figure 7.2. The velocity of point B of the body and of the vertical projection of point B*

### 7.1.3. Body and feet reference trajectories

As the $\mathrm{CoP_d}$ is a reference position for point $\overline{B}$, the vector $\underline{r}^{\overline{B}C}$ in equation (7.8), represents a position error for point $\overline{B}$. As the frames *fD* and *fC* are in this case equal, the points $\overline{B}$ and *B* should move in parallel planes, i.e. point $\overline{B}$ moves in the ground plane and point *B* in a parallel plane at a constant distance, and hence their velocity in the plane will be equal. The body controller will use the difference between point $\overline{B}$ and the $\mathrm{CoP_d}$ to create a control signal for the coordination of the legs, in the form of a reference velocity for the motion of point *B* by

$$\underline{v}_r^{NB} = \boldsymbol{P}_B \underline{r}^{\overline{B}C} + \boldsymbol{B}_B \frac{{}^{C}d\underline{r}^{\overline{B}C}}{dt} \tag{7.16}$$

where $\boldsymbol{P}_B$ and $\boldsymbol{B}_B$ are diagonal position and velocity feedback gain matrices, respectively.

The reference velocity $\underline{v}_r^{NB}$, in equation (7.16), along with the desired angular velocity set by the operator are used to create velocity references for each leg, during the support phase, using equation (3.31) in section 3.3. The reference velocity for leg *i* is then

$$\underline{v}_{i,\,r}^{BP} = -\underline{v}_r^{NB} - {}^{N}\underline{\omega}_d^{C} \times \underline{r}_i^{BP} \tag{7.17}$$

where $\underline{r}_i^{BP}$ is the sensed position of foot *i* relative to point *B*. The reference position trajectory during the support phase is found by integrating equation (7.17) with the landing position as initial condition

$$\underline{r}_{i,r}^{BP}(t) = \underline{r}_i^{BP}(t_i) + \int \underline{v}_{i,r}^{BP} dt \tag{7.18}$$

where $t_i$ is the time instant when the foot lands, i.e. if the time $t = 0$ at the beginning of a stride, the instant at which foot *i* is set down are $t_i = (n + \varphi_i)T$, where *n* is a positive integer.

The landing position for each leg, i.e. the position where the foot should be placed at the end of the transfer phase, is calculated relative to the position of the virtual vehicle, using equation (6.21), where the boundary condition is chosen such that $t_c = \beta T/2$, i.e. the vector $\underline{r}_{i,c}^{DP}$ is the position of the foot at the middle of the support phase, giving

$$\begin{aligned}
\begin{bmatrix} {}^{C}r_i^{DP(1)}(\varphi_i T) \\ {}^{C}r_i^{DP(2)}(\varphi_i T) \end{bmatrix} &= \begin{bmatrix} c\omega_d\frac{\beta T}{2} & -s\omega_d\frac{\beta T}{2} \\ s\omega_d\frac{\beta T}{2} & c\omega_d\frac{\beta T}{2} \end{bmatrix}\left(\begin{bmatrix} r_{i,c}^{DP(1)} \\ r_{i,c}^{DP(2)} \end{bmatrix} + \frac{1}{\omega_d}\begin{bmatrix} 0 & 1 \\ -1 & 0 \end{bmatrix}\begin{bmatrix} v_d^{(1)} \\ v_d^{(2)} \end{bmatrix}\right) \\
&\quad -\frac{1}{\omega_d}\begin{bmatrix} 0 & 1 \\ -1 & 0 \end{bmatrix}\begin{bmatrix} v_d^{(1)} \\ v_d^{(2)} \end{bmatrix} \\
{}^{C}r_i^{DP(3)}(\varphi_i T) &= r_{i,c}^{DP(3)}
\end{aligned} \tag{7.19}$$

where ${}^{C}r_{i,c}^{DP(3)}$ is a constant and the same for all the legs, equal to the desired height $h_n$ of the robot. However, as the desired angular velocity appears in the denominator of equation (7.19), a Taylor approximation for small angular velocities, was used in the implementation to avoid zero division.

Equation (7.19) gives the landing position for the feet relative to the virtual vehicle. In order to determine where the feet should be placed relative to the body, the position of the body relative to the virtual vehicle has to be known at the time instants $t_i$, i.e. the vector $\underline{r}_i^{BP}(t_i)$ has to be known in advance. This in order to be able to

plan a reference trajectory for the feet relative to the body during the transfer phase, from the lift off to the landing position. The position of the foot relative to the body can be expanded as

$$\underline{r}_i^{BP}(t_i) = \underline{r}^{BC}(t_i) - \underline{r}^{DC}(t_i) + \underline{r}_i^{DP}(t_i) \tag{7.20}$$

where $\underline{r}^{DC}(t_i)$ is the position of the CoP relative to the virtual vehicle

$$\underline{r}^{DC}(t_i) = \sum_i \eta_i \underline{r}_i^{DP}(t_i) \tag{7.21}$$

and can be calculated using equation (6.28) for the event at time $t_i$. The term $\underline{r}^{BC}(t_i)$ is the position of the CoP relative to the body and is unknown at the time of the lift off, as it depends on future values. Instead the current value $\underline{r}^{BC}(t)$ can be used, motivated by that

$$\underline{r}^{BC} = -h\underline{n}_3 + \underline{r}^{\bar{B}C} \tag{7.22}$$

where the first term on the right hand side is approximately constant while the foot is in the air, and the second term is the position error between point $\overline{B}$ and the $\mathrm{CoP_d}$, which should be small.

### 7.1.4. Control of gait parameters

There are many exact and approximate relationships between the gait parameters, that can be used in the control of the gait. Kumar, and Waldron (1989) made an extensive investigation of these relationships. The main gait parameters are the cycle time $T$, the duty factor $\beta$ and the relative phase $\varphi_i$ of the legs. Derived gait parameters are the duration of the support phase, $T_s = \beta T$, and the duration of the transfer phase, $T_a = (1-\beta)T$.

There are several limitations on how the gait parameters can be selected, for instance, due to limitation in the kinematic workspace of the legs and the available maximum velocity of the feet. For creeping gaits, i.e. when the duty factor is larger than or equal to 0.75, the duration of the transfer phase $T_a$ is less than the duration

of the support phase $T_s$ as

$$T_a = \frac{1-\beta}{\beta} T_s \leq \frac{1}{3} T_s \tag{7.1}$$

If the distance that the foot has to travel, is approximately equal for the support and the transfer phase, the foot should have a velocity that is at least three times larger during the transfer phase than the support phase. Any limitation in the maximum velocity of the foot will therefore set a lower limit on the duration of the transfer phase.

The length of the stroke is dependent on the velocity of the robot and the duration of the support phase. The length of the stroke, i.e. the length of trajectory that the foot travels during support relative to the virtual vehicle, was given by equation (6.22) in section 6.2, and is

$$|\lambda| = T_s \sqrt{(v_d^{(1)} - \omega_d r_c^{(2)})^2 + (v_d^{(2)} + \omega_d r_c^{(1)})^2} \tag{7.2}$$

The duration of the support phase $T_s$ can then be used to maintain the foot trajectory within the workspace of the leg, by reducing the stroke.

Therefore, it can generally be said, in the case of $\beta \geq 0.75$, that limitation in kinematic workspace provides an upper limit on the support time $T_s$, and the maximum foot velocity provides a lower limit on the transfer time $T_a$.

The approach, chosen here, for the control of the gait parameters is very simplified, as it is based on the foot trajectories relative to the virtual vehicle, and does not take into account the motion of the body relative to the virtual vehicle. If the desired angular velocity is assumed to be small, the length and width of the foot trajectories, projected onto the ground plane, can be approximated by

$$\begin{aligned} l_i^{(1)} &= \left| r_i^{DP(1)}(T_s) - r_i^{DP(1)}(0) \right| = T_s \upsilon_i^{(1)} \\ l_i^{(2)} &= \left| r_i^{DP(2)}(T_s) - r_i^{DP(2)}(0) \right| = T_s \upsilon_i^{(2)} \end{aligned} \tag{7.3}$$

where

$$\begin{aligned} \upsilon_i^{(1)} &= \left| v_d^{(1)} - \omega_d r_{c,i}^{(2)} \right| \\ \upsilon_i^{(2)} &= \left| v_d^{(2)} + \omega_d r_{c,i}^{(1)} \right| \end{aligned} \tag{7.4}$$

The two dimensional ground plane workspace of the feet is simplified to be a rectangle, with side lengths $l_{max}^{(1)}$ and $l_{max}^{(2)}$, centered around point $P_{i,c}$, i.e. the point where the foot is at the middle of the support phase, as shown in figure 7.3. The condition on the duration of the support phase is then that

$$T_s = \beta T \leq min \frac{l_{max}^{(j)}}{\upsilon_i^{(j)}} \tag{7.5}$$

In this simplified gait controller, the duration of the transfer phase will be limited to a minimum time $T_{a,min}$. Consequently this results in a minimum cycle time of $T_{min} = T_{a,min} / (1 - \beta)$ for a given $\beta \geq 0.75$. Given a time $T_s$ for the support phase, a limit on the choice of duty factor can then be found as

$$\beta \leq \frac{T_s}{T_s + T_{a,min}} \tag{7.6}$$

The algorithm for the control of the gait parameters duty factor and cycle time can be summarized as follows: Nominal values are set for the duty factor and the cycle time as $\bar{\beta}$ and $\bar{T}$, respectively. The time for the support phase is chosen such that

$$T_s = min \left\{ \bar{\beta} \bar{T}, \frac{l_{max}^{(j)}}{\upsilon_i^{(j)}} \right\} \tag{7.7}$$

The duty factor is chosen such that

$$\beta = min \left\{ \bar{\beta}, \frac{T_s}{T_s + T_{a,min}} \right\} \tag{7.8}$$

and the cycle time is finally calculated by

$$T = \frac{T_s}{\beta} \tag{7.9}$$

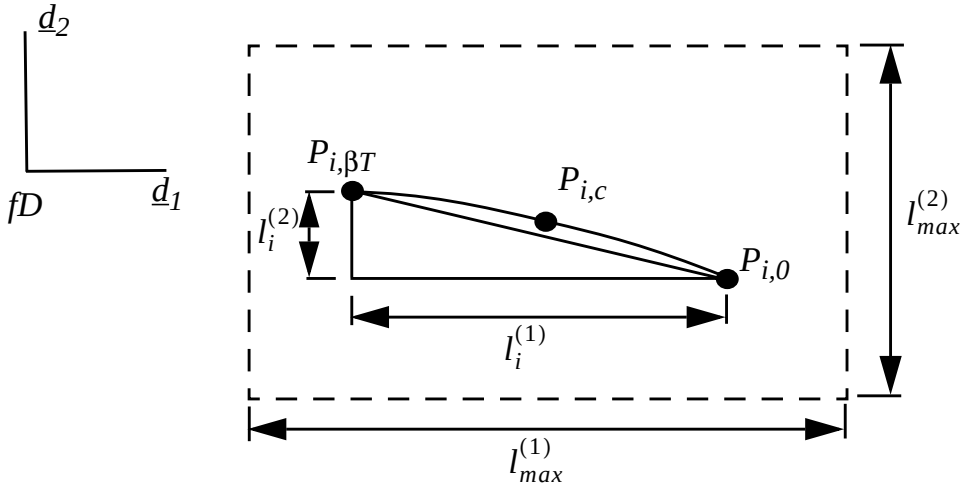


*Figure 7.3. Approximative kinematic workspace of a leg in the ground plane. Point $P_{i,0}$ is the landing position of the foot relative to the virtual vehicle, $P_{i,c}$ the position in the middle of the support phase, and $P_{i,\beta T}$ the position at lift off.*

For WARP1, the algorithm results in, for increasing desired speed, that when the feet reach the boundary of the allowed workspace, using the nominal gait parameters, the gait parameter controller will start to reduce the duration of the support phase, by reducing the cycle time. As the speed is further increased, the limitation on the minimum duration of the transfer phase will start to reduce the duty factor, in which case the duration of the transfer phase will remain constant.

The relative phase for each leg was for a nonsingular crawl gait set as in equation (2.3) in section 2.4. The relative phase for leg 3 is chosen such that the crawl gait is close to singular by choosing $\varphi = \beta - \delta\varphi$ where $\delta\varphi$ is a small positive number. In the resulting gait the front leg will be lifted closely after a hind leg on the same side is set down, such that the time difference between the two events is equal to $\delta\varphi T$. It should be noted that in order to maintain three feet on the ground at all times, the duty factor is limited by $\beta \geq 0.75 + \delta\varphi$.

### 7.1.5. Leg control

Each leg is controlled by a simple cartesian stiffness/damping controller (Hardarson, et al., 1999). The control law is given by

$$\underline{\tau}_i = \boldsymbol{J}_i^T[\boldsymbol{P}_i({}^B\underline{r}_{i,r}^{BP} - {}^B\underline{r}_i^{BP}) + \boldsymbol{B}_i({}^B\underline{v}_{i,r}^{BP} - {}^B\underline{v}_i^{BP}) + {}^B\underline{f}_{i,r}^{P}] \tag{7.10}$$

where $\underline{\tau}_i$ is the vector of output torques at the joints, $\boldsymbol{P}_i$ and $\boldsymbol{B}_i$ are the position and velocity feedback gain matrices for leg *i*, respectively, and $\boldsymbol{J}_i$ is the Jacobian of the position of the foot relative the body

$$J_i(\underline{\theta}_i) = \frac{\partial {}^B\underline{r}_i^{BP}}{\partial \underline{\theta}_i} \tag{7.11}$$

where $\underline{\theta}_i$ is the vector of joint angles for leg *i*, as discussed in chapter 3. The last term in equation (7.10) is a force reference, $f_{i,r}^P$, which is output in an open loop manner. In this case the output is chosen to compensate for the weight of the robot, i.e. it is opposite the desired ground reaction force for leg *i*,

$$f_{r,i}^P = \eta_i m\underline{\gamma} = -\eta_i m a_G \underline{n}_3 \tag{7.12}$$

which is equal to the portion of the total weight each leg should support according to the planned motion of the $CoP_d$.

## 7.2. Experimental results

The experiments where done with WARP1, using the experimental setup, described in Ridderström, et al. (2000), and Ridderström and Ingvast (2001a). The tool-chain used in the development and implementation is shown in figure 7.4. Models and analytical expressions, such as kinematic relationships, are derived in the computer algebra system *Maple*, using the *Sophia* language (Lesser, 1995), which are then exported to C-code using the macro package *Exmex* (Lennartsson, 1999). These models and expressions can then be used to build and simulate controllers in *Matlab/Simulink*, which is a system that combines numerical computations with high level graphical programming. Finally, the Matlab toolbox, *Real-Time Workshop*, is used to transform the Matlab/Simulink diagram into C-code, that can be compiled, with a real-time kernel from the *xPC* toolbox, and downloaded to the *target computer*. The target computer is a standard PC-computer that

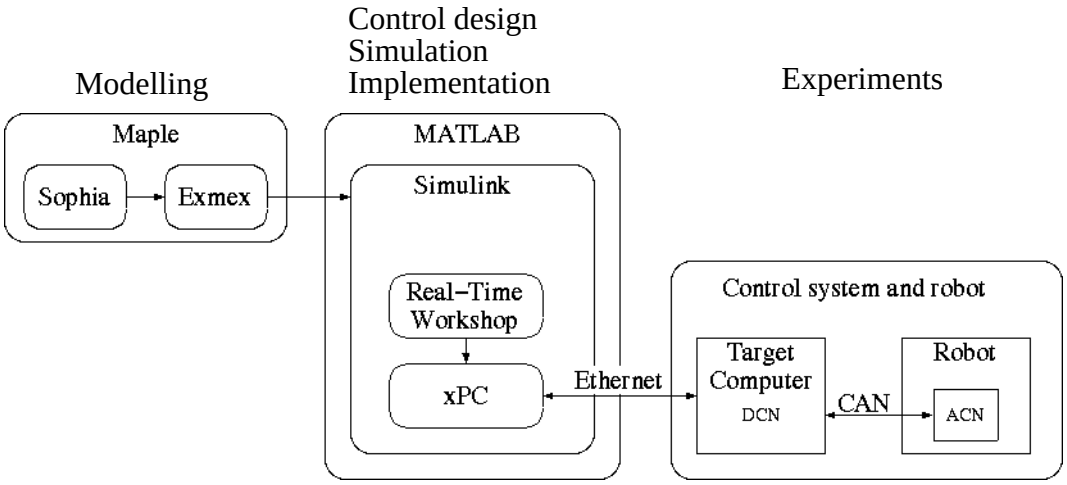


*Figure 7.4. Tool chain used in the development and implementation of the controller (from Ridderström, and Ingvast, 2000a).*

executes the controller code for the robot. Currently, the target computer is not onboard the robot, but communicates with four smaller computer nodes (*ACN*) on the robot, through a CAN-bus. The ACN:s perform I/O functions, such as reading sensors and send the readings to the target computer, and output desired voltages to the motors.

An external measurement system, V-Scope VS-100 from Litek Advanced Systems Ltd., is used to measure the robot position in the lab. It consists of two transmitters, that are placed on the robot, and three stationary receivers. Each transmitter sends out one infrared signal and one ultrasound signal at the same time. These signals are detected by the three receivers, where the time difference between the arrival of the two signals is used to calculate the distance of the transmitter from each receiver. Given the known distances between the three receivers, the position of the transmitter can be found in space by triangulation. The two transmitters are placed on the robot such that the yaw of the robot can be calculated. The current setup of the measurement system, used for the experiments, has an accuracy in the horizontal plane of $\pm 5$ mm, and the accuracy for the yaw estimation is $\pm 0.03$ rad (Karlsson, 2002). The clocks of the measurement system and the logging of experimental data from the robot are not synchronized, so the synchronization has to be done manually.

Only results using the six parameter controller in equation (7.13) are presented in this section. The motivation is that the 12 parameter model showed no significant improvement compared to the 6 parameter model. Further, the 12 parameter model required a higher sampling time when run on the target computer, which in turn deteriorate the performance of the joint controllers.

### 7.2.1. Walking straight forward

In the first experiment, the robot is commanded to walk straight forward on a horizontal plane. The robot starts from standstill and the desired velocity is first ramped up to 0.05 m/s, and then, after 45 s, to 0.08 m/s.

To evaluate how well the robot tracks the desired velocity, the external measurement system V-Scope is used. Figure 7.5 shows the velocity, where the desired velocity $v_d^{ND(1)}$, set by the operator is shown as a dash-dot line in all the figures. Figure 7.5*a* shows the desired velocity of the CoP ${}^{C}\underline{v}^{NC}$, calculated from the derivatives of the support ratios and the sensed positions of the feet. Figure 7.5*b* shows the reference velocity ${}^{C}\underline{v}_r^{NB}$ for the body, from equation (7.16). Figure 7.5*c* shows the derived velocity from the V-Scope measurements of the position of the robot. The estimate of the yaw of the robot is used to rotate the measured velocities such that they correspond to a frame which has the first axis in the direction of motion of the robot, i.e. the frame is approximately equal to frame *fB*. Figure 7.5*d* shows the moving average of the measured velocities, where a sliding window of width equal to the cycle time *T* is used to calculate the average velocity of the robot for a whole stride. The average velocity is approximately 10% less than the desired velocity, where the average velocity is 0.045 m/s when the desired is 0.05 m/s, and the average velocity 0.07 when the desired is 0.08 m/s.

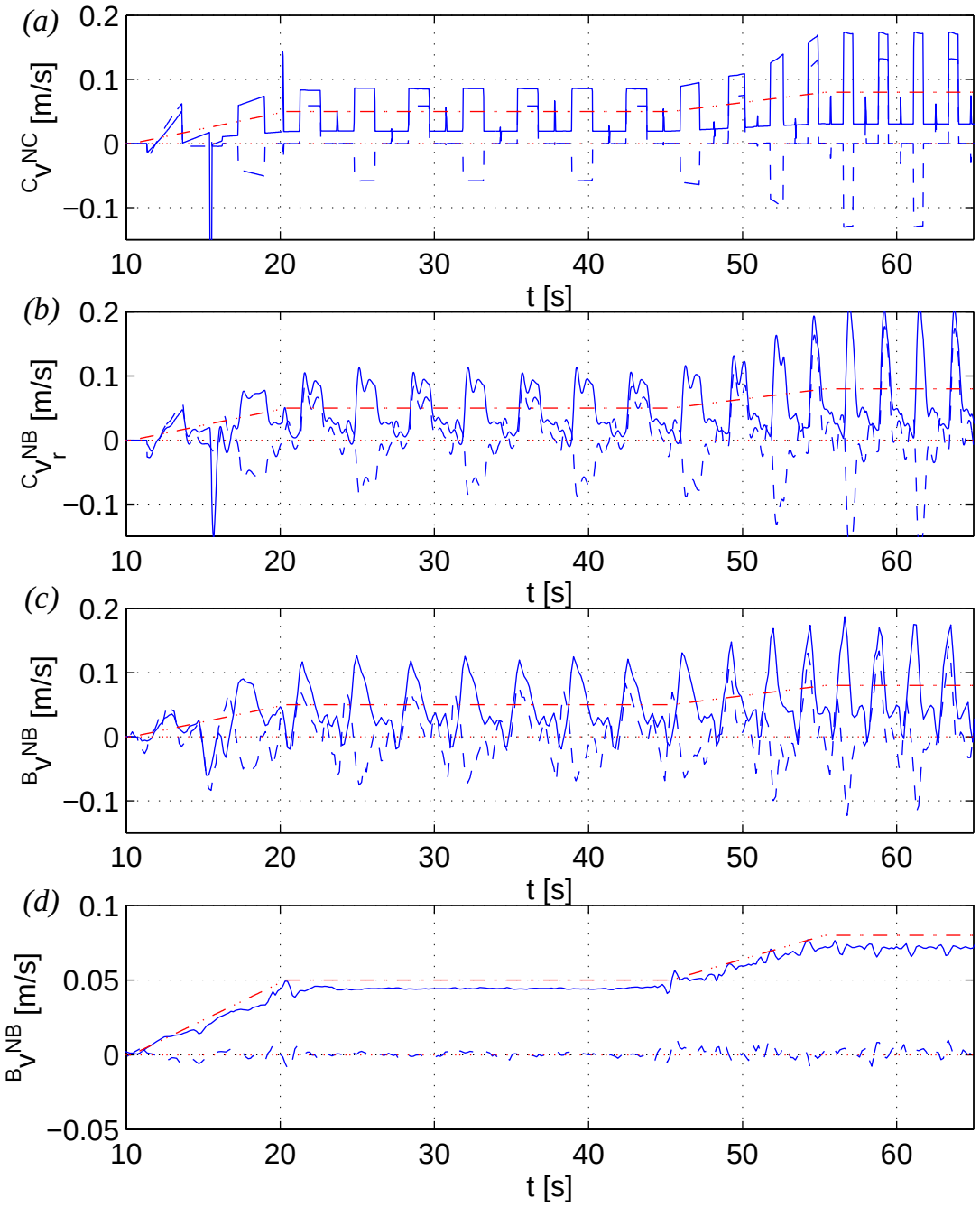


*Figure 7.5. The velocity of the robot when walking forward. In all a)-d) $v^{ND(1)}$ (dash-dot) and $v^{ND(2)}$ (dotted). a) The desired velocity of $CoP_d$, $v^{NC(1)}$ (solid) and $v^{NC(2)}$ (dashed). b) The reference body velocity, $v_r^{NB(1)}$ (solid) and $v_r^{NB(2)}$ (dashed). c) The filtered estimate of the velocity from the measurement system, $v^{NB(1)}$ (solid) and $v^{NB(2)}$ (dashed). d) The moving average for one stride of the velocity from the measurement system, $v^{NB(1)}$ (solid) and $v^{NB(2)}$ (dashed).*

Figure 7.6 shows the shortest distance between point $\overline{B}$ and an edge of the support surface (solid line), i.e. the distance *min* $\Lambda_j$ where *j* is the number of an edge. The dashed line is the support stability margin $\Lambda_m$, which is equal for all the edges in this case, and is chosen as 0.07 m. The dash-dot line is the shortest distance of the desired CoP to an edge of the support surface. Figure 7.7 shows the elements of vector ${}^{C}\underline{r}^{\overline{B}C}$, i.e. the error in the tracking of $\mathrm{CoP_d}$ by the point $\overline{B}$, where the dashed line shows the magnitude $\left\| {}^{C}\underline{r}^{\overline{B}C} \right\|$ of the error, i.e. the distance of point $\overline{B}$ from point *C*. It should be noted that the body controller is not active the first 11 s, hence the error for that time period.

Figure 7.6 shows that point $\overline{B}$ is too close to an edge of the support surface for certain time instants. These time instants correspond to the events $\varphi_1$, $\psi_4$, $\varphi_2$, and $\psi_3$, i.e. the events when a front leg is placed and a hind leg is lifted. At these events, the desired CoP is constrained to be a distance equal to $\Lambda_m$ from the edge, according to equation (7.10). Unfortunately, the error between point $\overline{B}$ and $\mathrm{CoP_d}$ can be as large as 4 cm, depending on the desired velocity, as can be seen in figure 7.7, that causes point $\overline{B}$ to violate the support stability margin. It should, however, be noted that in these cases the edge that $\overline{B}$ is to close to is a diagonal edge, in which case, in the event that the robot tips over, the fall can be braked by the leg that is in the air.

Figure 7.6 also shows that for certain time periods, the $\mathrm{CoP_d}$ is too close to an edge of the support surface. These time instants again correspond to the events $\varphi_1$, $\psi_4$, $\varphi_2$, and $\psi_3$. Although the support ratios are calculated such that the $\mathrm{CoP_d}$ should fulfill equation (7.10), these calculations are based on the desired positions of the feet. If the desired velocity is varying, the actual positions of the feet do not correspond to the desired positions of the feet. For instance, in the case of a step change in the desired velocity, it would take the robot one stride cycle, i.e. when all the legs have been lifted and replaced once, until the actual position of the feet correspond with the desired position of the feet. Error in the positioning of the feet or slipping will also have the effect that the $\mathrm{CoP_d}$ will not be correct. However, the $\mathrm{CoP_d}$ will always remain within the boundary of the support surface, as there are always at least three support ratios that are larger than zero.

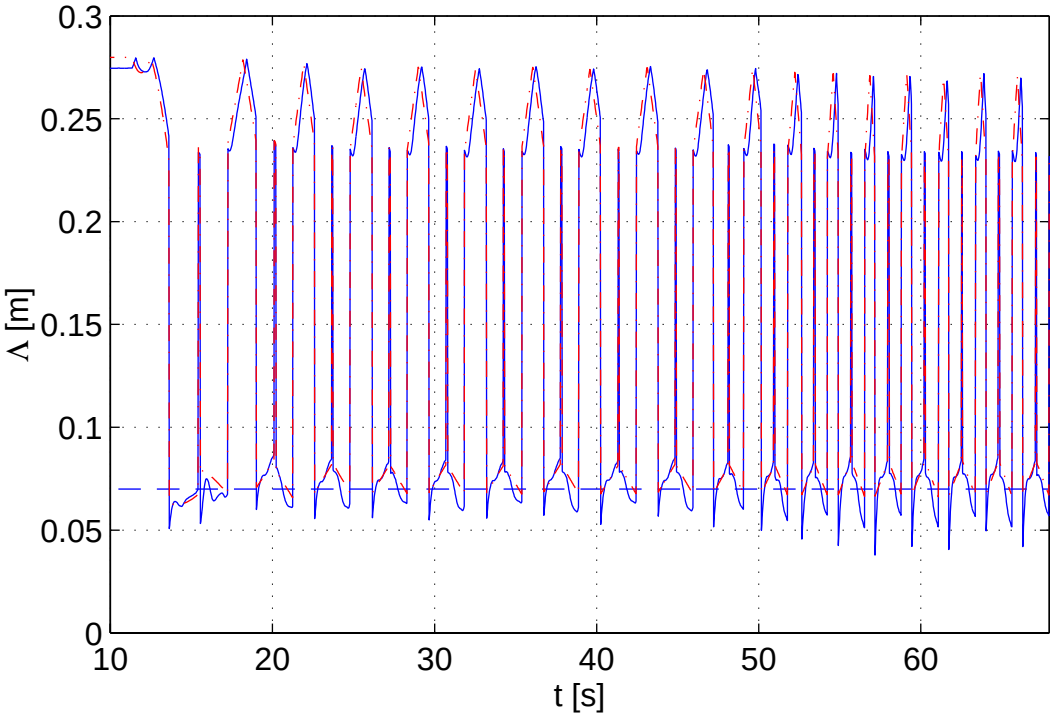


*Figure 7.6. The shortest distance of point $\bar{B}$ (solid), and $CoP_d$ (dash-dot), from an edge of support surface. The dashed line is the SSM ($\Lambda_m$ = 0.07 m).*

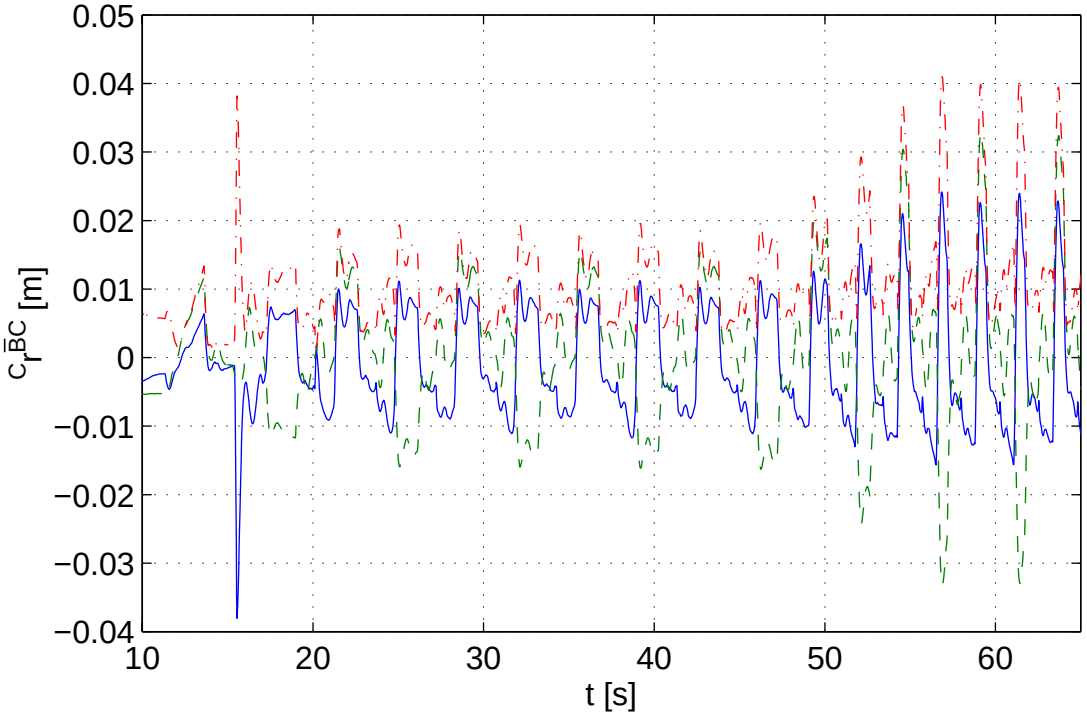


*Figure 7.7. The error vector ${}^{C}\underline{r}^{\bar{B}C}$ between point $\bar{B}$, and the $COP_d$, ${}^{C}r^{\bar{B}C(1)}$ (solid), ${}^{C}r^{\bar{B}C(2)}$ (dashed), $\left\|{}^{C}\underline{r}^{\bar{B}C}\right\|$ (dash-dot).*

Figure 7.8 shows the gait diagram for the first three strides. The gait diagram for each event is generated by selecting the foot with the highest support ratio to be the reference point. The position of the other feet and the point $\overline{B}$, are then plotted relative to the chosen reference foot for the duration of time between two events. The solid line inside the support surface, is the motion of the vertical projection of point $B$, i.e. point $\overline{B}$, where 'o' and 'x' denote the starting and end position, respectively.

Figure 7.9 shows the measured position of the robot in space as a solid line, using the V-Scope, where the robot starts at point (0,0). The dashed line is the average position of the robot for one stride, and the dash-dot line is the desired position of the robot, calculated by integrating the desired velocities, i.e. if (x,y) denote the position of the robot then

$$\begin{aligned} \dot{x} &= v_d^{ND(1)} \cos\phi - v_d^{ND(2)} \sin\phi \\ \dot{y} &= v_d^{ND(1)} \sin\phi + v_d^{ND(2)} \cos\phi \end{aligned} \tag{7.13}$$

where $\dot{\phi} = \omega_d$, $x(0) = y(0) = 0$ and $\phi(0)$ is equal to the average of the measured yaw of the robot before it starts walking.

The support ratios for the whole experiment are shown in figure 7.10. The difference in the support ratios for different velocities is mainly due to the difference in cycle time, where the cycle time reduces with increasing velocity. The shape of the support ratios, i.e. the values of the support ratio parameters, does not change much after a forward velocity of approximately 0.03 m/s has been reached. This is due to that the legs of the robot reach their kinematic limits at about that speed, in which case the desired position of the legs will not change for increasing forward velocity.

This experiment has shown that the robot is capable of walking statically balanced using the approach presented in chapter 6, at a constant desired velocity. Although the support stability margin (SSM) is violated at some time instances, the vertical projection of point $\overline{B}$ remains within the support surface. In order to guarantee that the motion satisfies the SSM, some uncertainty due to the tracking error could be added to the SSM. The experiment also shows some of the downsides of the imple-

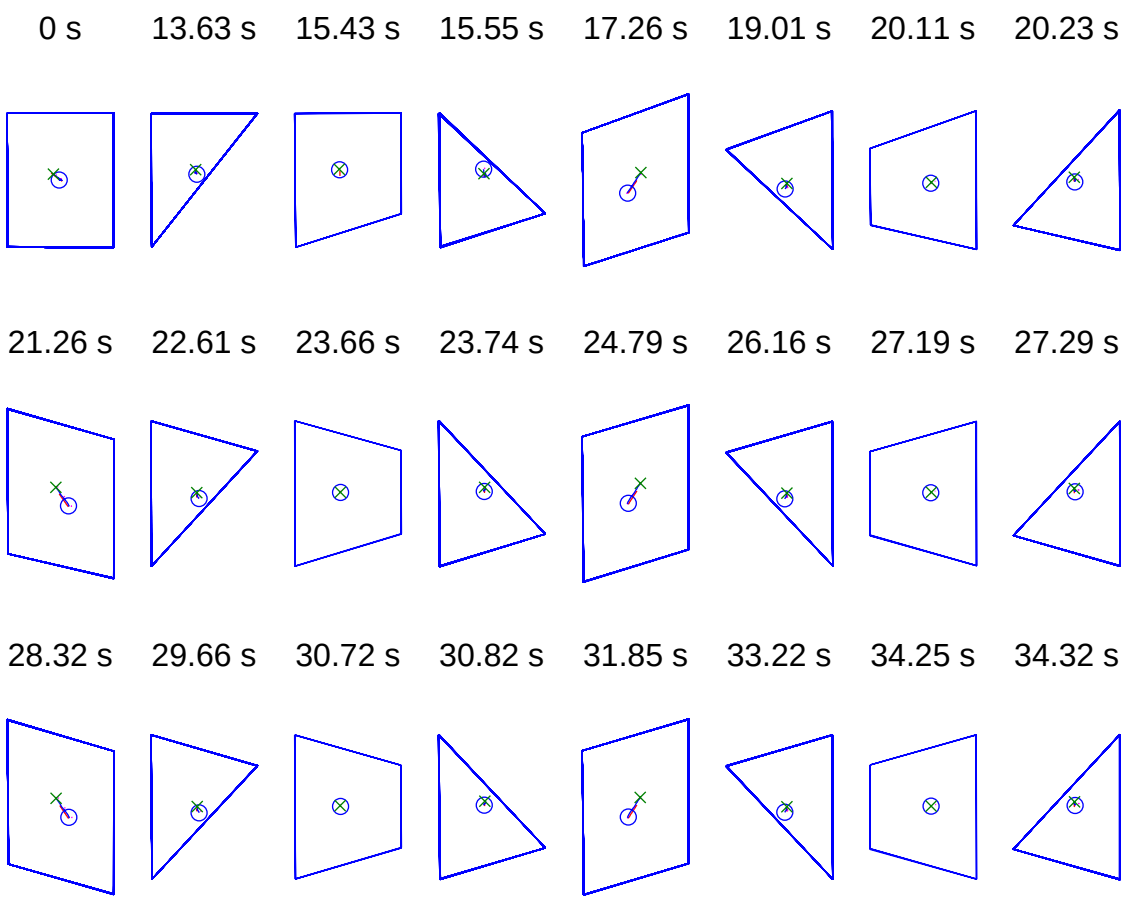


*Figure 7.8. Gait diagram for the robot for the first three strides, each row is one stride. The motion of point $\bar{B}$ between the events is shown as a solid line, where the mark 'o' denotes the position of point $\bar{B}$ at the beginning and 'x' at the end.*

mentation. The desired velocity of the CoP has large step-wise variations that cause jerky motion of the robot, as seen in figure 7.5. This may be the cause of the poor tracking of the desired CoP as can be seen in figure 7.7, which in turn led to violation of the SSM and that the tracking of the desired velocity is not satisfactory. Furthermore, the $\mathrm{CoP}_\mathrm{d}$ can only be guaranteed to remain within the boundary of the support stability margin for constant desired velocity, due to that the support ratios are calculated based on desired positions of the feet.

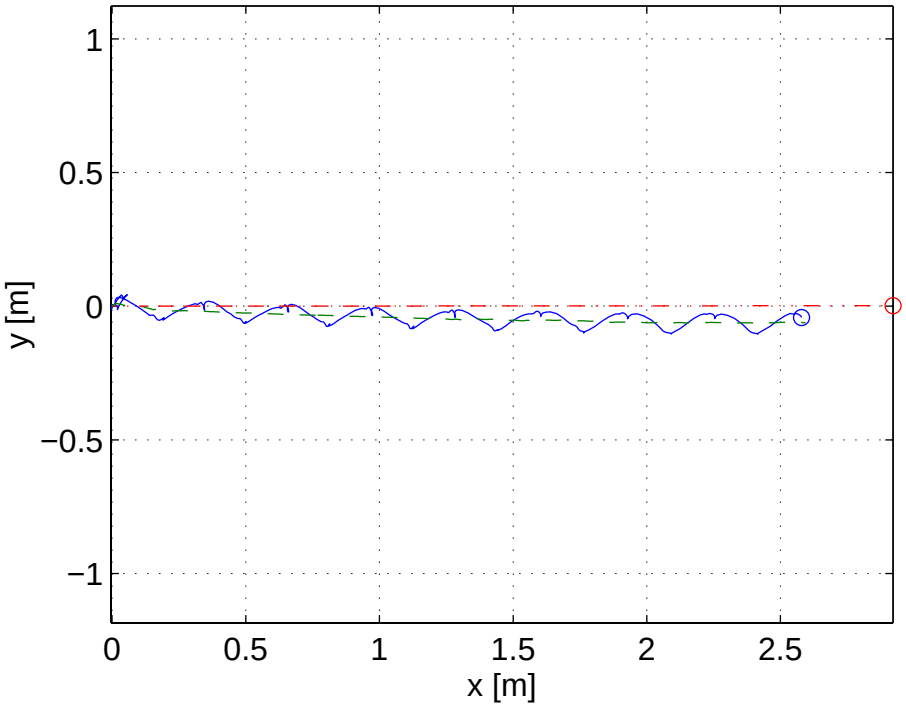


*Figure 7.9. Measured position of the robot in the lab (solid), the averaged position of the robot for one stride (dashed), and the desired position (dash-dot). The circles 'o' denote the end positions.*

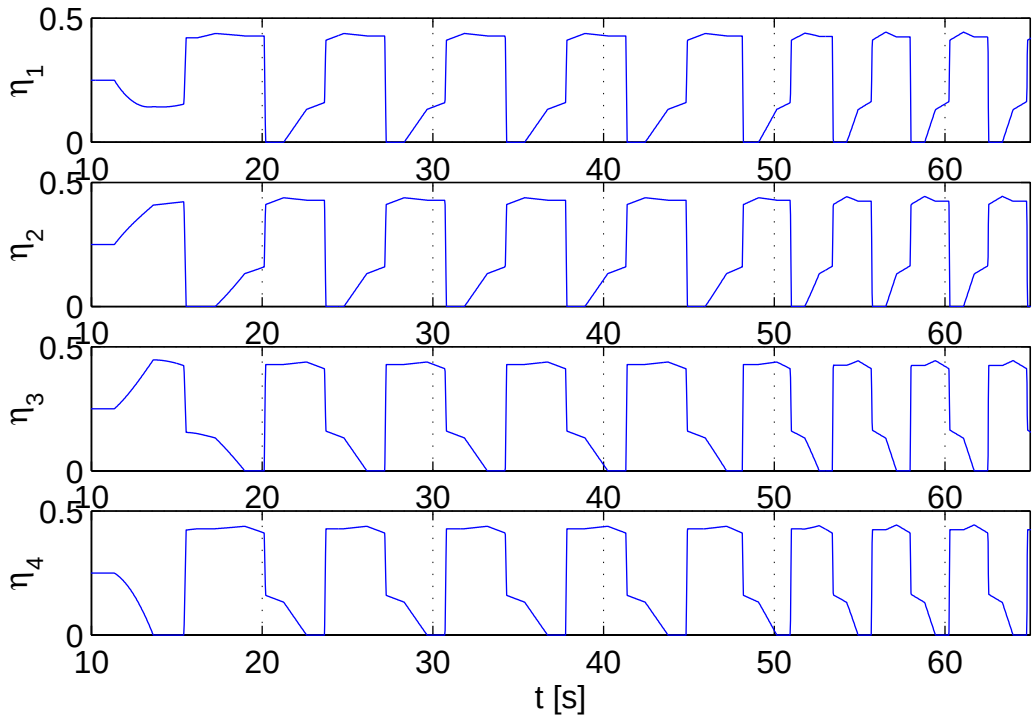


*Figure 7.10. The support ratios ($\eta_i$).*

### 7.2.2. Walking and turning

The second experiment demonstrates the robot turning. The robot walks forward with a velocity of $v_d^{ND(1)} = 0.05$ m/s and turning rate $\omega_d = \pi/80$ rad/s (i.e. the robot is turning to the left). The resulting velocity of the robot is shown in figure 7.11 and the resulting angular velocity is shown in figure 7.12. The velocity error between the averaged velocity and the desired is approximately 10%, for both the forward and the angular velocity.

Figure 7.13 shows the support ratio for one stride. The support ratios for the right legs, leg 2 and 4, support more of the weight, i.e. the robot shifts its weight more to the right side when turning left. Figure 7.14 shows the distance of point $\overline{B}$ and $\mathrm{CoP_d}$ from an edge of the support surface. In this case, the $\mathrm{CoP_d}$ is slightly less than the SSM, at the time instants that correspond to the events $\varphi_1$, $\psi_4$, $\varphi_2$, and $\psi_3$, even though the robot is walking with a constant velocity. The error in the position of $\overline{B}$ relative to $\mathrm{CoP_d}$ is shown in figure 7.15. Probable reasons for why the $\mathrm{CoP_d}$ is slightly less than the SSM could be that the feet slip slightly while turning or that there is a small error in the positioning of the feet at landing. In either case the support surface will not exactly match the desired support surface, on which the calculations of the support ratios are based. Figure 7.16 shows the gait diagram for the first three strides. Looking closely at the diagrams, that correspond to the events $\varphi_1$ and $\varphi_2$, i.e. number 1 and 5 in each row, it can be seen that there are slight changes in the shape during the time period between the events, seen by thicker lines of the boundary. This suggests that the front feet slip as they land. The reason for this can be seen in figure 7.11*b* and *c*, where the reference velocity $v_r^{NB(1)}$ is suddenly negative at the same instant as the front feet are placed, i.e. the robots jerks backwards at the same time as the feet land.

Figure 7.17 shows the motion of the robot, where the solid line is the measured position of the robot, the dashed line is the averaged position over one stride, and the dash-dot line is the desired position of the robot. The backwards jerk in the motion of the robot, mentioned above, can be seen in figure 7.17.

The main purpose of this experiment has been to demonstrate that the robot can turn while maintaining static balance. It also shows the effect of the step-wise varying velocity of the $\mathrm{CoP_d}$, which in this case causes the front feet to slip.

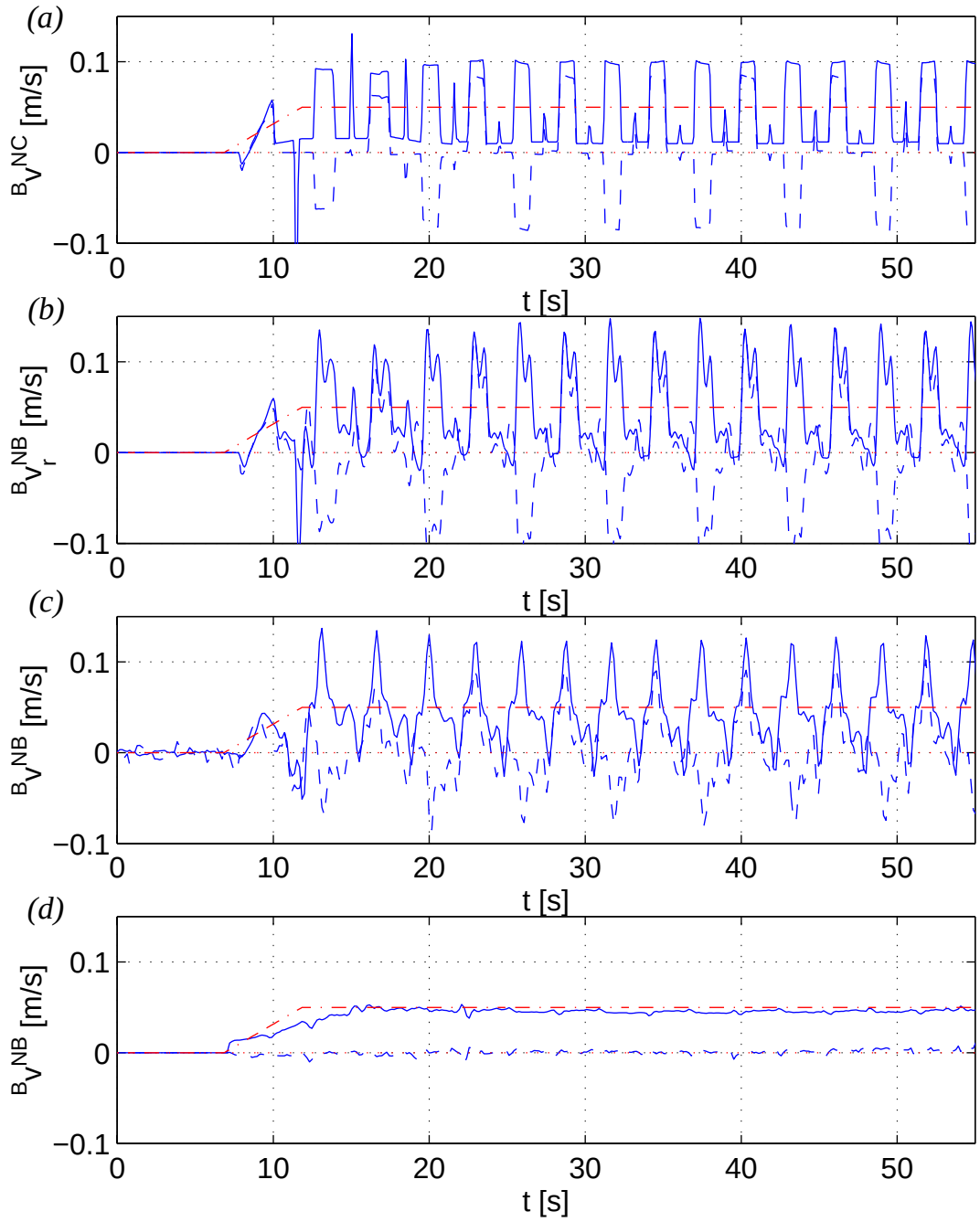


*Figure 7.11. The velocity of the robot when desired velocity is 0.05 m/s and desired turning rate is π/80 rad/s. In all a)-d) $v^{ND(1)}$ (dash-dot) and $v^{ND(2)}$ (dotted). a) The desired velocity of $CoP_d$, $v^{NC(1)}$ (solid) and $v^{NC(2)}$ (dashed). b) The reference body velocity, $v_r^{NB(1)}$ (solid) and $v_r^{NB(2)}$ (dashed). c) The filtered estimate of the velocity from measurement system, $v^{NB(1)}$ (solid) and $v^{NB(2)}$ (dashed). d) The moving average for one stride of the velocity from measurement system, $v^{NB(1)}$ (solid) and $v^{NB(2)}$ (dashed).*

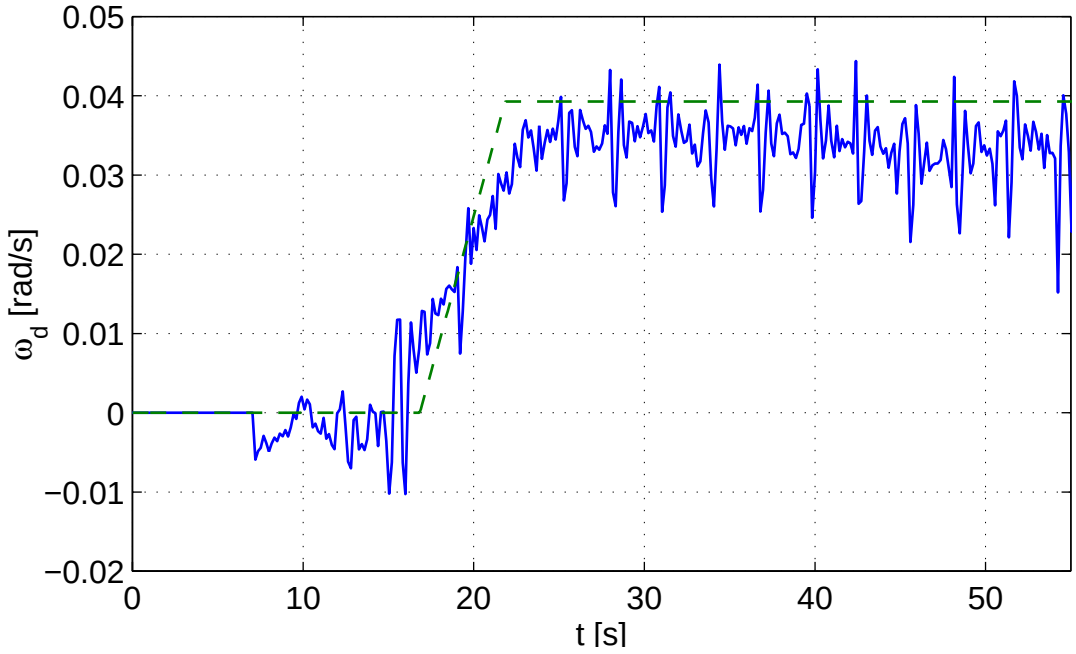


*Figure 7.12. The averaged measured angular velocity of the robot (solid), and the desired angular velocity (dashed).*

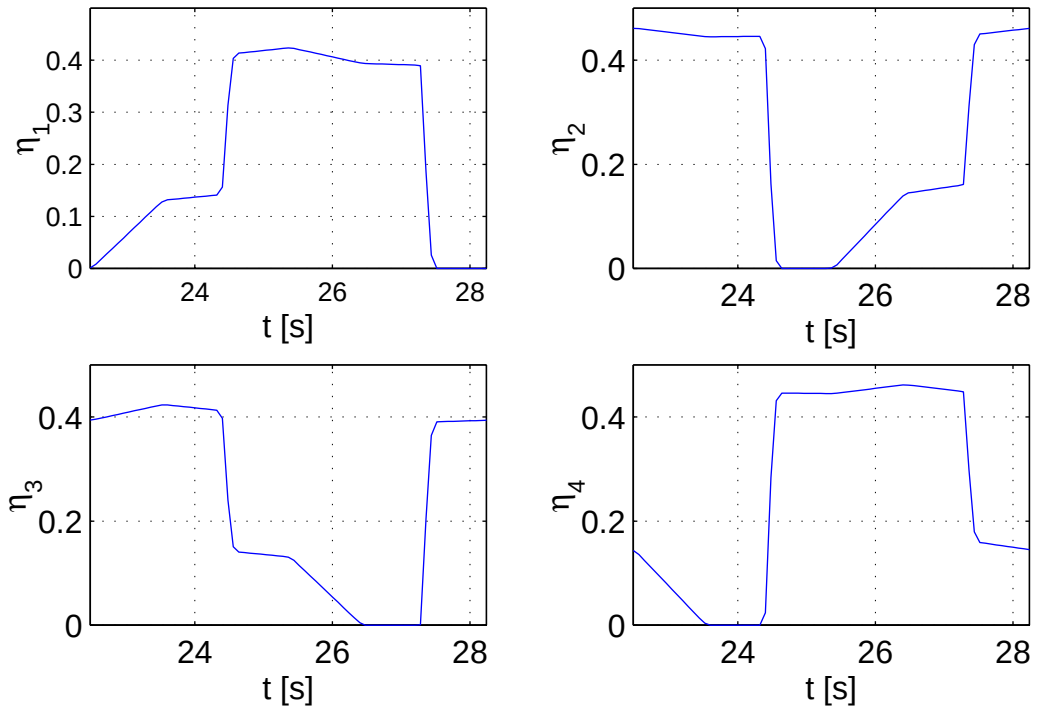


*Figure 7.13. The support ratios ($\eta_i$) for one stride.*

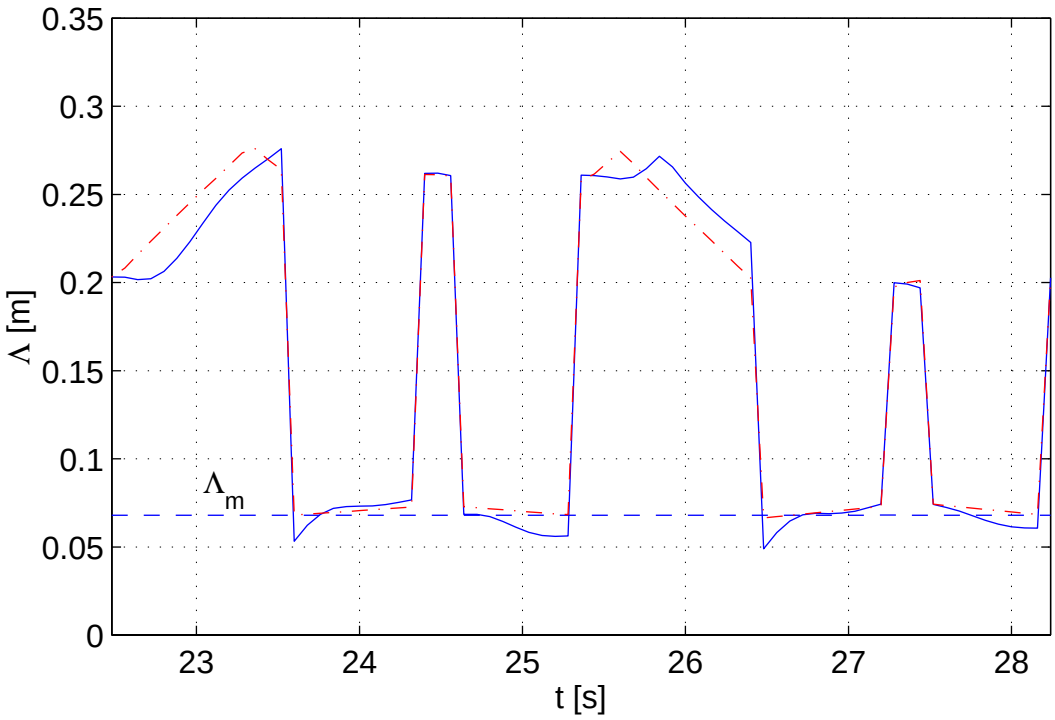


*Figure 7.14. The shortest distance of $\bar{B}$ (solid), and $CoP_d$ (dash-dot) from an edge of support surface, for one stride. The dashed line is the SSM ($\Lambda_m$=0.07 m).*

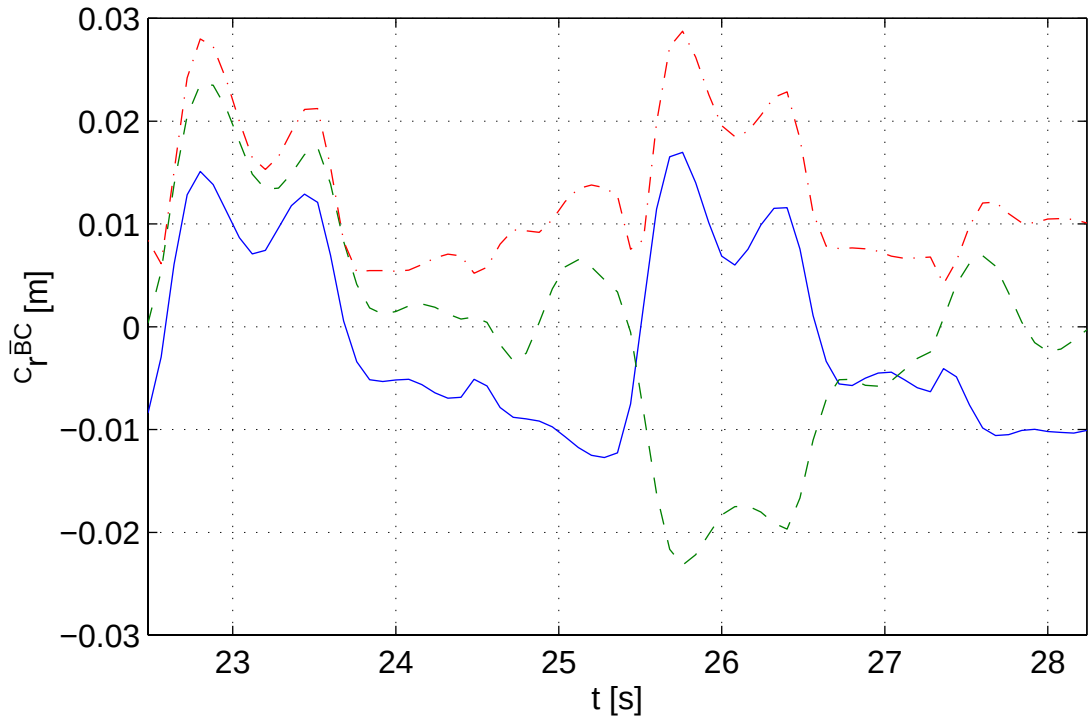


*Figure 7.15. The error vector ${}^{C}\underline{r}^{\bar{B}C}$ between point $\bar{B}$, and the $COP_d$, ${}^{C}r^{\bar{B}C(1)}$ (solid), ${}^{C}r^{\bar{B}C(2)}$ (dashed), $\left\|{}^{C}\underline{r}^{\bar{B}C}\right\|$ (dash-dot), for one stride.*

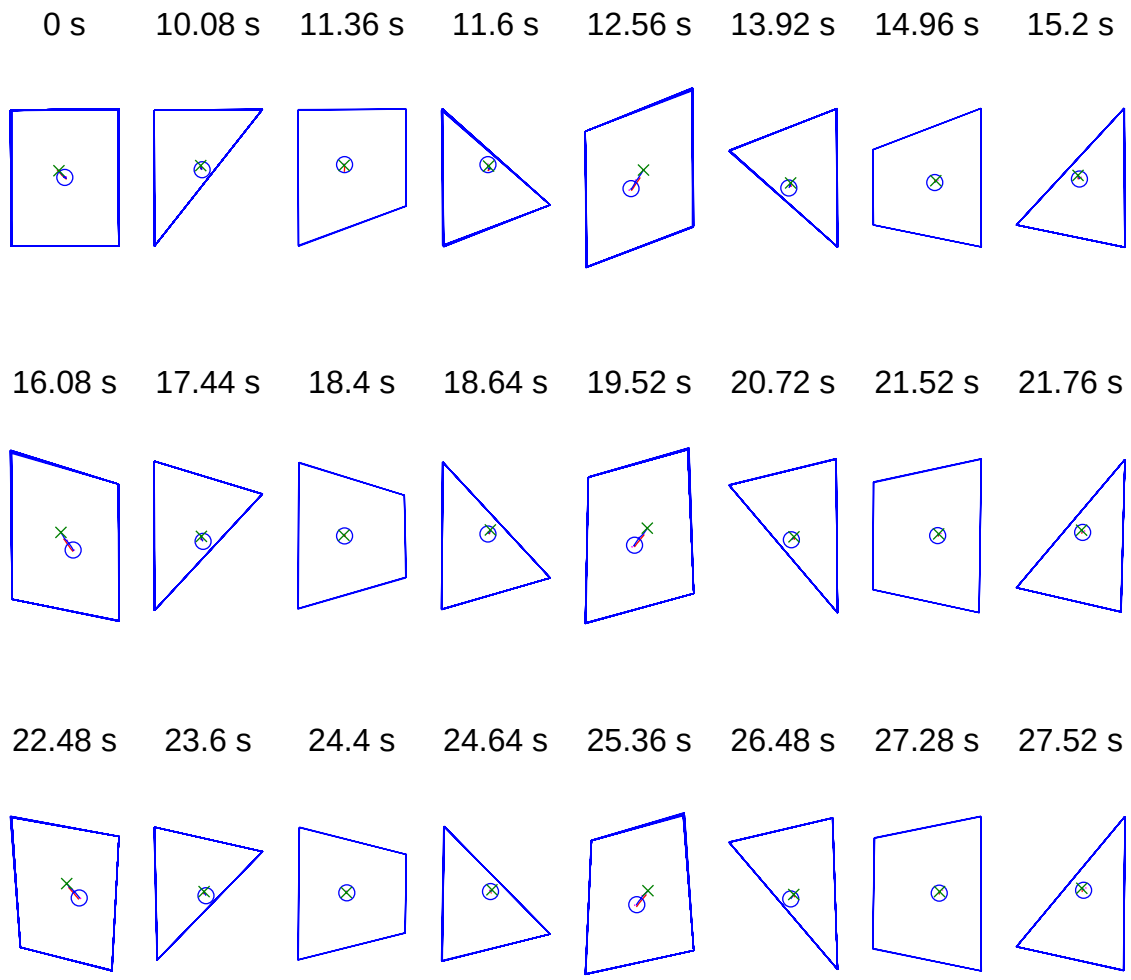


*Figure 7.16. The gait diagram of the robot for the first three strides, when the desired velocity is 0.05 m/s and angular velocity is π/80 rad/s, each row is one stride. The motion of point $\bar{B}$ between the events (solid), where the mark 'o' denotes the position at the beginning and 'x' at the end.*

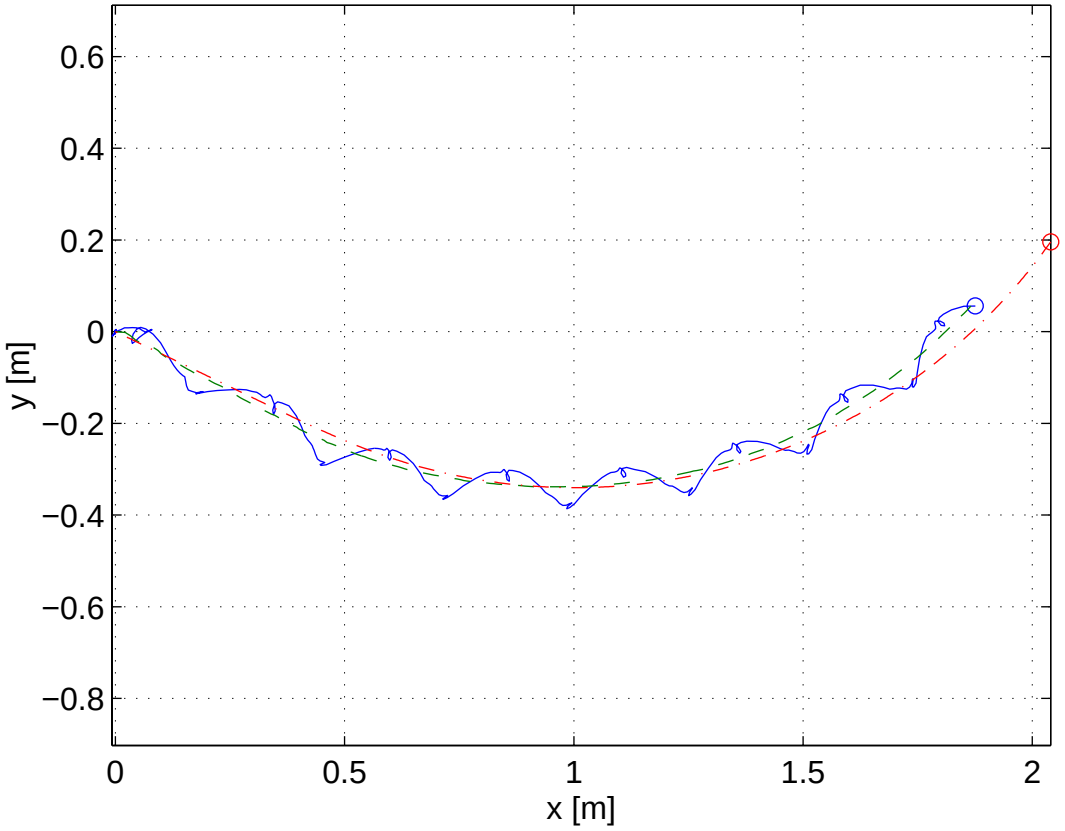


*Figure 7.17. Measured position of the robot in the lab (solid), the averaged position of the robot for one stride (dashed), and the desired position (dash-dot). The circles 'o' denote the end positions.*

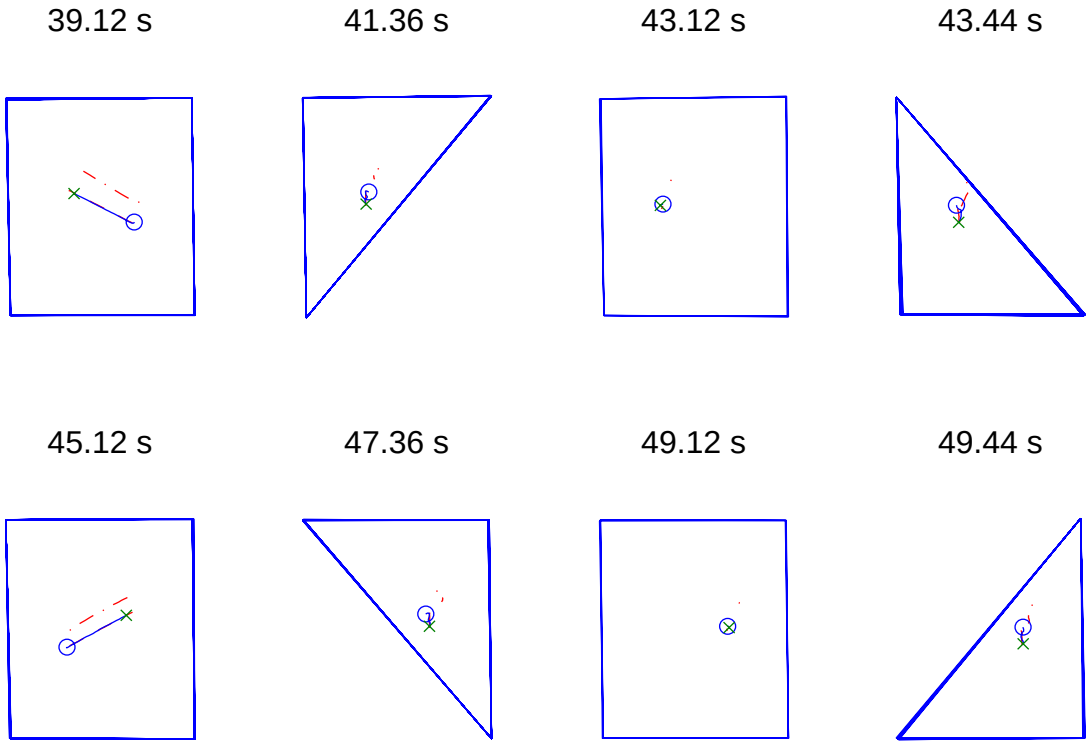


*Figure 7.18. Gait diagram for one stride. The motion of point $\bar{B}$ between the events (solid), where the mark 'o' denotes the position at the beginning and 'x' at the end, normal projection of B (dash-dot).*

### 7.2.3. Stepping and walking on an incline

The final experiments demonstrate the robot stepping and walking on an incline. When the robot is stepping, it is lifting its legs in a normal crawl gait step cycle but is not moving in any direction. Figure 7.18 shows one stride when the robot is standing on an incline of approximately 6 degrees, such that the front end is higher than the hind end. The solid line inside the support surfaces, is the motion of the vertical projection of point *B*, i.e. point $\bar{B}$, where 'o' and 'x' denote the starting and end position, respectively. The dash-dot line is the motion of the projection of point *B* along the estimated normal $\underline{c}_3$ to the plane.

Figure 7.19 shows the results of the estimate of ${}^{C}\underline{n}_3$, i.e. the third axis of *fN*, expressed in *fC*. Figure 7.19*a* shows the attitude angles defining *fC* relative to *fN*, i.e. the angles $\varphi_c^{(2)}$ and $\varphi_c^{(3)}$ calculated using equation (5.30). Figure 7.19*b* shows

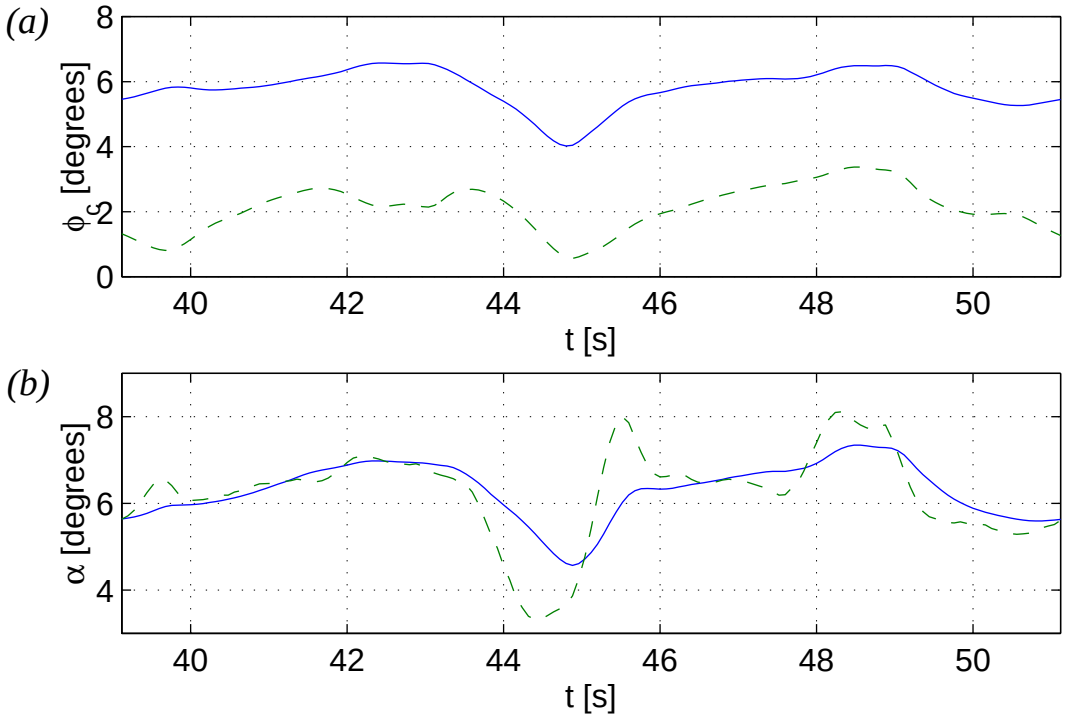


*Figure 7.19. Estimation of attitude of the ground plane. a) The rotations defining the attitude of frame fC relative to frame fN, $\varphi_c^{(2)}$ (solid), $\varphi_c^{(3)}$ (dashed). b) The angle $\alpha_c$ between the vectors $\underline{c}_3$ and $\underline{n}_3$ (solid), and $\alpha_b$ between $\underline{b}_3$ and $\underline{n}_3$ (dashed)*

the angle $\alpha_c$ between the normal vector $\underline{c}_3$ to the plane and the vertical vector $\underline{n}_3$, where the angle is calculated by $\underline{c}_3 \cdot \underline{n}_3 = {}^C n_3^{(3)} = \cos(\alpha_c)$ (solid line), and the angle $\alpha_b$ between the vector $\underline{b}_3$ to the plane and the vertical vector $\underline{n}_3$ (dashed line). The robot has a problem once, during the time period when leg 2 is lifted and placed, i.e. during 43.44 - 45.12 s. The robot tips slightly before the leg 2 is set down again, resulting in that leg 3 loses ground contact briefly.

Figure 7.20 shows a gait diagram when the robot is on a sideways incline, such that the right side is higher than the left side. The inclination is slightly less in this case, or approximately 4 degrees. As seen in figure 7.21*b*, by the $\alpha_b$, the body is pitching an rolling. The estimate of the attitude of the ground plane in figure 7.21*a* remains, however, fairly constant.

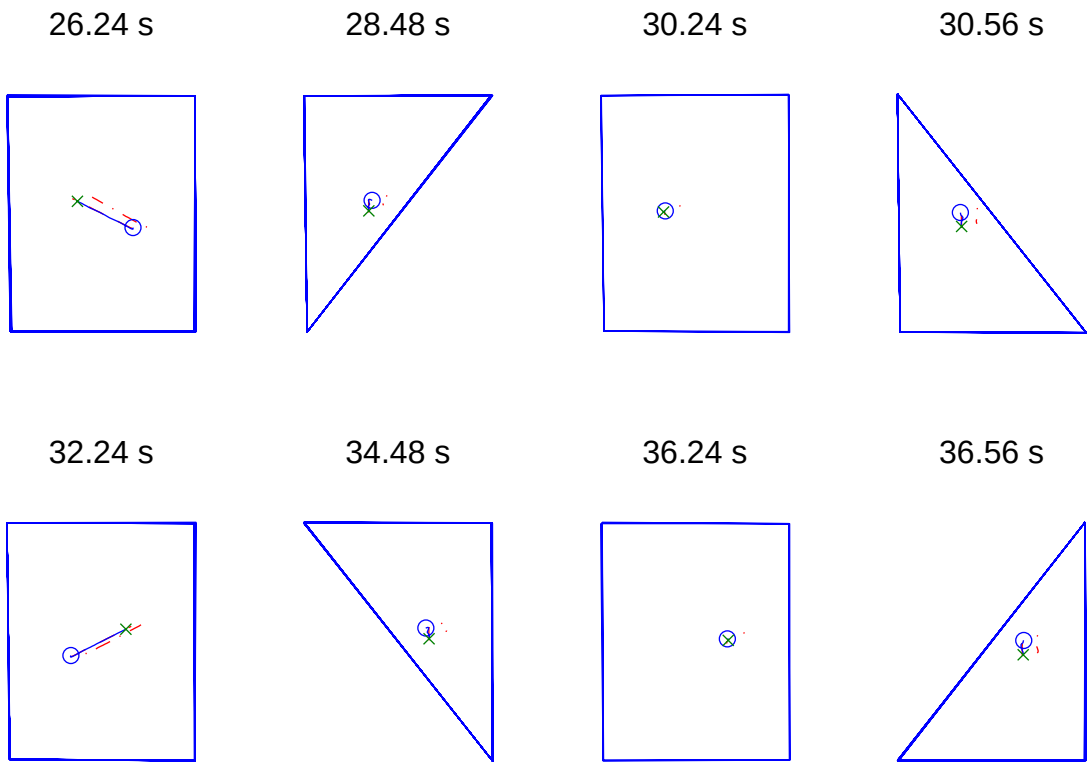


*Figure 7.20. Gait diagram for one stride. The motion of point $\bar{B}$ between the events (solid), where the mark 'o' denotes the position of point $\bar{B}$ at the beginning and 'x' at the end, normal projection of B (dash-dot).*

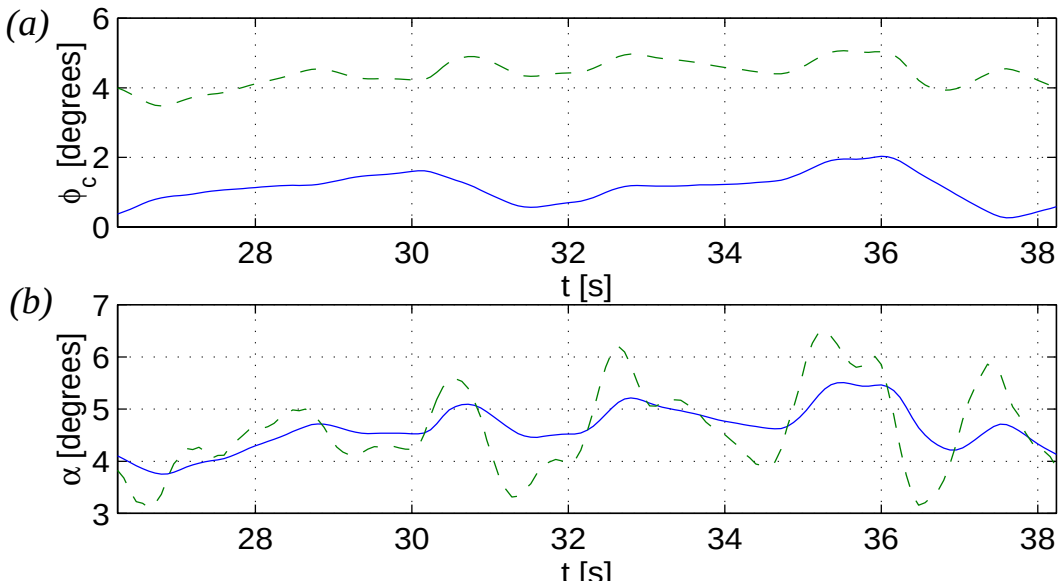


*Figure 7.21. Estimation of attitude of the ground plane. a) The rotations defining frame fC relative to frame fN, $\varphi_c^{(2)}$ (solid), $\varphi_c^{(3)}$ (dashed). b) The angle $\alpha_c$ between the vectors $\underline{c}_3$ and $\underline{n}_3$ (solid), and $\alpha_b$ between $\underline{b}_3$ and $\underline{n}_3$ (dashed)*

In the last experiment the robot walks forward with a velocity of 0.05 m/s, first on a horizontal plane and then up an incline of approximately 6 degrees. When going up on the incline, there is a 6 cm step, which the robot does not know of. Figure 7.22 shows gait diagrams for the robot as it is going from the horizontal plane to the incline. Figure 7.23 shows the estimation of the attitude of the ground plane during that time period. The reason for the jump in the estimation, after about 37 s, is that one of the feet slipped off the step.

The experiment shows some problems with the implementation. The control of the landing of the feet and the lack of adaption to the terrain, results in that in some cases the feet are not in ground contact when they are supposed to. Instead the ground contact is established when the robot starts shifting its weight over onto a newly placed foot, resulting in a tipping motion over to a new support surface. This can be seen in figure 7.23 as the estimate of the attitude of the ground plane is fluctuating. Figure 7.24 shows the shortest distance of point $\overline{B}$ and $\mathrm{CoP_d}$ to an edge of the support surface, and as can be seen, that point $\overline{B}$ is too close to an edge of the support surface, where the largest errors occur during the time periods when the front feet are in the air.

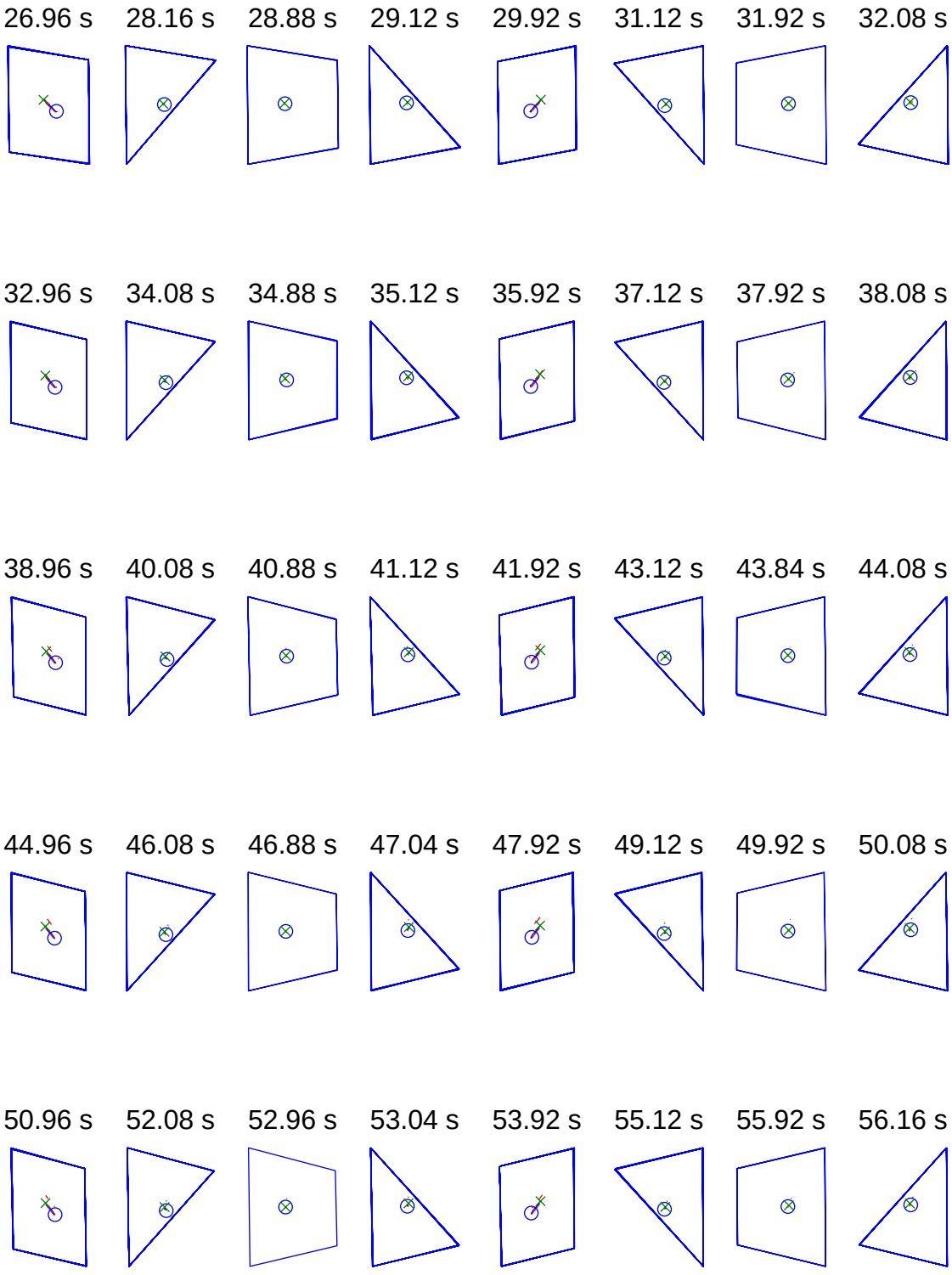


*Figure 7.22. Gait diagram for five strides, when walking from a horizontal to an inclined plane. The motion of point $\bar{B}$ between the events (solid), where the mark 'o' denotes the position of point $\bar{B}$ at the beginning and 'x' at the end, normal projection of B (dash-dot).*

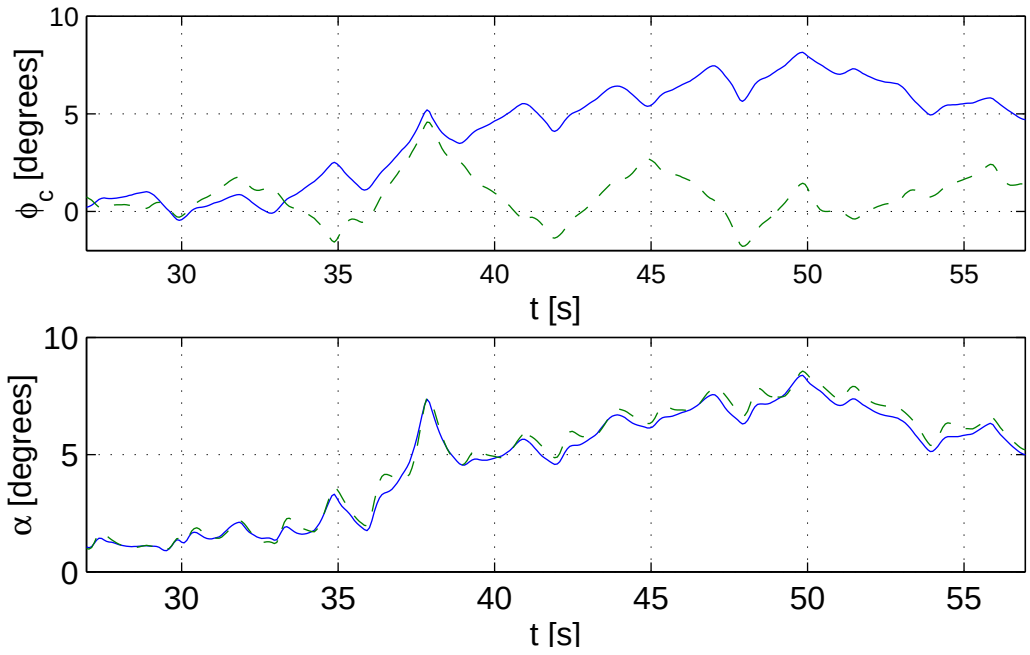


*Figure 7.23. Estimation of attitude of the ground plane. a) The rotations defining frame fC relative to frame fN, $\varphi_c^{(2)}$ (solid), $\varphi_c^{(3)}$ (dashed). b) The angle $\alpha_c$ between the vectors $\underline{c}_3$ and $\underline{n}_3$ (solid), and $\alpha_b$ between $\underline{b}_3$ and $\underline{n}_3$ (dashed)*

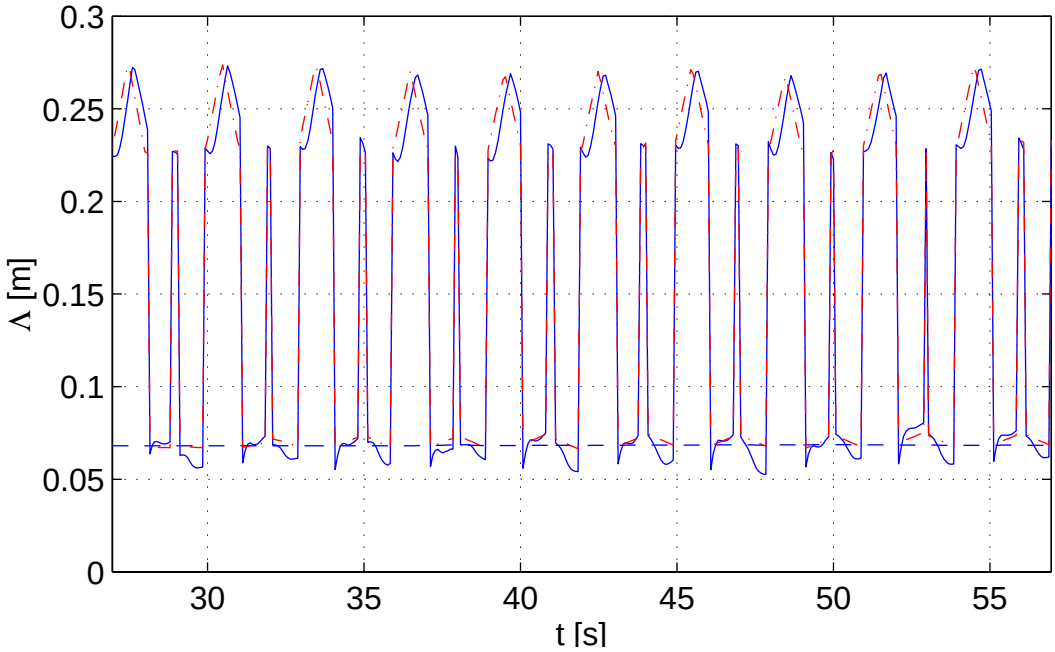


*Figure 7.24. he shortest distance of $\bar{B}$ (solid), and $CoP_d$ (dash-dot) from an edge of support surface. The dashed line is the SSM ($\Lambda_m$= 0.07 m).*

# 8. DISCUSSION

The focus of this thesis has been to develop and implement a method to achieve a statically balanced gait for a quadruped robot. As a goal, this has been accomplished. The center of pressure, i.e. the point where the resultant of the ground reaction forces at the feet acts, is used to develop a stability measure, the support stability margin (SSM), which is then used in the planning of a statically balanced body motion. The SSM is used to set appropriate bounds on the motion of the robot, to account for potentially destabilizing forces or moments. The motion of the robot is planned by determining the supporting force for each leg, which in turn will determine how the robot should shift its weight in order to remain statically balanced. The approach proposed in this thesis, therefore, solves simultaneously the problem of determining a statically balanced motion trajectory for the body, as well as, the distribution of forces to the feet, to compensate for the weight of the robot. The experimental results demonstrate that the quadruped robot WARP1 is able to walk statically balanced on both horizontal and inclined ground.

In this thesis work, the support stability margin was only used to plan the motion of the robot in a feedforward manner. However, the support stability margin can also be used to detect the risk of instability while walking, to allow the robot to take appropriate action to avoid tipping over or to recover from failure.

Several components of the controller for the robot can be refined or further developed, and more components can be added, in order to increase the performance of the robot and to provide the capability of handling more general types of terrain, as

will be discussed in section 8.2. Further investigation are also needed on the effect of different ground properties, for instance material properties, such as the friction and the stiffness of the ground, or geometric properties, such as handling steps and other obstacles. Another interesting challenge would be to investigate whether the approach, presented in this thesis can be extended such that a natural transition to dynamically balanced gaits, such as trotting, can be achieved.

## 8.1. The results of the experiments

In chapters 5 and 6, no assumptions are made that are specific to the robot WARP1, and the approach is general for most quadruped robots. The requirements of the approach are that the position of the feet and the attitude of the robot can be measured. Furthermore, the legs must have the necessary degrees of freedom to allow the robot to position the feet in a three dimensional space. On the other hand, chapter 7 presented an implementation that is more specific to WARP1, although quadruped robots with similar structure should be able to use it.

The main drawback of WARP1 is the size of the space in which the leg can provide the forces necessary to support the robot, i.e. this space is smaller than the kinematic workspace of the legs. For instance, the calculation of the support ratios resulted in that the front legs should support almost half the weight of the robot towards the end of the support phase, i.e. if the robot is walking straight forward, when the foot is farthest behind the hip joint. This limits the length of the stroke of the foot, i.e. the robot has to take rather short steps, which in turn limits the maximum velocity of the robot.

Another problem with WARP1 is its relatively heavy legs. When the robot is walking at higher velocities, the inertial forces acting on the robot, due to the motion of the legs in transfer phase, were quite noticeable, and furthermore, the impact when the legs land is quite large. The heavy legs also result in that the CoG is moving a lot, so the uncertainty in position of CoG, added to the SSM, is quite large.

Given a constant desired velocity, set by the operator, the robot has an error in the average velocity that is almost 10% less than the desired. One probable reason is that the desired velocity of the CoP has large step-wise variations that are very hard for the robot to track. They also cause jerky motion of the robot, which in turn can

cause the feet to slip, thereby the position of the feet will not correspond to the calculated support ratios. As will be discussed in the next section, certain improvements can be made that are likely to improve the velocity tracking.

## 8.2. Future work

The goal of the WARP project is to have a walking robot that can handle difficult terrain. As a step towards that goal, several improvements can be made on the controller presented in this thesis, here two smaller steps are identified. The first involves improving on the ability to handle uneven terrain, and the second involves improving on the velocity tracking and the smoothness of the body trajectory.

### 8.2.1. Adaption to the terrain

To improve the ability to handle uneven terrain, the controller should be able to adapt to the terrain it is walking on. In the implementation, presented in this thesis, the height of the legs were fixed, where it was assumed that the terrain the robot is walking on is approximately planar. However, if the ground is not planar, for instance when going up a step as in the experiments in section 7.2.3, this could cause a foot to lose ground contact as the robot is moving. Another problem could be that a foot, that should be placed, would not find any ground contact, or hit the ground earlier than expected causing a large impact. There are two improvements that can be done, better control of the landing of the feet and active control of the height and attitude of the robot.

The control of the leg during landing can be improved by making it able to handle minor variations in the terrain. For instance, if no ground contact is established, the foot could be moved further downwards, until ground contact is found, or if no ground contact is found, a warning should be sent to a higher control level which would take other actions. On the other hand, if the foot hits the ground earlier than expected, the leg should switch to support phase directly, using the actual landing position as the initial condition for the reference position trajectory during the support phase. Methods to accomplish this were studied in Hardarson, et al. (1999).

The second improvement is active control of the height and attitude of the body of the robot. The goal of the attitude controller, given the estimate of the attitude and distance to the ground plane, would be to maintain the body parallel with the

ground plane at a desired height above the plane. This can be accomplished without interfering with the current controller by only varying the height of the legs, normal to the ground plane. One method, that could potentially be adopted for this purpose, is described in Ridderström and Ingvast (2001b).

### 8.2.2. The support ratio

There were two problems noted with the current calculations of the support ratios. The first is that the support ratios are calculated based on the desired positions of the feet. If the desired velocity is varying, the calculated support ratios do not correspond to the real positions of the feet. There are two problems with this, the desired velocity of the CoP will not be correct and there is a risk that the support stability margin might be violated.

One approach might be to calculate the support ratio parameters by using the actual position of the feet, and predicting one stride ahead in time, using the desired position of the feet. In that case the support ratios would correspond with the desired velocity and the current support pattern.

The second problem is that due to the piece-wise linearly varying support ratios, the desired velocity of the CoP is piece-wise constant. As shown by the experiments in section 7.2, the desired velocity of the CoP showed large variations. To reduce these variations, a term can be added to equation (6.33), that would punish large variations in the velocity of the CoP, for instance

$$\frac{1}{2}\int_0^T (\underline{v}^{NC}(t))^T (\underline{v}^{NC}(t))dt + \sum_i (\underline{v}^{NC}(t_i^+) - \underline{v}^{NC}(t_i^-))^T \boldsymbol{Q} (\underline{v}^{NC}(t_i^+) - \underline{v}^{NC}(t_i^-)) \quad (7.14)$$

where $Q$ is a weight matrix, and $t_i^+$ and $t_i^-$ are the time instants just prior and after the event $i$ of the gait, respectively. Alternatively, it could be investigated whether a more smooth function for the support ratios can be found, such that the desired velocity of the CoP would be a continuous function.

Improvements on the support ratio calculations would result in better velocity tracking, smoother motion and improvement of the stability.

## 8.3. Conclusion

In order to justify the development of walking robots for practical purposes, their potential for handling certain types of difficult terrain should be utilized. This thesis work has dealt with statically balanced gaits for quadruped robots. The main emphasis has been on the stability of such gaits and how they can be accomplished. The motivation for studying statically balanced gaits is that they can be executed arbitrarily slow. This is beneficial in the event that the terrain is uncertain and the robot has to search for footholds, as the robot can remain balanced at all times. There is, however, further work that has to be done before the walking robot WARP1 will be able to handle more general types of terrain.

# 9. REFERENCES


M. Ahmadi, and M. Buehler (1995), A control strategy for stable passive running, *Proc. IEEE/RSJ Conf. on Intelligent Robots and Systems*, **3**: 152-157

M. Ahmadi, and M. Buehler (1997), Stable control of a simulated one-legged running robot with hip and leg compliance, *IEEE Trans. on Robotics and Automation*, **13(1)**: 96-104

A. Albu-Schäffer, and G. Hirzinger (2000), State feedback controller for flexible joint robots: A globally stable approach implemented on DLR's light-weight robots, *Proc. IEEE/RSJ Int. Conf. on Intelligent Robots and Systems*,**2**: 1087-93

R.M. Alexander (1984), The gaits of bipedal and quadrupedal animals, *Int. J. Robotics Research* **3(2)**: 49-59.

R.McN. Alexander (1988), *Elastic mechanisms in animal movements*, Cambridge University Press, Cambridge

R.M. Alexander (1989), Optimization and gaits in the locomotion of vertebrates, *Physiological Reviews* **69(4)**: 1199-1227.

R. McN. Alexander (1990), Three uses of springs in legged locomotion, *Int. J. Robotic Research*, **9(2)**: 53-61

T. Arakawa, and T. Fukuda (1997), Natural motion generation of a biped locomotion robot using the hierarchical trajectory generation method consisting of GA, EP layers, *Proc. IEEE Int. Conf. on Robotics and Automation*, **1**: 211-16

K. Arikawa, and S. Hirose (1996), Development of quadruped walking robot TITAN-VIII, *Proc. IEEE/RSJ Int. Conf. on Intelligent Robots and Systems*, **1**: 208-14

J.E. Bares, and W.L. Whittaker (1993), Configuration of autonomous walkers for extreme terrain, *Int. J. Robotic Research*, **12(6)**: 535-59

R.D. Beer, H.J. Chiel, and L.S. Sterling (1990), A biological perspective on autonomous agent design, *Robotics and Autonomous Systems*, **6**: 169-86

M. Buehler, R. Battaglia, A. Cocosco, G. Hawker, J. Sarkis, and K. Yamazaki (1998), SCOUT: A simple quadruped that walks, climbs, and runs, *Proc. IEEE Int. Conf. on Robotics and Automation*, **2**: 1707-12

J.-S. Chen, F.-T. Cheng, K.-T. Yang, F.-C. Kung, and Y.-Y. Sun (1998), Solving the optimal force distribution problem in multilegged vehicles, *Proc. IEEE Int. Conf. on Robotics and Automation*, **1**: 471-6

F.-T. Cheng, and D.E. Orin (1990), Efficient algorithm for optimal force distribution - The compact-dual LP method, *IEEE Trans. on Robotics and Automation*, **6(2)**: 178-87

S. Cordes, K. Berns, M. Eberl, and W. Ilg (1997), On the design of a four-legged walking machine, *Proc. IEEE Int. Conf. on Robotics and Automation*, **1**: 65-70

J. De Schutter, H. Bruyninckx, W.-H. Zhu and M. W. Spong (1997), Force control: a bird's eye view, *IEEE CSS/RAS Int. Workshop on Control problems in Robotics and Automation: Future Directions*, San Diego, CA

J. Denavit, and R.S. Hartenberg (1955), A kinematic notation for lower-pair mechanisms based on matrices, *J. Applied Mechanics*, p. 215-26

B. Eriksson (1998), *A survey on dynamic locomotion control strategies for legged vehicles*, Technical report, TRITA-MMK 1998:1, Dept. of Machine Design, Royal Institute of Technology, Stockholm

K.S. Espenscheid, R.D. Quinn, R.D. Beer, and H.J. Chiel (1996), Biologically based distributed control and local reflexes improve rough terrain locomotion in a hexapod robot, *Robotics and Automation*, **18**: 59-64

X. Gao, and S.M. Song (1992), A stiffness matrix method for foot force distribution of walking vehicles, *IEEE Trans. on Systems, Man, and Cybernetics*, **22(5)**: 1131-8

J.F. Gardner (1991), Characteristics and approximations of optimal force distributions in walking machines on rough terrain, *Proc. Int. Conf. on Advanced Robotics*, p. 613-8

A. Ghasempoor, and N. Sepehri (1995), A measure of machine stability for moving base manipulators, *Proc. IEEE Int. Conf. on Robotics and Automation*, **3**: 2249-54

D.M. Gorinevsky, and A.Y. Schneider (1990), Force control in locomotion of legged vehicles over rigid and soft surfaces, *Int. J. Robotics Research*, **9(2)**: 4-23

A. Goswami (1999), Postural stability of biped robots and the foot-rotation indicator (FRI) point, *Int. J. Robotics Research*, **18(6)**: 523-33

M. Guihard, and P. Gorce (1996), A new way to tackle position/force control for pneumatic robots, *Proc. IEEE Int. Conf. on Intelligent Robots and Systems*, **2**: 603-10

A. Halme, I. Leppänen, M. Montonen, and S. Ylönen (2001), Robot motion by simultaneously wheel and leg propulsion, *Proc. Int. Conf. on Climbing and Walk-*

*ing Robots (CLAWAR'01)*, p. 1013-20

F. Hardarson, K. Benjelloun, T. Wadden, and J. Wikander (1998), Biologically inspired design and construction of a compliant robot leg for dynamic walking, *Proc. of the 6th UK Mechatronics Forum International Conference*, p. 367-72

F. Hardarson, B. Eriksson, C. Ridderström, T. Wadden, and J. Wikander (1999), Experiments with impedance control of a single compliant leg, *Int. Conf. on Climbing and Walking Robots (CLAWAR'99)*, p. 319-32

F. Hardarson (1999), *Principles of legged robots: Design and control of a single leg prototype*, Licentiate Thesis, Dept. of Machine Design, Royal Institute of Technology, Stockholm, TRITA-MMK 1999:10, ISSN1400-1179,ISRN KTH/MMK--99/10--SE

F. Hardarson, and J. Wikander (2000), Robust torque control of a flexible, geared, DC-motor driven robot joint, *Proc. 1st IFAC Conf. on Mechatronic Systems*, **2**: 659-64

M. Hildebrand (1965), Symmetrical gaits of horses, *Science*, **150**: 701-8

K. Hirai, M. Hirose, Y. Haikawa, and T. Takenaka (1998), The development of Honda humanoid robot, *Proc. IEEE Int. Conf. on Robotics and Automation*, **2**: 1321-6

S. Hirose, K. Yoneda, and I. Arai (1991), Design of prismatic quadruped walking vehicle TITAN VI, *Int. Conf. on Advanced Robotics*, **1**: 732-8

S. Hirose, H. Tsukagoshi, and K. Yoneda (2001), Normalized energy stability margin and its contour of walking vehicles on rough terrain, *Proc. IEEE/RSJ Int. Conf. on Intelligent Robots and Systems*, **1**: 181-6

N. Hogan (1984), Adaptive control of mechanical impedance by coactivation of antagonist muscles, *IEEE Trans. on Automatic Control*, **ac-29(8)**: 681-9

N. Hogan (1985), Impedance control: An approach to manipulation, Part 1-Theory, Part II-Implementation, Part III-Applications, *J. Dynamic Systems, Measurements, and Control*, **107**: 1-24

V. Hugel, and P. Blazevic (1999), Towards efficient implementation of quadruped gaits with duty factor of 0.75, *Proc. IEEE Int. Conf. on Robotics and Automation*, **3**: 2360-65

K. Inagaki, and H. Kobayashi (1993), A gait transition for quadruped walking machine, *Proc. IEEE/RSJ Int. Conf. on Intelligent Robots and Systems*, **1**: 525-31

J. Ingvast, C. Ridderström, F. Hardarson, and J. Wikander (2001), Improving a trotting robot's gait by adapting foot reference offsets, *Proc. Int. Conf. on*

*Climbing and Walking Robots (CLAWAR'01)*, p. 711-8

A. Isidori (1995), *Nonlinear Control Systems*, Springer-Verlag, London

S. Ito, and H. Kawasaki (2000), A standing posture control based on ground reaction forces, *Proc. IEEE/RSJ Int. Conf. on Intelligent Robots and Systems*, **2**: 1340-5

D.-O. Kang, Y.-J. Lee, Y.S. Hong, and Z. Bien (1997), A study of an adaptive gait for a quadruped walking robot under external forces, *Proc. IEEE Int. Conf. on Robotics and Automation*, **4**: 2777-82

H. Karlsson (2002), to be published, Master thesis, MMK 2002:41 MDA193, Dept. of Machine Design, Royal Institute of Technology, Stockholm

C.A. Klein, K.W. Olsson, and D.R. Pugh (1983), Use of force and attitude sensors for locomotion of a legged vehicle over irregular terrain, *Int. J. Robotics Research*, **2(2)**: 3-17

C.A. Klein, and S. Kittivatcharapong (1990), Optimal force distribution for the legs of a walking machine with friction cone constraints, *IEEE Trans. on Robotics and Automation*, **6(1)**: 73-85

T.-W. Koo, and Y.-S. Yoon (1999), Dynamic instant stability measure for quadruped walking robot, *Robotic*a, **17**: 59-70

V.R. Kumar, and K.J. Waldron (1988), Force distribution in closed kinematic chains, *IEEE J. Robotics and Automation*, **4(6)**: 657-64

V.R. Kumar, and K.J. Waldron (1989), Adaptive gait control for a walking robot, *J. Robotic Systems*, **6(1)**: 49-76

R. Kurazume, S. Hirose, and K. Yoneda (2001), Feedforward and feedback dynamic trot gait control for a quadruped walking vehicle, *Proc. IEEE Int. Conf. on Robotics and Automation*, **3**: 3172-80

H. Lehtinen (1996), Force control for walking on soft terrain, *Robotica*, **14**: 165-72

A. Lennartsson (1999), *Efficient multibody dynamics*, Doctoral Thesis, Department of Mechanics, Royal Institute of Technology, Stockholm, TRITA-MEK 1999:01, ISSN 0348-467X, ISRN KTH/MEK/TR--99/01--SE

M. Lesser (1995), *The analysis of complex nonlinear mechanical systems: A computer algebra assisted approach*, World Scientific, Singapore

B.-S. Lin, and S.M. Song (1993), Dynamic modelling, stability and energy efficiency of a quadrupedal walking machine, *Proc. IEEE Int. Conf. on Robotics and Automation*, **3**: 367-73

H. Lind (1993), *A distributed implementation of dynamic control on a direct-drive*

*robot system*, Doctoral Thesis, Dept. of Machine Elements, Royal Institute of Technology, Stockholm, TRITA-MAE 1993:3, ISSN 0282-0048, ISRN KTH/ MAE/R--93/3--SE

H. Liu, and B. Wen (1997), Force distribution for the legs of a quadruped walking vehicle, *J. of Robotics Systems*, **14(1)**: 1-8

D.W. Marhefka, and D.E. Orin (1998), Quadratic optimization of force distribution in walking machines, *Proc. IEEE Int. Conf. on Robotics and Automation*,**1**: p. 477-83

T. McGeer (1990), Passive dynamic walking, *Int. J. Robotics Research*, **9(2)**: 62-82

R.B. McGhee, and A.A. Frank (1968), On the stability properties of quadruped creeping gaits, *J. Mathematical Biosciences*, **3**: 331-351

T.A. McMahon (1985), The role of compliance in mammalian running gaits, *J. Experimental Biology*, **115**: 263-82

D.A. Messuri, and C.A. Klein (1985), Automatic body regulation for maintaining stability of legged vehicle during rough terrain locomotion, *IEEE J. Robotics and Automation*, **RA-1(3)**: 132-41

E.Z. Moore, and M. Buehler (2001), Stable stair climbing in a simple hexapod, *Int. Conf. on Climbing and Walking Robots (CLAWAR'01)*, p. 603-9

R.M. Murray, Z. Li, and S. Sastry (1994), *A mathematical introduction to robotic manipulation*, CRC Press

P.V. Nagy, S. Desa, and W.L. Whittaker (1994), Energy-based stability measures for reliable locomotion of statically stable walkers: Theory and application, *Int. J. Robotics Research*, **13(3)**: 272-87

M.A. Nahon, and J. Angeles (1992), Real-time force optimization in parallel kinematic chains under inequality constraints, *IEEE Trans. on Robotics and Automation*, **8(4)**: 439-50

G.M. Nelson, R.D. Quinn, R.J. Bachmann, W.C. Flannigan, R.E. Ritzmann, and J.T. Watson (1997), Design and simulation of a cockroach-like hexapod robot, *Proc. IEEE Int. Conf. on Robotics and Automation*, **2**: 1106-11

G.M. Nelson and R.D. Quinn (1998), Posture control of a cockroach-like robot, *Proc. IEEE Int. Conf. on Robotics and Automation*, **1**: 157-162

R. Ortega, and M. W. Spong (1988), Adaptive motion control of rigid robots: a tutorial, *Proc. IEEE Conf. on Decision and Control*, **2**: 1575-84

E.G. Papadopoulos, and D.A. Rey (1996), A new measure of tipover stability mar-

gin for mobile manipulators, *Proc. IEEE Int. Conf. on Robotics and Automation*, **4**: 3111-6

L. Petterson (1999), *Control system architecture for a walking robot*, Licentiate Thesis, TRITA-MMK 1999:3, Dept. of Machine Design, Royal Institute of Technology, Stockholm

F. Pfeiffer, J. Eltze, and H.-J. Weidemann (1995), Six-legged technical walking considering biological principles, *Robotics and Automation*, **14**: 223-32

J. Pratt, P. Dillworth, and G.A. Pratt (1997), Virtual model control of a bipedal walking robot, *Proc. IEEE Int. Conf. Robotics and Automation*, **1**: 193-8

J. Pratt, and G. Pratt (1999), Exploiting Natural Dynamics in the Control of a three-dimensional bipedal walking simulation, *Int. Conf. on Climbing and Walking Robots (CLAWAR'99)*, p. 797-807

R.D. Quinn, and K. Espenschied (1993), Control of a hexapod robot using biologically inspired neural network, In: *Biological neural networks in invertebrate neuroethology and robotics*, Academic press, p. 365-81

M.H. Raibert (1986), *Legged robots that balance*, Cambridge, Massachusetts: MIT Press

H. Rehbinder (2001), *State estimation and limited communication control for nonlinear robotic systems*, Doctoral Thesis, Dept. of Mathematics, Royal Institute of Technology, Stockholm, TRITA-MAT-01-OS-09, ISSN 1401-2294, ISRN KTH/OPT SYST/DA 01/05-SE

C. Ridderström (1999), *Legged locomotion control: A literature study*, Technical Report, Dept. of Machine Design, Royal Institute of Technology, Stockholm, TRITA-MMK 1999:27, ISSN 1400-1179, ISRN KTH/MMK/R--99/27--SE

C. Ridderström, J. Ingvast, F. Hardarson, M. Gudmundsson, M. Hellgren, J. Wikander, T. Wadden, and H. Rehbinder (2000), The basic design of the quadruped robot WARP1, *Int. Conf. on Climbing and Walking Robots (CLAWAR)*, p. 87-94

C. Ridderström, and J. Ingvast (2001a), Combining control design tools - From modelling to implementation, *Proc. IEEE Int. Conf. on Robotics and Automation*, **2**: 1327-33

C. Ridderström, and J. Ingvast (2001b), Quadruped posture control based on simple force distribution - A notion and trial, *Proc. IEEE/RSJ Int. Conf. on Intelligent Robots and Systems*, **4**: 2326-31

C. Ridderström (2002), Stability of statically balanced stances for legged robots

with compliance, *to be presented at IEEE Int. Conf. on Robotics and Automation*

C.L. Shih, Y.Z. Li, S. Chung, T.T. Lee, and W.A. Gruver (1990), Trajectory synthesis and physical admissability for a biped robot during the single support phase, *Proc. IEEE Int. Conf. on Robotics and Automation*, **3**: 1646-52

D. Shirley and J. Matijevic (1995), Mars Pathfinder microrover, *Autonomous Robots*, **2**:283-89

F.M. Silva, and J.A.T. Machado (2001), Goal-oriented biped walking based on force interaction control, *Proc. IEEE Int. Conf. on Robotics and Automation*, **4**: 4122-7

S.M. Song, and K.J. Waldron (1989), *Machines that walk: The adaptive suspension vehicle*, Massachusetts: MIT Press

M.W. Spong (1987), Modelling and control of elastic joint robots, *J. Dynamic Systems, Measurements, and Control*, **109**: 310-19

H. Takeuchi (2001), Development of MEL horse, *Proc. IEEE Int. Conf. on Robotics and Automation*, **3**: 3165-71

D.J. Todd (1985), *Walking machines: An introduction to legged robots*, Kogan Page Ltd., London

P. Tomei (1991), A simple PD controller for a robot with elastic joints, *IEEE Trans. on Automatic Control*, **36(10)**: 1208-13

C. Tzafestas, N.K. M'Sirdi, N. Manamani (1997), Adaptive impedance control applied to a pneumatic legged robot, *J. Intelligent and Robotic Systems*, **20**: 105-129

M. Vukobratovic, and J. Stepanenko (1972), On the stability of anthropomorphic systems, *J. Mathematical Bioscience*, **15**: 1-37

T. Wadden (1998), *Neural control of locomotion in biological and robotic systems*, Doctoral Thesis, TRITA-NA-P9809, Dept. of Numerical Analysis and Computing Science, Royal Institute of Technology, Stockholm

K.J. Waldron (1986), Force and motion management in legged locomotion, *IEEE J. Robotics and Automation*, **RA-2(4)**: 214-20

D. Wettergreen, C. Thorpe, and R. Whittaker (1993), Exploring Mount Erebus by walking robot, *Robotics and Autonomous Systems*, **11**: 171-85

J. Yamaguchi, A. Takanishi, and I. Kato (1995), Experimental development of a foot mechanism with shock absorbing material for acquisition of landing surface position information and stabilization of dynamic biped walking, *Proc.*

*IEEE Int. Conf. on Robotics and Automation*, **3**: 2892-9

J. Yamaguchi, and A. Takanishi (1997), Development of a biped walking robot having antagonistic driven joints using nonlinear spring mechanism, *Proc. IEEE Int. Conf. on Robotics and Automation*, **2**: 799-804

K. Yoneda, H. Iiyama, and S. Hirose (1994), Sky-hook suspension control of quadruped walking vehicle, *Proc. IEEE Int. Conf. on Robotics and Automation*, **2**: 999-1004

K. Yoneda, and S. Hirose (1995), Dynamic and static fusion gait of a quadruped walking vehicle on a winding path, *Advanced robotics*, **9(2)**: 125-36

D. Zhou, and K.H. Low (1999), A friction constraint method for the force distribution of quadruped robots, *Proc. IEEE/ASME Int. Conf. on Advanced Intelligent Mechatronics*, p. 866-71

D. Zhou, and K.H. Low (2001), Combined use of ground learning model and active compliance to the motion control of walking robotic legs, *Proc. IEEE Int. Conf. on Robotics and Automation*, **3**: 3159-64

## APPENDIX A: THE LAGRANGE EQUATIONS

One of the standard methods for deriving the equations of motion for mechanical systems are the Euler-Lagrange equations. This method will be used here as it highlights some of the properties of the system. The Euler-Lagrange equations are

$$\frac{d}{dt}\frac{\partial L}{\partial \underline{\dot{q}}} - \frac{\partial L}{\partial \underline{q}} = \underline{f} \tag{A.1}$$

where $\underline{q}$ is the vector of generalized coordinates, $\underline{f}$ is the vector of generalized forces acting on the system, and $L$ is the Lagrangian, corresponding to the difference between the kinetic energy, $T$, and the potential energy, $P$, i.e. the Lagrangian is $L = T\text{-}P$.

Robotic systems have two important properties. The potential energy is only a function of the generalized coordinates, i.e. potential energy can be expressed as $P(\underline{q})$, and the kinetic energy is a quadratic function of the derivatives of the generalized coordinates

$$T(\underline{q}, \underline{\dot{q}}) = \frac{1}{2}\underline{\dot{q}}^T \boldsymbol{D}(\underline{q})\underline{\dot{q}} = \frac{1}{2}\sum_{i,\,j} D^{ij}(\underline{q})\dot{q}^i\dot{q}^j \tag{A.2}$$

where $\boldsymbol{D}(\underline{q})$ is the inertia matrix. The inertia matrix is always positive definite and symmetric. The Lagrangian can then be written as

$$L = \frac{1}{2}\underline{\dot{q}}^T \boldsymbol{D}(\underline{q})\underline{\dot{q}} - P(\underline{q}) \tag{A.3}$$

From the Lagrange equation get that

$$\boldsymbol{D}(\underline{q})\underline{\ddot{q}} + \dot{\boldsymbol{D}}(\underline{q})\underline{\dot{q}} - \frac{1}{2}\frac{\partial}{\partial \underline{q}}(\underline{\dot{q}}^T \boldsymbol{D}(\underline{q})\underline{\dot{q}}) + \frac{\partial}{\partial \underline{q}}P(\underline{q}) = \underline{f} \tag{A.4}$$

Each row $k$ of the vector expression can be expressed in sums as

$$\sum_{j\,=\,1}^{n} (D^{kj}(\underline{q})\ddot{q}^j + \dot{D}^{kj}(\underline{q})\dot{q}^j) - \frac{\partial}{\partial q^k}\left(\frac{1}{2}\sum_{i,\,j} D^{ij}(\underline{q})\dot{q}^i\dot{q}^j\right) + \frac{\partial}{\partial q^k}P(\underline{q}) = f^k \tag{A.5}$$

The term $\dot{D}^{kj}(\underline{q})$ can be written as

$$\dot{D}^{kj}(\underline{q}) \;=\; \frac{d}{dt}D^{kj}(\underline{q}) \;=\; \sum_{i}\frac{\partial}{\partial q^{i}}D^{kj}(\underline{q})\dot{q}^{i} \tag{A.6}$$

so equation (A.5) can be written as

$$\sum_{j}D^{kj}(\underline{q})\ddot{q}^{j} + \sum_{i,\,j}\left(\frac{\partial}{\partial q^{i}}D^{kj}(\underline{q}) - \frac{1}{2}\frac{\partial}{\partial q^{k}}D^{ij}(\underline{q})\right)\dot{q}^{i}\dot{q}^{j} + \frac{\partial}{\partial q^{k}}P(\underline{q}) \;=\; f^{k} \tag{A.7}$$

The second term on the left hand side of equation (A.6) can be written as, using the symmetry of the inertia matrix

$$\sum_{i,\,j}\left(\frac{\partial}{\partial q^{i}}D^{kj} - \frac{1}{2}\frac{\partial}{\partial q^{k}}D^{ij}\right)\dot{q}^{i}\dot{q}^{j} \;=\; \frac{1}{2}\sum_{i,\,j}\left(\frac{\partial}{\partial q^{i}}D^{kj} + \frac{\partial}{\partial q^{j}}D^{ki} - \frac{\partial}{\partial q^{k}}D^{ij}\right)\dot{q}^{i}\dot{q}^{j} \tag{A.8}$$

Define the coefficients

$$c^{kji}(\underline{q}) \equiv \frac{1}{2}\left\{\frac{\partial}{\partial q^{i}}D^{kj}(\underline{q}) + \frac{\partial}{\partial q^{j}}D^{ki}(\underline{q}) - \frac{\partial}{\partial q^{k}}D^{ij}(\underline{q})\right\} \tag{A.9}$$

which are known as Christoffel symbols (of the first kind) (Ortega, and Spong, 1988).

Define now vector $\underline{h}$ which is the partial derivative of the potential energy function

$$h^{k}(\underline{q}) \equiv \frac{\partial}{\partial q^{k}}P(\underline{q}) \tag{A.10}$$

and a matrix $\boldsymbol{C}$ which elements are

$$C^{kj}(\underline{q},\,\underline{\dot{q}}) \equiv \sum_{i\,=\,1}^{n} c^{kji}(\underline{q})\dot{q}^{i} \tag{A.11}$$

and get finally by inserting into equation (A.6) that

$$\sum_{j}D^{kj}(\underline{q})\ddot{q}^{j} + \sum_{j}C^{kj}(\underline{q},\,\underline{\dot{q}})\dot{q}^{j} + h^{k}(\underline{q}) \;=\; f^{k} \tag{A.12}$$

or in vector form that

$$\boldsymbol{D}(\underline{q})\underline{\ddot{q}} + \boldsymbol{C}(\underline{q},\,\underline{\dot{q}})\underline{\dot{q}} + \underline{h}(\underline{q}) \;=\; \underline{f} \tag{A.13}$$

The vector $\boldsymbol{C}(\underline{q}, \underline{\dot{q}})\underline{\dot{q}}$ contains the centrifugal and coriolis forces, where the centrifugal forces are terms of type $(\dot{q}^j)^2$, and the coriolis forces are the terms of type $\dot{q}^i\dot{q}^j$ where $i \neq j$. Comparing to equation (A.4), the vector of centrifugal and coriolis forces are equal to

$$\boldsymbol{C}(\underline{q}, \underline{\dot{q}})\underline{\dot{q}} = \dot{\boldsymbol{D}}(\underline{q})\underline{\dot{q}} - \frac{1}{2}\frac{\partial}{\partial \underline{q}}(\underline{\dot{q}}^T \boldsymbol{D}(\underline{q})\underline{\dot{q}}) \tag{A.14}$$

independent of how the matrix $\boldsymbol{C}$ is defined.

Some fundamental properties of the equations of motion are (Ortega, and Spong, 1988; Albu-Schäffer, and Hirzinger, 2000)

- The inertia matrix $\boldsymbol{D}(\underline{q})$ is symmetric, positive definite and both $\boldsymbol{D}$ and $\boldsymbol{D}^{-1}$ are uniformly bounded as function of $\underline{q} \in \Re^n$. The norm is bounded by

$$\lambda_{min} \leq \left\| \boldsymbol{D}(\underline{q}) \right\| \leq \lambda_{max} \tag{A.15}$$

  with $\lambda_{min}$, $\lambda_{max} > 0$, the minimum and maximum eigenvalues of $\boldsymbol{D}$.
- The matrix $\boldsymbol{N}(\underline{q}, \underline{\dot{q}}) = \dot{\boldsymbol{D}}(\underline{q}) - 2\boldsymbol{C}(\underline{q}, \underline{\dot{q}})$ is scew symmetric, where $\boldsymbol{C}$ is defined using the Christoffel symbols. However, independent of how $\boldsymbol{C}$ is defined, $\underline{\dot{q}}^T(\dot{\boldsymbol{D}} - 2\boldsymbol{C})\underline{\dot{q}} = 0$ is always true. This reflects that the centrifugal and coriolis forces are fictitious and don't do any work.
- The gravity potential energy, $P_G$, with

$$\underline{g}(\underline{q}) = \frac{\partial P_G}{\partial \underline{q}} \tag{A.16}$$

  is dominated by some quadratic for a suitably chosen $\alpha$:

$$\left| P_G(\underline{q}_d) - P_G(\underline{q}) + (\underline{q} - \underline{q}_d)\underline{g}(\underline{q}_d) \right| \leq \frac{1}{2}\alpha \left\| \underline{q} - \underline{q}_d \right\|^2 \tag{A.17}$$

  or equivalently:

$$\left\| \underline{g}(\underline{q}_d) - \underline{g}(\underline{q}) \right\| \leq \alpha \left\| \underline{q} - \underline{q}_d \right\| \tag{A.18}$$

## APPENDIX B: EQUATIONS OF MOTION FOR A QUADRUPED

This appendix is based on Koo, and Yoon (1999). For shortness of notation let $\underline{r}_B = \underline{r}^{NB}$, $\underline{r}_{ij} = \underline{r}_{ij}^{NL}$, $\underline{v}_B = \underline{v}^{NB}$, $\underline{v}_{ij} = \underline{v}_{ij}^{NL}$, $\omega_B = {}^N\underline{\omega}^B$ and $\omega_{ij} = {}^N\underline{\omega}_{ij}^L$. The kinetic energy for each component is composed of two parts, one due to translation and one due to rotation. The kinetic energy for the robot's body is then

$$T_B = \frac{1}{2} m_B \underline{v}_B^T \underline{v}_B + \frac{1}{2} \underline{\omega}_B^T \boldsymbol{I}_B \omega_B \tag{B.1}$$

where $m_B$ and $\boldsymbol{I}_B$ are the mass and inertia matrix of the robot's body, respectively. In the same manner the kinetic energy for the links of leg $i$ is

$$T_i = \frac{1}{2} \sum_{j=1}^{3} \{ m_{ij} \underline{v}_{ij}^T \underline{v}_{ij} + \underline{\omega}_{ij}{}^T \boldsymbol{I}_{ij} \underline{\omega}_{ij} \} \tag{B.2}$$

where $m_{ij}$ and $\boldsymbol{I}_{ij}$ are the mass and the inertia matrix, respectively, for link $j$ of leg $i$. The total kinetic energy of the whole robot is then

$$T(\underline{q}, \dot{\underline{q}}) = T_B(\underline{q}_B, \dot{\underline{q}}_B) + \sum_{i=1}^{4} T_i(\underline{q}, \dot{\underline{q}}) \tag{B.3}$$

It should be noted the kinetic and potential energy are independent on which frame the vectors are defined in. However, in some cases it is desirable to express the vectors in a specific frame. In that case it should be remembered that the inertia matrix is specified in the same frame. The inertia matrix is a constant matrix in the frame of the its component, but if the vectors are expressed in other frames then the inertia matrix has multiplied with the corresponding rotation matrix. For example the inertia matrix for the body when expressed in the world frame is

$${}^N\boldsymbol{I}_B = {}^N\boldsymbol{R}^B \cdot {}^B\boldsymbol{I}_B \cdot {}^B\boldsymbol{R}^N \tag{B.4}$$

The kinetic energy for the body can be expressed, using the derivative of the generalized coordinates, as

$$T_B(\dot{\underline{q}}_B) = \frac{1}{2} m_B \dot{\underline{x}}_B^T \dot{\underline{x}}_B + \frac{1}{2} \dot{\underline{\phi}}_B^T ({}^N\Phi^B)^T \cdot {}^N\boldsymbol{I}_B \cdot {}^N\Phi^B \dot{\underline{\phi}}_B \tag{B.5}$$

where following relation was used

$$ {}^{N}\underline{\omega}^{B} = {}^{N}\mathbf{\Phi}^{B}(\underline{\phi}_{B})\dot{\underline{\phi}}_{B} \tag{B.6} $$

The kinetic energy for each leg can be expressed as functions of the generalized coordinates,

$$ T_i = \frac{1}{2}\sum_{j=1}^{3}\{m_{ij}({}^{N}\underline{v}_{ij})^{T}\cdot{}^{N}\underline{v}_{ij} + \underline{\omega}_{ij}{}^{T}\cdot{}^{N}\boldsymbol{I}_{ij}\underline{\omega}_{ij}\} \tag{B.7} $$

where the vectors in equation (B.7) are all expressed in *fN*,

$$ {}^{N}\underline{v}_{ij} = \dot{\underline{x}}_{B} + {}^{N}\boldsymbol{R}^{B}\cdot{}^{B}\boldsymbol{J}_{ij}^{L}\cdot\dot{\underline{\theta}}_{i} - {}^{N}\tilde{\underline{\boldsymbol{r}}}_{ij}^{BL}\cdot{}^{N}\mathbf{\Phi}^{B}\dot{\underline{\phi}}_{B} \tag{B.8} $$

where

$$ {}^{B}\boldsymbol{J}_{ij}^{L} = \frac{\partial^{B}\underline{r}_{ij}^{BL}}{\partial\underline{\theta}_{i}} \tag{B.9} $$

is the Jacobian, and ${}^{N}\tilde{\underline{\boldsymbol{r}}}_{ij}^{BL}$ is the dual matrix of the vector ${}^{N}\underline{r}_{ij}^{BL}$. The angular velocity, when expressed in *fN*, is

$$ \underline{\omega}_{ij} = {}^{N}\mathbf{\Phi}^{B}\dot{\underline{\phi}}_{B} + {}^{B}\mathbf{\Phi}_{ij}^{L}\dot{\underline{\theta}}_{i} \tag{B.10} $$

where the relationship between the angular velocity vector and the generalized coordinates is

$$ {}^{B}\mathbf{\Phi}_{ij}^{L} = \frac{{}^{N}\partial^{B}\underline{\omega}_{ij}{}^{L}}{\partial\dot{\underline{\theta}}_{i}} \tag{B.11} $$

The inertia matrix is then

$$ \boldsymbol{D}(\underline{q})\ddot{\underline{q}} = \begin{bmatrix} \boldsymbol{D}_{x} & \boldsymbol{D}_{x\phi}^{T} & \boldsymbol{D}_{x\theta1}^{T} & \boldsymbol{D}_{x\theta2}^{T} & \boldsymbol{D}_{x\theta3}^{T} & \boldsymbol{D}_{x\theta4}^{T} \\ \boldsymbol{D}_{x\phi} & \boldsymbol{D}_{\phi} & \boldsymbol{D}_{\phi\theta1}^{T} & \boldsymbol{D}_{\phi\theta2}^{T} & \boldsymbol{D}_{\phi\theta3}^{T} & \boldsymbol{D}_{\phi\theta4}^{T} \\ \boldsymbol{D}_{x\theta1} & \boldsymbol{D}_{\phi\theta1} & \boldsymbol{D}_{\theta1} & \mathbf{0} & \mathbf{0} & \mathbf{0} \\ \boldsymbol{D}_{x\theta2} & \boldsymbol{D}_{\phi\theta2} & \mathbf{0} & \boldsymbol{D}_{\theta2} & \mathbf{0} & \mathbf{0} \\ \boldsymbol{D}_{x\theta3} & \boldsymbol{D}_{\phi\theta3} & \mathbf{0} & \mathbf{0} & \boldsymbol{D}_{\theta3} & \mathbf{0} \\ \boldsymbol{D}_{x\theta4} & \boldsymbol{D}_{\phi\theta4} & \mathbf{0} & \mathbf{0} & \mathbf{0} & \boldsymbol{D}_{\theta4} \end{bmatrix} \begin{bmatrix} \ddot{\underline{x}}_{B} \\ \ddot{\underline{\phi}}_{B} \\ \ddot{\underline{\theta}}_{1} \\ \ddot{\underline{\theta}}_{2} \\ \ddot{\underline{\theta}}_{3} \\ \ddot{\underline{\theta}}_{4} \end{bmatrix} \tag{B.12} $$

where all the submatrices are of size $3 \times 3$ and given by

$$
\begin{aligned}
\boldsymbol{D}_x &= \left( m_B + \sum_{i,\,j} m_{i,\,j} \right) \boldsymbol{I}_{3\times 3} \\
\boldsymbol{D}_\phi(\underline{\phi}_B, \underline{\theta}_{1\to 4}) &= ({}^N\boldsymbol{\Phi}^B)^T \cdot {}^N\boldsymbol{I}_B {}^N\boldsymbol{\Phi}^B \\
&\quad + \sum_{i=1}^{4} \sum_{j=1}^{3} \{ m_{ij} ({}^N\tilde{\underline{\boldsymbol{r}}}_{ij}^{BL} \cdot {}^N\boldsymbol{\Phi}^B)^T \cdot {}^N\tilde{\underline{\boldsymbol{r}}}_{ij}^{BL} \cdot {}^N\boldsymbol{\Phi}^B + ({}^N\boldsymbol{\Phi}^B)^T \cdot {}^N\boldsymbol{I}_{ij} \cdot {}^N\boldsymbol{\Phi}^B \} \\
\boldsymbol{D}_{x\phi}(\underline{\phi}_B, \underline{\theta}_{1\to 4}) &= -\sum_{i=1}^{4} \sum_{j=1}^{3} \{ m_{ij} {}^N\tilde{\underline{\boldsymbol{r}}}_{ij}^{BL} \cdot {}^N\boldsymbol{\Phi}^B \} \\
\boldsymbol{D}_{x\theta i}(\underline{\phi}_B, \underline{\theta}_i) &= \sum_{j=1}^{3} \{ m_{ij} {}^N\boldsymbol{R}^B \cdot {}^B\boldsymbol{J}_{ij}^L \} \\
\boldsymbol{D}_{\phi\theta i}(\underline{\phi}_B, \underline{\theta}_i) &= \sum_{j=1}^{3} \{ ({}^N\boldsymbol{\Phi}^B)^T \cdot {}^N\boldsymbol{I}_{ij} \cdot {}^B\boldsymbol{\Phi}_{ij}^L - m_{ij} ({}^N\tilde{\underline{\boldsymbol{r}}}_{ij}^{BL} \cdot {}^N\boldsymbol{\Phi}^B)^T \cdot {}^N\boldsymbol{R}^B \cdot {}^B\boldsymbol{J}_{ij}^L \} \\
\boldsymbol{D}_{\theta i}(\underline{\phi}_B, \underline{\theta}_i) &= \sum_{j=1}^{3} \{ m_{ij} ({}^B\boldsymbol{J}_{ij}^L)^T \cdot {}^B\boldsymbol{J}_{ij}^L + ({}^B\boldsymbol{\Phi}_{ij}^L)^T \cdot {}^N\boldsymbol{I}_{ij} \cdot {}^B\boldsymbol{\Phi}_{ij}^L \}
\end{aligned}
\tag{B.13}
$$

The vector of centrifugal and coriolis forces is then equal to

$$
\underline{c}(\underline{q}, \dot{\underline{q}}) = \dot{\boldsymbol{D}}(\underline{q})\dot{\underline{q}} - \frac{1}{2}\frac{\partial}{\partial \underline{q}}(\dot{\underline{q}}^T \boldsymbol{D}(\underline{q})\dot{\underline{q}}) \tag{B.14}
$$